POLITECNICO DI MILANO

Corso di Laurea Specialistica in Ingegneria Biomedica

Facoltà di Ingegneria dei Sistemi

Dipartimento di Bioingegneria

Tesi di Laurea Specialistica

A COMPUTATIONAL MULTISCALE ANALYSIS OF SPIDER SILK MECHANICAL PROPERTIES

Relatori: Prof. Alberto REDAELLI

Prof. Markus J. BUEHLER

Correlatore: Dr. Sinan KETEN

Autore:

Andrea NOVA

Matricola 720178

Anno Accademico 2009-2010

...while the land of the free

is the home of the brave.

Acknowledgments

I express my profound gratitude for all the people and the institutions that have supported, guided and inspired the path of my academic career, making it an extraordinary experience of knowledge, passion and life.

I would like first to acknowledge Politecnico di Milano, a truly international university, who first gave me a solid and comprehensive engineering education, and then made it possible for me to live fantastic international experiences, first at the Royal Institute of Technology in Stockholm, Sweden and finally at the Massachusetts Institute of Technology, Cambridge, MA, United States of America.

I thank Prof. Redaelli for his guidance, his supervision and his visionary ideas for my academic and research career. I particularly appreciate his intellectual rigor, coupled at the same time by a profound and constant human touch.

I express my enormous gratitude to Prof. Buehler, who introduced me to the fascinating world of spider silk and the nano-structural analysis of bio-inspired materials. I greatly acknowledge his excellent mentorship, his support, his constant guidance and his tenacity. He is an extraordinary scientist, a never-ending source of inspiration, a phenomenal teacher and a great man.

I am really thankful to Sinan Keten, a great advisor, an inspiring researcher, a superb drummer and a friend. I express my gratitude to him for his constant and insightful supervision, for his suggestions and for his help in all situations. I wish him all the best as neo-professor at Northwestern University in Chicago, Illinois.

I thank all my peers at LAMM for the suggestions, for the excellent and sometimes surreal discussions, for the Hollywood-style pictures and for all the friendship we shared in these months: Steven Cranford, Dipanjan Sen, Alfonso Gautieri, Andre Garcia, Raffaella Paparcone, Graham Bratzel, Melis Arslan, Zhao Qin, Zhiping Xu.

I express gratitude, respect and obligation to M.I.T., one of the most amazing places on Earth, an authentic ἀγορά of knowledge, for paving the way of my future career and for printing few words forever in my mind: ‘Everything is possible’.

I thank the American Dream, for making me dare and look further.

I thank all my friends in Italy, Sweden and in the United States, for the fantastic moments spent together, for their support and joy through my whole academic career. In particular I thank Spider&friend at Politecnico di Milano.

I am grateful to Gianpaolo and Liann, for their help and their kindness and for being a constant and reliable landmark in my ever-changing and unstable American adventure.

Finally, I am endless thankful to my all-awesome family, for all their support, their faith in me, their patience and their unconditioned love. I must thank them, first and uppermost, for making this fantastic life of mine ultimately possible.

List of journal publications

A. Nova, S. Keten, N. M. Pugno, A. Redaelli and M. J. Buehler, "Molecular and nanostructural mechanisms of deformation, strength and toughness of spider silk fibrils", *Nano Letters,* DOI: 10.1021/nl101341w

A. Nova, S. Keten, S. Cranford, D. Sen, A. Redaelli and M. J. Buehler, "Mechanics of spider silk fibrils", in submission.

List of Figures

List of Tables

Abstract

Spider silk is one of the strongest, most extensible and toughest biological materials known, exceeding the properties of many engineered materials including steel. Silks feature a hierarchical architecture where highly organized, densely H-bonded beta-sheet nanocrystals are arranged within a semi-amorphous protein matrix consisting of 3_1-helices and beta-turn protein structures. By using a bottom-up molecular-based approach, here a first spider silk mesoscale model is developed, bridging the scales from Angstroms to hundreds of nanometers. Thanks to a one-dimensional model of the silk unit cell, it is first demonstrated that the specific nanoscale combination of a crystalline phase and a semi-amorphous matrix is crucial to achieve the unique properties of silks. These results reveal that the superior mechanical properties of spider silk can be explained solely by structural effects, where the geometric confinement of beta-sheet nanocrystals combined with highly extensible semi-amorphous domains is the key to reach great strength and great toughness, despite the dominance of mechanically inferior chemical interactions such as H-bonding. The one-dimensional model described in this thesis work directly shows that semi-amorphous regions govern the silk behavior at small deformation, unraveling first when silk is being stretched and leading to the large extensibility of the material. Conversely, beta-sheet nanocrystals play a significant role in defining the mechanical behavior of silk at large-deformation levels. In particular, the ultimate tensile strength of silk is controlled by the strength of beta-sheet nanocrystals, which is directly

related to their size: small beta-sheet nanocrystals are crucial to reach outstanding levels of strength and toughness. A molecular dynamics parametric two-dimensional study is also performed, with the aim to understand and foresee how parameters such as crystal density, level of pre-stretch, structural homogeneity and degree of hydration affect the overall silk mechanical behavior. Results from both models, coupled with a mechanistic insight, directly explain recent experiments, where it was shown that a significant change in the strength and toughness can be achieved solely by tuning the size of beta-sheet nanocrystals and the structural parameters of the silk network. These findings help to unveil the material design strategy that enables silks to achieve superior material performance despite simple and inferior material constituents.

Spider silk is a strong and tough fibrous biological protein material with a hierarchical structure that has evolved to fulfill multiple functions of efficiently storing and dissipating mechanical energy, making it one of the toughest and most versatile materials known. Silks belong to the broader class of biological structures that have evolved as critical material components in biological systems, in order to provide structural support and energy conversion. From a biological point of view, spiders take advantage of the unique mechanical features when using silk threads to support their own weight and to absorb kinetic energy to capture prey. From an engineering perspective, silk has been utilized in various technological fields including parachutes, medical sutures, and more recently, tissue regeneration and many other biomedical applications. Experimental and computational investigations

of the structure of silks at the nanoscale revealed that there exist two fundamental structural constituents in silks: highly organized anti-parallel beta-sheet nanocrystals and a semi-amorphous phase that consists of less orderly protein structures. Thereby, the anti-parallel beta-sheet nanocrystals play a key role in defining the mechanical properties as they provide stiff orderly cross-linking domains embedded in a semi-amorphous matrix that consists of less orderly beta-structures, 3_1 helices and beta-turns. Similar to their role in other mechanical proteins, it has been hypothesized that H-bond arrays in beta-sheet nanocrystals reinforce the polymeric network under mechanical stretch, by forming interlocking regions that transfer the load between chains. In particular, Termonia's pioneering empirical two-phase model based on experimental data has been instrumental in explaining the importance of the ratio and size of crystalline and semi-amorphous domains, at a time when large-scale atomistic simulations of spider silk constituents were impossible due to the lack of suitable force fields and computational resources. More recently, macroscale experiments demonstrated that when the size of beta-sheet nanocrystals is reduced by moderating the reeling speed or by infiltrating, silk displays enhanced toughness and greater ultimate strength, exceeding that of steel and other engineered materials. However, despite progress in experimental, theoretical and computational studies, thus far no model exists to that enables a rigorous understanding of the role of the two fundamental constituents of silks at the intermediate "composite" level. This progress has partly been hindered due to a lack of appropriate atomistic models of silks, and a lack of a thorough understanding of the mechanical behavior of silk's constituents at the nanoscale. Both issues have recently been addressed through protein structure

identification methods and large-scale molecular simulation studies, where the molecular structure and mechanical signature of the two key constituents of silks has been identified. As a result, we are now in a position to understand the fundamentals of the origin of silk's unique material properties at the mesoscale by deriving parameters directly from an atomistic level without the need to introduce experimental parameters, an issue that will be addressed in this thesis work.

General method of this work is to utilize key material and structural parameters from atomistic calculations on spider silk constituents and to develop a fundamental understanding of silk's exceptional performance by linking the molecular structure and mechanisms to its larger-scale mechanical behavior at scales of hundreds of nanometers. To provide a fundamental description of spider silk mechanics from a bottom-up perspective, and to elucidate the design strategy behind the making of silks, a simple coarse-grained model is used, whose parameters are directly informed from atomistic simulation results. A simple combination of beta-sheet nanocrystals as well as semi-amorphous regions is modeled by beads connected via nonlinear springs in serial arrangement, in order to represent a unit cell of the silk two-phase nanostructure. We consider both a one-dimensional and two-dimensional implementation of the model. We first focus on the one-dimensional setup, and apply the model to simulate the mechanical deformation of silk according to uniaxial tensile loading conditions. The following two-dimensional geometry that is developed is based on a random network, with the aim to describe the entangled arrangement of silk polypeptide chains. Nodes represent the stiff poly-alanine beta-sheet

nanocrystals, while the bonds between nodes represent the inter-crystalline semi-amorphous regions. While a MATLAB in-house made code is used for the 1D model, LAMMPS molecular dynamics simulations are performed at 300 K for the two-dimensional system, applying tensile stretching at constant deformation rate, with a timestep of 1 fs and for varying system and boundary conditions. Results are then post-processed to extract relevant information regarding silk's mechanical behavior and regarding the effect of multiple parameters on the protein assembly.

The analysis in both 1D and 2D model starts by considering a system with a beta-sheet nanocrystal size of 3 nm that reflects the size of naturally-spun silks. It is found that the resulting stress-strain curve displays the characteristic shape experimentally observed in silks, that is characterized by an early yield point that leads to a significant softening and is followed by a severe stiffening effect. A detailed analysis of the results reveals that the initial regime is characterized by a relatively high tangent modulus, owing to the homogeneous stretching of semi-amorphous regions that are rich in hydrogen bonding in the form of 3_1-helices and beta-turns. The onset of rupture of the hydrogen bonds in the semi-amorphous domains leads to yielding at strain values of around 15% in both models, and evident from a sudden drop in the tangent stiffness. During the plateau regime, protein chains in the semi-amorphous region gradually align along the pulling direction, a mechanism that is mediated by the significant hidden length of polypeptide stored in this geometry. At a strain value of around 50%, the stress-strain curve enters a final covalent high-stiffness regime. At this point, the semi-amorphous region has been completely stretched out and the beta-

sheet nanocrystals begin to sustain larger strains. When the applied force reaches the maximum tensile strength, varying for different systems and different parameters in the study, individual beta-strands are completely pulled out, and failure occurs at a stress of the order of GPa, in quantitative agreement with results from experimental studies. A systematic variation of the beta-sheet nanocrystal size of up to 10 nm is then considered in the two models, and its impact on the mechanical properties is studied to quantify the dependence of the crystal size on the overall mechanical behavior. The motivation for this analysis is to validate earlier hypotheses, showing that small changes in the crystal size translate to altogether different overall mechanical response in spider silk. The most important finding is the observation that the size of beta-sheet nanocrystals—at otherwise completely identical conditions—severely affects the mechanical response. The analysis clearly shows that larger-crystal systems (*i.e.* 6.5 nm and 10 nm beta-sheet nanocrystals) have a behavior that deviates significantly from the reference small-crystal case, especially at high levels of deformation. Silk fibrils with larger beta-sheet nanocrystals break at significantly lower stress values, and also show a shorter and much softer third regime. These findings hold both for a one-dimensional and a two-dimensional system, where the entanglement of polypeptide chains is represented by a coarse-grained random network. Both systems provide evidence that the size of the beta-sheet nanocrystals drastically affects the overall mechanical response, with smaller-crystal systems showing enhanced properties in terms of maximum tensile strength and dissipated energy. The extension from the one-dimensional unit cell to a two-dimensional network model gives coherent results and confirms that the mechanical properties and

deformation mechanisms of silk—in particular the sensitivity of the properties with respect to the size of beta-sheet nanocrystals—are well preserved when increasing the complexity of the system. Most importantly, the similarity of the results throughout different scales confirms that our approach of coarse-graining the spider-silk unit cell into a one-dimensional model is suitable to capture the key physics of material deformation. To deepen our understanding of the silk unit-cell mechanics, an accurate analysis of the deformation mechanisms at different strain levels has been performed, showing how each regime of deformation is associated with specific molecular-level mechanics. The overall analysis of these data shows that beta-sheet nanocrystals play a significant role in defining the mechanical behavior of silk only at high-deformation levels, while the initial behavior is mainly governed by deformation of the semi-amorphous phase. This concept has been hypothesized in earlier experimental studies, but is here for the first time shown from a molecular perspective and with a direct link to underlying molecular mechanisms. The analysis put forth here reveals that the contribution of the beta-sheet nanocrystals to deformation tends to decrease significantly as the size of beta-sheet nanocrystals is increased. In the small-crystal system, beta-sheet nanocrystals start to play a significant role once the semi-amorphous region begins to stiffen at around 50% strain, and dominates deformation when the stick-slip mechanisms of beta-sheet nanocrystal deformation is triggered. In the larger-crystal case, the beta-sheet nanocrystal contribution increases more gradually, and reaches a maximum just before the system breaks, that is, shortly after the semi-amorphous region enters the covalent hard-stretching regime. If we compare the semi-amorphous region deformation in the two cases of crystal size, we observe

that the breaking point is reached earlier in large-crystal systems, when semi-amorphous regions are less stretched. This is an important observation, which suggests that the change of the beta-sheet nanocrystal size prevents the material to take full advantage of the entire potential (hidden length) of the semi-amorphous regions in terms of extensibility and energy dissipation capacity. In addition to the study of the silk unit cell, the development of a two-dimensional mesoscale model has been crucial to identify and explain key features of spider silk behavior that cannot be justified by a simple one-dimensional model, such as crystal concentration and structural homogeneity. Molecular dynamics tools have been used to simulate the variation of a variety of system conditions, and to perform a parametric study of their effect on the overall silk's mechanical behavior. A complete understanding of the mechanical signature of silk requires indeed the development of a model that can also take into account key physical phenomena such as the effect system hydration, the effect of crystal density and homogeneity, as well as the level of pre-stretch of the protein chains. The robustness and flexibility of the current model, together with its results, have been checked by validating computational evidences with experiments, showing great agreement but opening at the same time interesting directions for future research, in the pursuit of an even better understanding of the phenomena underlying silk's behavior.

The importance of this computational study of silk's behavior at the nanoscale comes from the fact that experimental techniques can only provide limited insight into the nanostructure of silk, making computing techniques the only suitable tool for such

investigation. One of the outcomes of this study is that its computational results are overall in excellent agreement with experimental data, where a similar variation of the beta-sheet nanocrystal size, as well as system and boundary conditions, was recently studied. In conclusion, one the most important finding of this thesis work is that it has revealed the mechanistic interplay of the two constitutive phases in silks, semi-amorphous regions and highly organized beta-sheet nanocrystals, and the effect of structural and boundary-condition changes on the overall mechanical behavior of silks. It is discovered that semi-amorphous regions unravel first when silk is being stretched, leading to the large extensibility of silk. Conversely, the large-deformation mechanical properties and ultimate tensile strength of silk are controlled by the strength of beta-sheet nanocrystals, which is directly related to their size. An important discovery is that small beta-sheet nanocrystals are crucial to reach outstanding levels of strength and toughness. These results have shown how the confinement of beta-sheet nanocrystals to the nanoscale is essential for the superior mechanical properties of silks, as it is crucial to reach high extensibility and high levels of stress. These findings also relate the characteristic yielding point in the stress-strain curve, observed universally for many silks, to the onset of failure of semi-amorphous regions when H-bonded 3_1-helices and beta-turns begin to rupture. Small-crystal systems guarantee the required cross-linking strength that is necessary for the semi-amorphous domains to fully extend and to enter a high-stiffness covalent regime when beta-sheet nanocrystals are being stretched and eventually fail. The resulting capacity to sustain large tensile force as well as extension enhances the strength and energy dissipation ability of the material. The two dimensional model

provided insight into the effect of different system parameters, and its development has opened new interesting research paths. These findings have impact beyond our understanding of silk mechanics, as they show that by solely controlling the structure at the nanoscale, a tailoring of material properties at the microscale is possible without the need to introduce new material constituents. This could provide us with a powerful alternative to the traditional engineering top-down approach of shaping materials to obtain specific properties, and enable the bottom-up design of complex structural materials. Thereby, the application of our findings to the design of synthetic materials could provide us with new material concepts based on inexpensive and abundant constituents. Technologically, we are not limited by "simple" natural building blocks such as amino acids. Therefore, the incorporation and transfer of the materials design strategies identified here into synthetic products could result in materials with significantly better performance, much higher levels of strength and toughness while reaching similar levels of extensibility.

Sommario

La seta aracnide è un materiale biologico dalle proprietà meccaniche sensazionali, tanto da eccedere le caratteristiche di molti materiali industriali, incluso l'acciaio, per quanto riguarda durezza e sforzo massimo a trazione per unità di volume. La seta aracnide è caratterizzata da una architettura gerarchica, dove nanocristalli formati da foglietti beta ad alto contenuto di legami idrogeno sono assemblati all'interno di una struttura proteica semi-amorfa che consiste di eliche 3_1 e ripiegamenti beta. Utilizzando un approccio dimensionale bottom-up e basato sulla conoscenza della struttura molecolare, in questo lavoro di tesi viene sviluppato il primo modello mesocala della seta aracnide, che crea un ponte tra la scala degli Angstroms e quella di centinaia di nanometri. Grazie ad un modello monodimensionale dell'unità base della seta aracnide, viene dimostrato che la specifica combinazione alla nanoscala di una fase cristallina e di una matrice semi-amorfa è cruciale per ottenere le proprietà uniche che caratterizzano la seta. Questi risultati rivelano che le superiori proprietà meccaniche possono essere spiegate tramite soli effetti strutturali, dove il confinamento geometrico di nanocristalli di foglietti beta, in combinazione con domini semi-amorfi altamente estensibili, è la chiave per raggiungere elevati livelli di sforzo e di durezza, nonostante la prevalenza di interazioni chimiche meccanicamente inferiori quali i legami a idrogeno. Il modello descritto in questa tesi mostra direttamente come le regioni semi-amorfe governino il comportamento meccanico della seta aracnide a bassi livelli di deformazione, svolgendosi e garantendo l'elevata estensibilità del materiale sottoposto a trazione. Al contrario, i nanocristalli giocano

un ruolo significativo nel definire il comportamento meccanico della seta aracnide ad elevati livelli di deformazione. In particolare, la resistenza a trazione è controllata dallo sforzo a rottura dei nanocristalli di foglietti beta, il quale a sua volta è inversamente correlato alla dimensione dei cristalli stessi: piccoli nanocristalli di foglietti beta sono cruciali per raggiungere livelli eccezionali di forza e durezza. Uno studio parametrico di dinamica molecolare su un sistema bidimensionale è stato inoltre effettuato, con lo scopo di comprendere e prevedere come parametri quali la densità di cristalli, il livello di pre-stretch, l'omogeneità strutturale e il grado di idratazione condizionano il comportamento meccanico complessivo della seta. Risultati da entrambi i modelli, accoppiati con la loro interpretazione meccanica, sono in grado di spiegare direttamente esperimenti recenti: è stato dimostrato che un cambiamento significativo nei valori di massimo sforzo e durezza può essere raggiunto modificando unicamente le dimensioni dei nanocristalli ed i parametri strutturali che definiscono la rete della seta aracnide. Questi risultati aiutano a svelare la strategia che permette alla seta aracnide di raggiungere prestazioni superiori, nonostante i semplici e meccanicamente inferiori costituenti elementari.

La seta aracnide è un materiale proteico fibroso, caratterizzato da livelli elevati di sforzo a rottura e di durezza. La sua struttura gerarchica si è evoluta in modo da adempiere a funzioni multiple di immagazzinamento e dissipazione di energia meccanica, rendendola uno dei materiali conosciuti più duri e versatili allo stesso tempo. La seta aracnide appartiene ad una classe più ampia di materiali biologici che si sono evoluti per adempiere a funzioni chiave in sistemi biologici, fornendo

supporto strutturale e conversione energetica. Dal punto di vista biologico, i ragni sfruttano le caratteristiche meccaniche uniche della seta per supportare il proprio peso e per assorbire energia cinetica nel catturare le prede. Da una prospettiva ingegneristica, la seta viene utilizzata in svariati campi tecnologici, che includono paracaduti, suture mediche e, più recentemente, rigenerazione di tessuti ed altre applicazioni biomediche. Come accennato, studi sperimentali e computazionali della struttura della seta alla nanoscala hanno rivelato l'esistenza di due costituenti strutturali fondamentali: nanocristalli di foglietti beta antiparalleli, altamente organizzati, e una fase semi-amorfa che consiste di strutture proteiche strutturalmente meno ordinate. I nanocristalli giocano un ruolo chiave nel definire le proprietà meccaniche, dal momento che forniscono domini rigidi e ordinatamente interconnessi, integrati alla matrice semiamorfa che consiste di strutture beta a minore livello di ordine ed eliche 3_1. E' stato ipotizzato che l'assemblaggio altamente ordinato di legami idrogeno all'interno dei nanocristalli agisca da rinforzo per la rete polimerica complessiva sotto stiramento meccanico, formando regioni a incastro che trasferiscono il carico tra le catene polipeptidiche. In particolare, il modello pionieristico ed empirico sviluppato da Termonia, unicamente basato su dati sperimentali, assume un ruolo fondamentale nel chiarire l'importanza del rapporto tra fasi e delle dimensioni dei domini cristallini. Questi studi sono stati sviluppati in un'epoca in cui simulazioni atomistiche a larga scala non erano possibili a causa della mancanza di force-field adeguati e risorse computazionali sufficientemente performanti. Più di recente, modulando la velocità di tessitura della seta aracnide o tramite infiltrazione metallica, esperimenti alla macroscala hanno dimostrato che una

diminuzione delle dimensioni dei nanocristalli determina una accresciuta durezza e un maggiore sforzo a rottura della seta. Tuttavia, nonostante i progressi nella conoscenza teoretica, computazionale e sperimentale della seta aracnide, non esiste tuttora un modello che permetta una comprensione rigorosa del ruolo dei due costituenti fondamentali della seta aracnide a livello composito intermedio. Questo progresso è in parte stato ostacolato dalla mancanza di modelli atomistici appropriati, oltre che dalla carenza di una comprensione dettagliata del comportamento meccanico dei costituenti della seta alla nanoscala. Entrambi i punti in questione sono stati recentemente affrontati attraverso metodi di identificazione della struttura proteica, nonchè da studi molecolari e simulazioni a larga scala. E' stato in questo modo possibile caratterizzare meccanicamente i due costituenti molecolari chiave nel determinare la risposta a trazione della seta aracnide. Come risultato, si è ora nella posizione di poter comprendere l'origine delle proprietà uniche della seta, direttamente partendo da un livello atomistico e senza la necessità di introdurre parametri sperimentali. È questo il punto chiave che verrà affrontato in questo lavoro di tesi.

Metodo generale di questo lavoro è quello di utilizzare parametri strutturali da calcoli atomistici, ed ottenere tramite un modello mesoscala una comprensione dell'origine delle prestazioni eccezionali della seta aracnide. Il fine è quello di connettere la struttura e i meccanismi molecolari della seta aracnide al suo comportamento meccanico complessivo, alla scala ampia di centinaia di nanometri. Per fornire una descrizione comprensiva della meccanica della seta aracnide seguendo un approccio

bottom-up, e per delucidare la strategia progettuale alla base della formazione della seta, i parametri del modello mesoscala sviluppato in questo progetto sono dedotti unicamente da risultati di simulazioni atomistiche. La combinazione di nanocristalli e di regioni semiamorfe è modellizzata da molle non lineari in disposizione seriale, rappresentando in questo modo la cella elementare bifase della seta aracnide e riflettendo la geometria fondamentale della sua nanostruttura. Viene considerata sia un' implementazione monodimensionale che un modello bidimensionale della seta. Ci si sofferma dapprima sul setup 1D, applicando il modello con l'obiettivo di simulare la deformazione meccanica della seta secondo condizioni di carico a trazione monoassiale. La geometria che viene in seguito sviluppata e descritta per il modello 2D è basata su una rete di nodi a generazione casuale, con l'obiettivo di descrivere la disposizione spaziale delle catene polipeptidiche. I nodi rappresentano i nanocristalli rigidi di foglietti beta, metre i legami tra i nodi rappresentano le regioni inter-cristalline semi-amorfe. Mentre uno script MATLAB è utilizzato per calcolare la risposta meccanica del modello monodimensionale, simulazioni di dinamica molecolare in LAMMPS vengono effettuate a 300 K per il modello 2D, applicando un carico a trazione con deformazione costante, con un timestep di 1 fs e per parametri variabili di sistema e di condizioni al contorno. I risultati sono successivamente sottoposti a post-processing, in modo da estrarre informazioni utili riguardanti il comportamento meccanico della seta aracnide e l'effetto di diversi parametri sulla rete proteica.

L’analisi meccanica sia nel sistema 1D che in quello 2D inizia considerando un sistema con dimensioni dei nanocristalli di 3 nm, tale da riflettere le dimensioni riscontrate nella seta in condizioni naturali. Viene mostrato che la curva sforzo-deformazione assume una forma sigmoidale, caratterizzata da un punto di snervamento, un plateau a bassa rigidezza e uno spiccato irrigidimento finale. Il regime iniziale, caratterizzato da un modulo tangente relativamente alto, è dovuto allo stiramento omogeneo delle regioni semiamorfe, ricche in legami idrogeno nella forma di eliche 3_1 e ripiegamenti beta. La rottura dei legami idrogeno nei domini semiamorfi porta allo snervamento della struttura per valori di deformazione di circa il 15% e determina un calo improvviso della rigidezza tangente. Durante il regime di plateau, le catene proteiche si allineano gradualmente lungo la direzione di trazione. Questo meccanismo è mediato dalla significativa ridondanza delle catene polimeriche nella configurazione descritta. Quando la curva sforzo-deformazione entra in un regime finale di elevata rigidezza, la regione semiamorfa è completamente estesa e i nanocristalli di foglietti beta iniziano a sostenere deformazioni più elevate. Quando infine la forza applicata raggiunge il valore massimo di sforzo a rottura, singole catene beta vengono completamente sfilate dal cristallo e il fallimento meccanico complessivo avviene ad uno sforzo massimo dell’ordine dei GPa, in accordo quantitativo con risultati di studi sperimentali. Viene considerato un incremento sistematico delle dimensioni del nanocristallo fino al valore di 10 nm in entrambi i modelli, studiandone l’impatto sulle proprietà meccaniche complessive. Lo studio ha come obiettivo la validazione di ipotesi precedenti, che mostrano come piccoli cambiamenti nelle dimensioni del cristallo si traducano in differenti risposte

meccaniche complessive. Importante risultato sta nell'osservazione che le dimensioni dei cristalli – a parità di altre condizioni – influenzano significativamente la risposta meccanica della seta. L'analisi mostra chiaramente che sistemi di cristalli più grandi (nanocristalli di 6.5 nm e 10 nm) hanno un comportamento che devia significativamente dal caso di riferimento (cristallo di 3 nm), specialmente ad elevati livelli di deformazione. Le fibrille di seta con nanocristalli più larghi vanno incontro a rottura a valori di sforzo significativamente più bassi, mostrando inoltre un regime finale molto meno rigido. Le osservazioni presentate nel modello 1D valgono anche per una rete polipeptidica bidimensionale. Entrambi i sistemi mostrano una significativa dipendenza dalle dimensioni dei nanocristalli, fornendo evidenza aggiuntiva che le dimensioni dei nanocristalli di foglietti beta influiscono drasticamente sulla risposta meccanica complessiva. L'estensione del modello ad un arrangiamento bidimensionale conferma che le proprietà meccaniche e i meccanismi di deformazione della seta aracnide vengono ben conservati quando la complessità del sistema viene aumentata. Altro risultato importante è il fatto che la similarità di risultati tra il modello monodimensionale e bidimensionale conferma che questo approccio mesoscala di modellizzazione della cella elementare della seta aracnide è in grado di rappresentare i fenomeni fisici chiave di deformazione del materiale. In entrambi i modelli, i risultati esposti in questa tesi dimostrano che anche un piccolo incremento nelle dimensioni del nanocristallo determina un decremento significativo del valore di sforzo a rottura del sistema e di conseguenza valori di durezza consistentemente più bassi sia per il sistema monodimensionale che per quello bidimensionale. Un'analisi dei meccanismi di deformazione, per livelli di

elongazione differenti e, per dimensioni dei nanocristalli variabili, mostra come ciascun regime di deformazione sia associato a specifici fenomeni meccanici a livello molecolare. L'analisi complessiva dei dati mostra che i nanocristalli di foglietti beta giocano un ruolo significativo nel definire il comportamento meccanico della seta aracnide solo ad elevati livelli di deformazione, mentre il comportamento meccanico iniziale è principalmente governata dalla deformazione della fase semiamorfa. Questo concetto è stato ipotizzato in studi sperimentali precedenti, ma viene qui per la prima volta mostrato secondo una prospettiva molecolare e con riferimento diretto ai meccanismi costitutivi sottostanti. Nel sistema di riferimento, i nanocristalli iniziano a giocare un ruolo significativo una volta che la ragione semiamorfa inizia a irrigidirsi, a valori di deformazione di circa 50%. Nel caso di cristalli più grandi, il contributo dei nanocristalli cresce più gradualmente e raggiunge un massimo appena prima della rottura del sistema, che avviene poco dopo che la regione semi-amorfa entra nel regime covalente finale. Il punto di rottura viene raggiunto prima nei sistemi con nanocristalli grandi, mentre le regioni semiamorfe non sono ancora completamente stirate. Questa osservazione suggerisce che il cambiamento delle dimensioni del nanocristallo impedisce al materiale di trarre pieno vantaggio delle potenzialità delle regioni semiamorfe in termini di estensibilità e capacità di dissipazione energetica, capitalizzando su legami sacrificali e sulla rottura di legami idrogeno. I risultati di questo studio sono complessivamente in eccellente accordo con i dati sperimentali, dove una variazione simile delle dimensioni dei nanocristalli e il suo impatto sulle proprietà meccaniche ad una scala superiore è stato recentemente riportato, mostrando un drastico calo in durezza conseguente all'aumento delle

dimensioni dei nanocristalli (negli esperimenti il cambiamento dimensionale dei nanocristalli viene ottenuto per mezzo del cambiamento della velocità di tessitura da parte del ragno).

Il contributo più importante dello studio esposto in questa tesi è il fatto di aver rivelato l'interscambio meccanicistico delle due fasi costitutive della seta aracnide, ovvero delle regioni semi-amorfe e dei nanocristalli di foglietti beta. E' stato computazionalmente dimostrato che le regioni semi-amorfe della seta si estendono per prime quando la seta viene stirata, portando alla elevata estensibilità del materiale. Al contrario, le proprietà meccaniche ad elevati livelli di deformazione e lo sforzo a rottura della seta aracnide sono controllati dal massimo sforzo dei nanocristalli, che è inversamente proporzionale alle loro dimensioni. Una scoperta importante è che nanocristalli di piccole dimensioni sono cruciali nel raggiungere eccezionali livelli di massimo sforzo e di durezza. Questi risultati mostrano che il confinamento dei nanocristalli alla nanoscala è essenziale per le superiori proprietà meccaniche della seta, dal momento che risulta cruciale nel raggiungere elevata estensibilità e alti livelli di sforzo. Questi risultati inoltre mettono in relazione il caratteristico punto di snervamento nella curva sforzo-deformazione con l'insorgere del cedimento di eliche 3_1 e ripiegamenti beta nelle regioni semi-amorfe. Sistemi con cristalli di piccole dimensioni garantiscono la forza di legame necessaria alle regioni semiamorfe per estendersi completamente e per entrare in un regime covalente ad alta rigidezza in cui i nanocristalli vengono stirati fino a rottura. La risultante capacità di sostenere una elevata forza a trazione ed elevati livelli di deformazione incrementa il

massimo sforzo a rottura e la capacità di dissipazione energetica del materiale. Questi risultati hanno un impatto che va oltre la conoscenza della meccanica della seta aracnide, dal momento che mostrano che solamente controllando la struttura alla nanoscala è possibile definire le proprietà del materiale alla micro e macroscala senza l'introduzione di alcuna nuova specie molecolare. Questo strumento può fornire una potente alternativa al tradizionale approccio top-down usato in ingegneria, che consiste nel dare forma a materiali per ottenere specifiche proprietà: l'approccio usato in questo studio permette invece di progettare materiali complessi seguendo una logica bottom-up. L'incorporazione e il trasferimento di strategie di progetto tipiche dei biomateriali nel progetto di prodotti sintetici potrà risultare in nuovi materiali con prestazioni meccaniche superiori, ovvero con livelli di sforzo a rottura e di durezza molto maggiori, mantenendo nel contempo simili livelli di estensibiltà.

Massachusetts
Institute of
Technology

A COMPUTATIONAL MULTISCALE ANALYSIS OF SPIDER SILK MECHANICAL PROPERTIES

Contents

Chapter 1

Background

Aim of this Chapter is to foster the curiosity of the reader, by introducing silk not only as the fascinating fiber that has driven a rich trade for centuries, but also as a natural biological material with exceptional mechanical properties.

Spider silk is first described and categorized among fibrous biological materials. The State of the Art in scientific knowledge is then presented, together with its possible applications as biomedical material.

The objectives of the work are then stated, underlying the progress from current knowledge and the challenges of this study in the short and in the long term.

1.1 Spider silk: an evolutionary marvel

Silk has carried with itself a stunning secret for ages: while traded from East to West as a luxury fabric, this intriguing biological fiber was hiding another astonishing feature, the one of being among the most mechanically outstanding fibers ever. Silk is perhaps the strongest, most extensible and toughest material on Earth, by far exceeding the properties of many engineered industrial materials [1-3].

Figure 1-1 shows the complexity and at the same time the beauty of a spider web, deadly trap for flies and insects, feeble and fragile at first glance but incredibly strong and tough when carefully studied.

Figure 1-2 shows the complex hierarchical organization of silk, where the secrets of this evolutionary marvel of nature have long been stored.

Figure 1-1: A spider web, carefully weaved across young tree offshoots. Remarkable is the perfect geometry of the whole structure, together with the fact that all load is carried by a single upper silk thread following a catenary curve [Figure reprinted by http://naturescrusaders.files.wordpress.com].

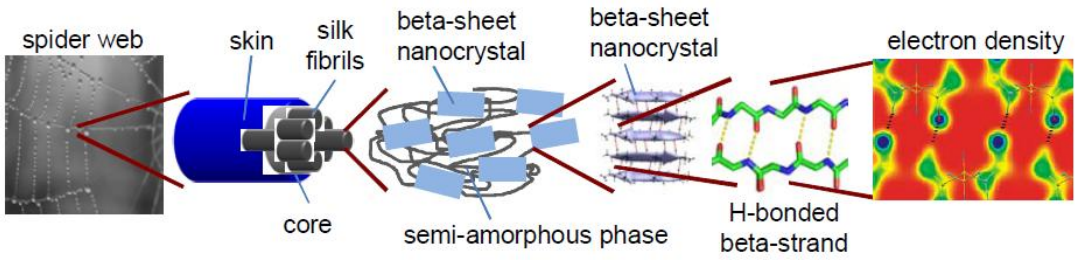

Figure 1-2: Hierarchical organization of silk. A multiscale representation of the structural organization of spider silk, from a level explored by quantum mechanics up to the macro-scale of the spider web. [Figure reprinted from Ref. [4]]

Commercial silk defines primarily the fiber spun by the silk moth *Bombyx Mori*; it is collected by unraveling the pupal cocoon of the insect and then it is weaved, machined and dyed in an infinite combination of shapes and colors. Nevertheless, spider dragline silk, although perceived as very different when looking at a spider web, is indeed very similar, at least in its general structure and mechanical properties, to the commercial *Bombyx* silk produced in vast quantities worldwide.

Spider silk is considerably stronger and significantly more extensible than any other silkworm silk. Both of them, however, show an initial high-stiffness that, at a yield point, gives way to a plateau and to a final-stiff covalent regime [5]. Figure 1-3 represents a series of experimental curves on spider silk threads, showing the typical three-regime behavior just described.

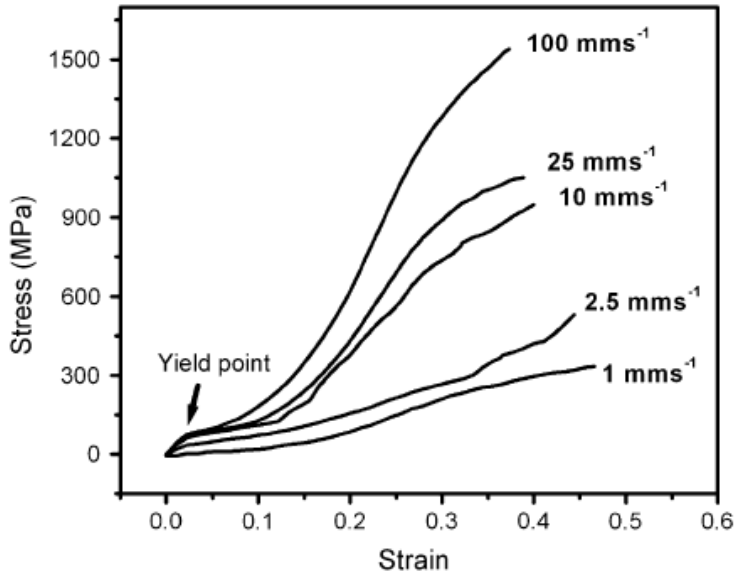

Figure 1-3: Experimental values for the silk characteristic curve at different reeling speed. An initial high stiffness regime is followed by a yield point, a plateau of varying length and a final stiff regime. The higher the reeling speed, the more pronounced this characteristic behavior [figure reprinted from Ref. [6]].

Spider silk is a powerful tool for spiders to achieve an effective energy management: according to evolutionary concepts and theories [7], in biology energy is the primary currency used by natural selection, where efficient energy management allows animals to accumulate reserves, ultimately converted into the following generation of individuals [7].

Silk's complex hierarchical structure has evolved to fulfill the vital function of efficiently storing and dissipating mechanical energy [3, 8, 9], making it an exceptionally tough and versatile material [2, 3]. Figure 1-4 schematically illustrates the interplay of scales that is crucial in silk, where mechanical properties at the nanoscale reflect on the overall macroscale behavior.

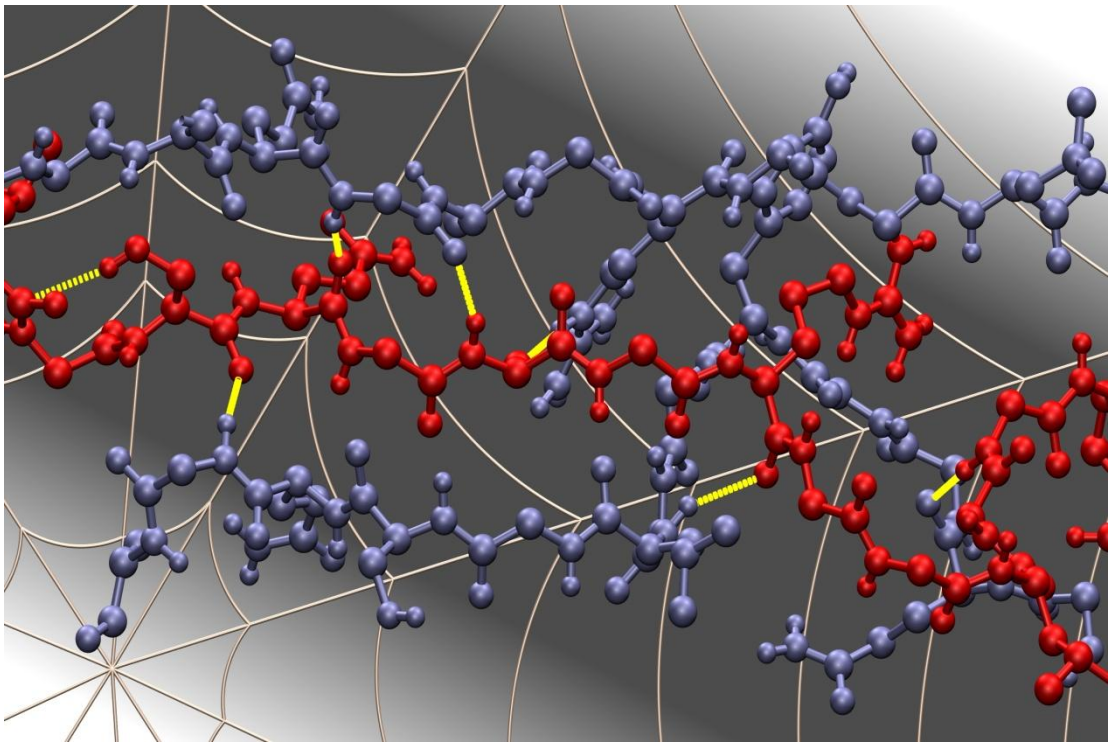

Figure 1-4: Macroscale and nanoscale interplay in spider silk. The enchanting geometric structure of the silk web is made possible by a complex and hierarchical nanoscale organization. Hydrogen bonds are key to interconnect residues of different protein molecules. [Figure reprinted from Ref. [10], image created by Steven Cranford].

For the spider, energy efficiency consists in a combination of optimal web engineering in terms of architecture and silk materials. For example, flies captured in the web arrive with kinetic energy that needs to be distributed both effectively and efficiently, that is with a minimum amount of material [11].

1.2 Hierarchical study of silk as a protein material

Proteins can be considered the constitutive bricks of life as we know it on Earth [12]. The primary structure of a protein, as a linear sequence of amino acids, is synthesized

by cells based on segments of DNA code, and this is made possible by covalent peptide bonds that link amino acids[13].

Through charge interactions and weak interactions such as hydrophobic effects, Van der Waals interactions and hydrogen bonding, proteins create folds and filamentous structures that are able to carry out physiological functions. Fibrous proteins are large assemblies of polypeptide chains that play mostly structural and mechanical functions [14]. The structure and mechanics of these materials, of which silk is an example, are largely controlled by a complex and intriguing arrangement of weak interactions at the nano-scale and in particular by hydrogen bonds [4].

The atomic microstructure of materials is the defining factor of their mechanical properties [15]. Mechanical behavior of biological materials features molecular unfolding or sliding under tensile loading, where particularly relevant is the rupture of hydrogen bonds, covalent cross-links and intermolecular entanglement [12, 16]. Different mechanisms operate at larger length scales: the overall mechanical behavior emerges as a result of geometrical parameters, chemical nature of the molecular interactions, as well as the structural arrangement of the protein elementary building blocks, across many hierarchical scales, from nano to macro.

As discussed in Ref. [12, 16], a trait of most biological materials is the occurrence of hierarchies and, at the molecular scale, the abundance of weak interactions. The presence of hierarchies in biological materials may be vital to take advantage of molecular and sub-molecular features, with the aim to enhance the material's mechanical properties [12, 16]. The nanoscale arrangement of molecules is often characterized by weak interactions, and a hierarchical arrangement allows to multiply their properties so that they become visible at larger scales, thus providing a link between structural organization and function [17]. In spider silk, weak interactions are used to produce a strong materials at moderate temperatures, using just a very limited quantity of energy [4, 18].

Promising strategies for probing biological materials at the nano-scale can now be developed by combining experiment and simulation concurrently, and at the same scales. These methods could eventually lead to the development of superior biomaterials through an improved understanding of the influence of nano-scale on the macro-scale. It is therefore reasonable to conclude that modeling and simulations have evolved from explaining experimental observations into predictive tools that complement experimental analyses [12] (see Figure 1-5).

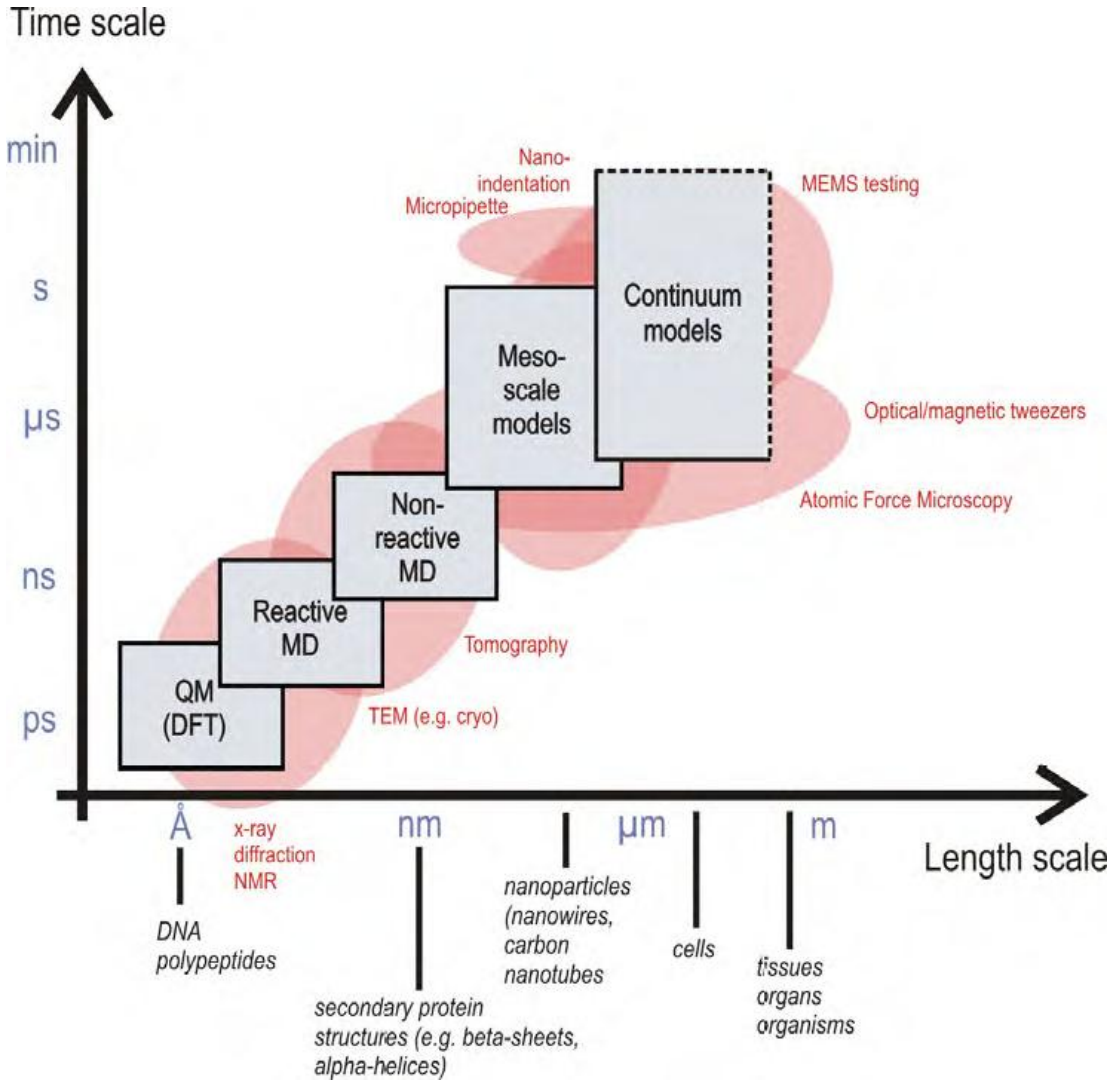

Figure 1-5: Different molecular hierarchies and computational tools used for multiscale analysis. From the Angstrom level up to the macroscale levels, the experimental and computational tools used at different scales are graphically represented (Figure reprinted from Ref. [12]).

The nanostructure of biological materials is crucial to understand the source of their mechanical properties such as fracture strength, failure mechanisms and elasticity, as discussed in Ref. [19, 20].

In protein materials, the molecular structure is directly linked to the chemistry of the molecules, in particular the primary structure consisting of individual amino acids [12, 21]. The source of silk's unique properties has been attributed to the specific secondary structures of proteins found in the repeating units of spider silk proteins [22].

Experimental and computational investigations of the structure of silks at the nanoscale revealed that there exist two fundamental structural constituents in silks, highly organized anti-parallel beta-sheet nanocrystals and a semi-amorphous phase that consists of less orderly protein structures [23-25]. Two distinct proteins are typically found in dragline silks with similar sequence across species [26]. One of the most studied silk from spiders, *N. Clavipes* dragline silk, contains MaSp1 and MaSp2 proteins, with significantly different chemical makeup [22, 27-29]. MaSp1 contains glycine (Gly) rich Gly-Gly-X (GGX) repeats with poly-alanine (poly-Ala) domains. Conversely, MaSp2 contains poly-Ala domains but it also contains a large number of proline residues in the glycine-rich regions.

Recent investigations revealed that anti-parallel beta-sheet crystals at the nanoscale [4, 30-32], consisting of highly conserved poly-(Gly[G]-Ala[A]) and poly-Ala repeats [22], play a key role in defining the mechanical properties of silk by providing stiff orderly cross-linking domains, in the form of beta-sheet nanocrystals embedded in a semi-amorphous matrix that consists predominantly of less orderly beta-structures, 3_1 helices and beta-turns [23, 24, 33, 34].

Figure 1-6 is a graphical representation of a group of silk unit cells, where the combination of poly(Ala) crystalline regions and semi-amorphous domains gives us an idea of the complexity of the overall entanglement of silk protein structures.

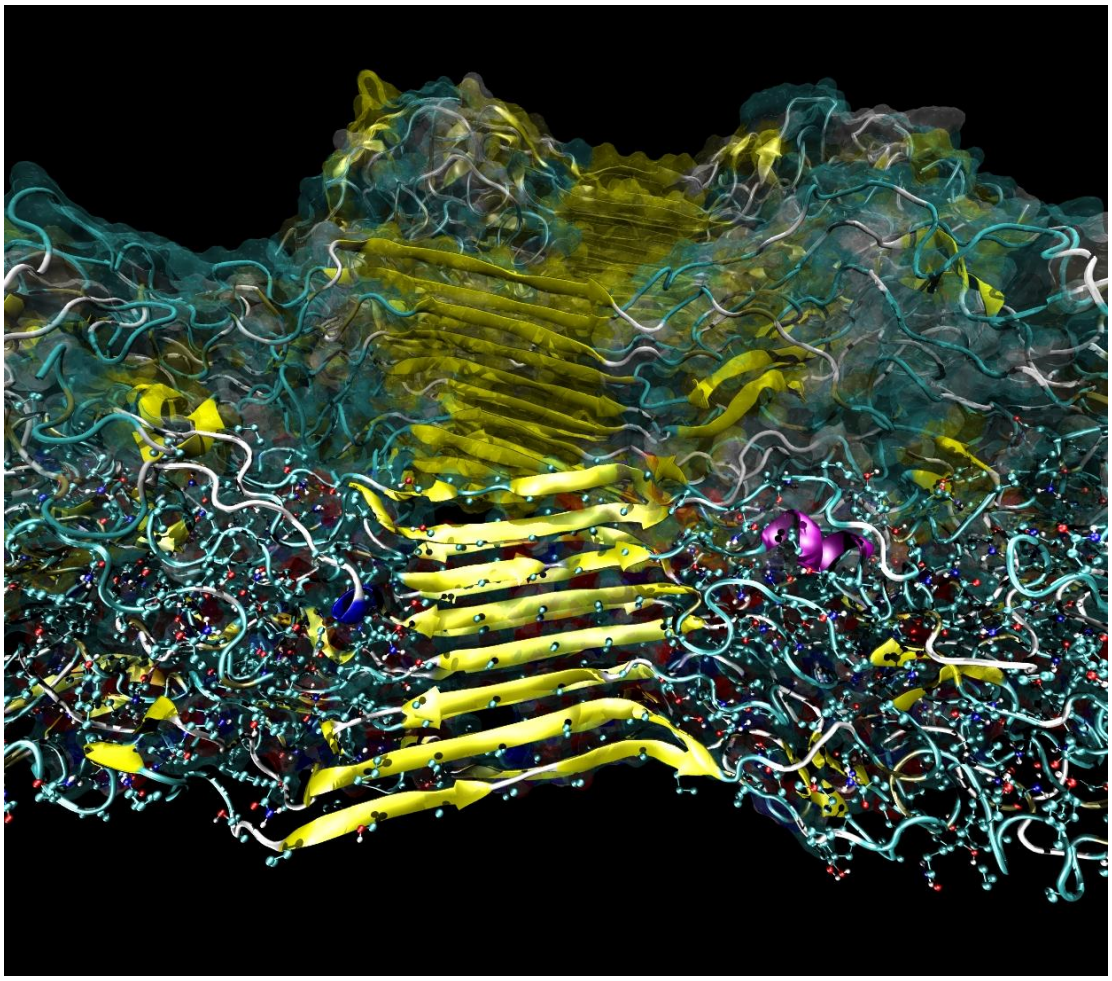

Figure 1-6: Graphical representation of spider silk unit cells. Silk constitutive unit cells are represented in a three-dimensional space. In the middle, the beta-sheet secondary structure of the poly(Ala) crystalline regions [courtesy Steven Cranford].

The existence of 3_1 helices, beta-turns and beta-spiral conformations has been suggested for the less-ordered structures of silk [23, 24, 33, 35], and has recently been directly identified by means of an atomistic-level structural model [36]. The use of atomistic simulations techniques turned out to be a necessary tool due to the fact that despite significant advances in experimental techniques, approaches such as solid

state NMR and x-ray diffraction can only provide limited insight into the atomic resolution structure for complex materials such as spider silk.

What is especially missing in the field of spider silk mechanics is a thorough understanding of the link between the atomistic and the macroscale-level mechanical description. A mesoscale model is the necessary tool to bridge this gap and correlate spider silk's properties at different scales.

1.3 State of the art

1.3.1 Silk as a biomaterial

Since its early development in China thousands of years ago, the use of silk throughout history has not been limited only to luxury fabric, and its usage in the form of medical sutures has been documented for centuries. What has been exploited are the remarkable mechanical properties of silk fibers produced both by silkworms and spiders.

More recent applications include not only parachutes but also a whole range of products where silk has been used to form a variety of biomaterials, such as gels, sponges and films for medical applications [5, 37, 38]. Figure 1-7 shows a microscope image of porous gradient silk sponges.

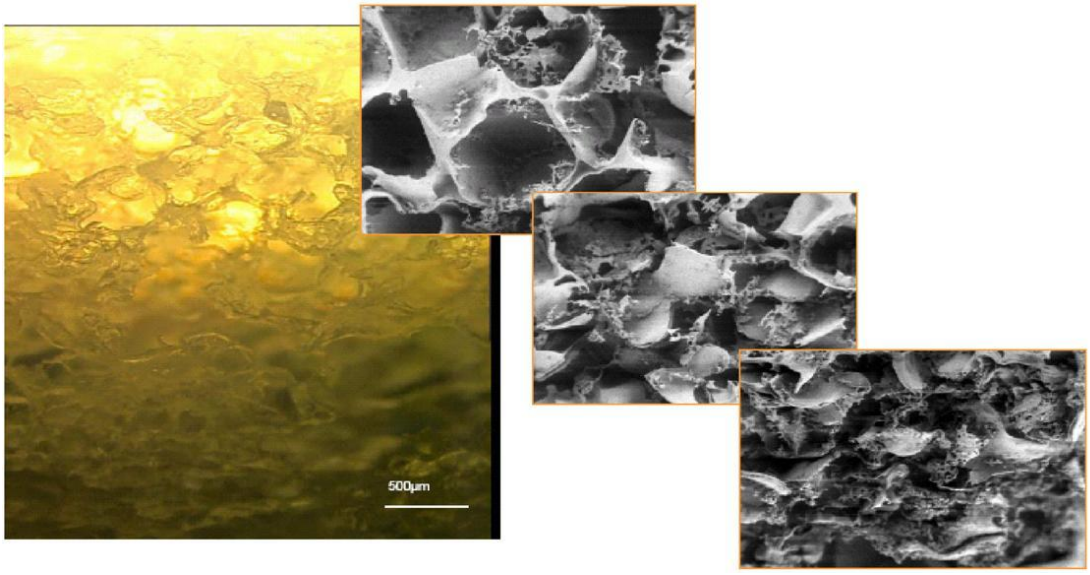

Figure 1-7: Silk sponges with different porosity. Porous gradient sponges are prepared by stacking a water-soluble porogen from smallest to largest: when the porogen is dissolved in water it leaves the sponge with a porous gradient. [Figure reprinted from Ref. [37]].

Through amino acid side-chain chemical modifications, silk's surface properties can be modified with the aim to immobilize cellular growth factors. Molecular engineering of silk sequences has been used to modify silks with specific features, such as cell recognition and mineralization [37].

Key point in the use of silk as biomaterial is that the degradability of silk biomaterials can be controlled by the mode of processing when obtained from spiders and is related to the content of beta-sheet nanocrystals. Multiple primary cells and cell lines have been successfully grown on different silk biomaterials to demonstrate a range of different biological outcomes [37, 38].

The advantage that silk biomaterials are highly biocompatible when studied *in vitro* and *in vivo* has been successfully employed in wound healing and in tissue engineering of bone, cartilage, tendon and ligament tissues [37].

1.3.2 Atomistic mechanical characterization of silk

1.3.2.1 Size dependence of spider silk strength and toughness

It is of major importance for the present study to investigate silk's structure and mechanics at its atomic and molecular scale, and in detail to analyze the contribution of each constitutive element in reaching silk's outstanding mechanical performances.

What makes silk one of the toughest materials known is the combination of exceptional mechanical properties, such as high tensile strength and great extensibility. The exceptional strength of silks, exceeding that of steel in terms of strength over density, arises from beta-sheet nanocrystals that consist of highly conserved poly-(Gly-Ala) and poly-Ala domains [4].

Recent findings from a series of large-scale molecular dynamics simulations [4] revealed that, when beta-sheet nanocrystals are confined to a few nanometers, they can achieve higher stiffness, strength and mechanical toughness than larger nanocrystals. Figure 1-8 shows the simulation setup of this recent work on the role of beta-sheet nanocrystals in spider silk [4]. These findings were used as input for the development of the mesoscale spider silk model described in this thesis work.

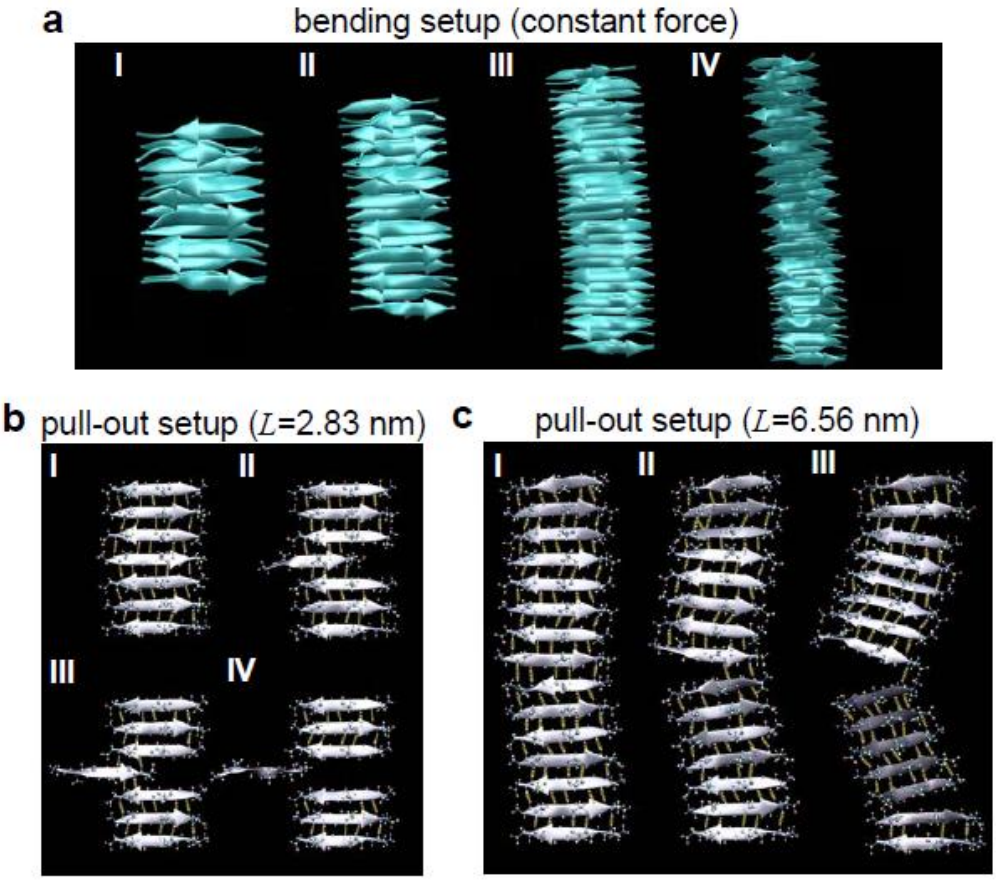

Figure 1-8: Bending and pull-out setup for silk beta-sheet nanocrystals of different size. a depicts a graphical representation of the geometry of crystals of different size in a bending setup, showing the deformation of the nanocrystal under applied force. b and c show snapshots of the geometry of crystals of different size when undergoing a pull-out simulation test [Figure reprinted from Ref. [4]].

What has been done thus far to explain silk's mechanical behavior at the atomic scale is to understand what are the defining characteristics of beta-sheet nanocrystals and to obtain mechanical parameters for their constitutive behavior [4]. Goal was to explore how size-effects can be exploited to create bioinspired materials with superior mechanical properties, in spite of relying on mechanically inferior, weak H-bonds.

Figure 1-9 summarizes the finding of this atomistic-level work [4] and the parameters represented here have been used as inputs for the current mesoscale model.

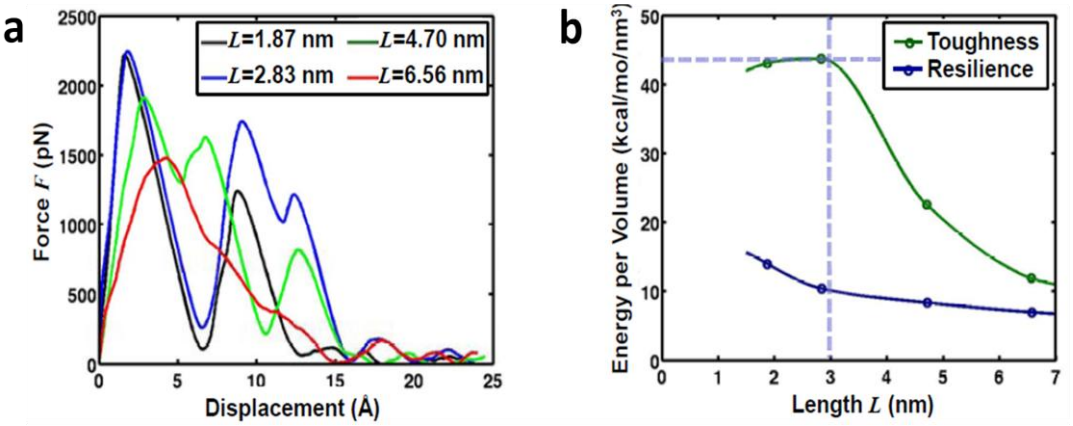

Figure 1-9: Mechanical behavior of spider silk nanocrystals undergoing pull-out simulations. a. Force-displacement behavior of a single silk beta-sheet-nanocrystal strand under the pull-out conditions represented in Figure 1-8. Different crystal sizes have been investigated, showing a drastic change in the mechanical response. b. Toughness and resilience values plotted as a function of crystal size. We notice how smaller beta-sheet nanocrystals can reach greater values of toughness and how an increase in crystal dimensions leads to a swift drop in toughness values. [Figure reprinted from Ref. [4]].

1.3.2.2 Physical reason for the relevance of hydrogen bonding in spider silk

When silk fibers are exposed to stretch, beta-sheet nanocrystals reinforce the partially extended and oriented macromolecular chains by forming interlocking regions that transfer the load between chains, similar to their function in other mechanical proteins [12, 24, 39-44]. Thereby, beta-sheet nanocrystals provide cohesion between the long polypeptide strands, enabling the amorphous domains to stretch significantly.

Fracture of beta-sheet nanocrystals occurs at large deformation and large loads [22]. Recent experiments demonstrated that when the size of beta-sheet nanocrystals is reduced by moderating the reeling speed or by metal infiltration, silk displays enhanced toughness and greater ultimate strength [6, 45, 46]. This is particularly intriguing, since H-bonds comprise the chemical bonds that underlie the beta-sheet nanocrystals structures, and are enlisted among weak chemical interactions [4].

It has recently been discovered that through crystal nanoconfinement, through a combination of uniform shear deformation and the emergence of dissipative molecular stick-slip deformation it is possible to significantly enhance silk's mechanical properties, by making the most efficient use of H-bonds and increasing the maximum values of strength and toughness [4].

What is still missing is a model able to unify all the gained knowledge and bring the understanding of the role of H bonding, beta sheet nanocrystals and semi-amorphous regions at an upper dimensional level.

1.4 Objectives of the work

Termonia's pioneering empirical two-phase model, based on experimental data, has been instrumental in explaining the importance of the ratio and size of beta-sheet nanocrystals embedded in semi-amorphous domains, at a time when large-scale atomistic simulations of spider silk constituents were impossible due to the lack of suitable force fields and computational resources [45].

Despite recent progress in experimental, theoretical and computational studies, thus far no model exists that enables a rigorous understanding of the role of the two fundamental constituents of silks at the intermediate "composite" level (*i.e.*, the silk fibril nanostructure as shown in Figure 1-2).

This progress has partly been hindered due to a lack of appropriate atomistic models of silks, and a lack of a thorough understanding of the mechanical behavior of silk's constituents at the nanoscale. Both issues have recently been addressed through protein structure identification methods and large-scale molecular simulation studies, where the molecular structure and mechanical signature of the two key constituents of silks has been identified [4, 10, 47].

As a result, conditions make now possible to understand the fundamentals of the origin of silk's unique material properties directly from an atomistic level without the need to introduce experimental parameters, an issue that will be addressed in this thesis work.

A specific goal of this work is to create the link between the understanding of silk mechanical behavior at the nanoscale and its macroscopic mechanical features. This is made possible by the development of two mesoscale models, first describing the silk unit cell mechanical behavior in a one-dimensional system and then developing a two-dimensional network for the description of the entangled network of proteins.

By utilizing a computational materials science approach, goal of this project is to understand the mechanical properties of spider silk from a fundamental level at the scale of tens, and potentially hundreds of nanometers. A multi-scale simulation approach is applied, explicitly considering the architecture of spider silk from the atomistic level up to the overall structure, supporting the structure-process-property paradigm of materials science.

Key material and structural parameters from atomistic calculations on dragline silk constituents are used to develop a mesoscale model and gain a fundamental understanding of the secrets of silk's exceptional performance, by linking the molecular structure and mechanisms to its larger-scale mechanical behavior.

In addition to understanding the structure and function of spider silk, the long-term goal of this work is to help develop a new engineering paradigm that encompasses the design of structures and materials, starting from the molecular level and creating new materials that mimic and exceed the properties of biological analogs.

The underlying belief is the fact that nature gives us an exceptionally rich source of inspiration for the design of new materials. Once the secrets of spider silk's makeup are unravel, science and technology can further enhance specific mechanical properties by applying the same building principles to different atomic and molecular species.

Chapter 2

One-dimensional mesoscale model of spider silk

Despite decades of research in silk's mechanical properties and its possible industrial applications, the mass-production of silk and other biomimetic materials remains a challenge, particularly due to silk's unique features that can only be achieved by the controlled self-assembly of the macromolecular constructs with molecular precision at the nanoscale.

A lack of full understanding of silk's complex hierarchical organization has created a gap of knowledge between what is known about silk's molecular organization at the atomistic level and silk's mechanical properties at the macroscopic scale.

The work described in this chapter aims to create a bridge between current knowledge of silk's molecular structure and silk's macroscopic mechanical behavior by mean of a mesoscale coarse-grained model. By using a bottom-up molecular-based approach, the first spider silk mesoscale model is described, bridging the scales from Angstroms to tens of nanometers, and thereby enabling the development of large-scale computational models of silk mechanics. It is here demonstrated that the specific nanoscale combination of a crystalline phase and a semi-amorphous matrix is crucial to achieve the unique properties of silks. Specific deformation mechanisms are analyzed and explained, and the results are found to agree well with experimental findings.

2.1 Materials and Methods

To provide a fundamental description of spider silk mechanics from a bottom-up perspective, and to elucidate the design strategy behind the making of silks, this chapter focuses on the description of the mechanical behavior of a simple one-dimensional coarse-grained model, whose parameters are directly informed from atomistic simulation results. The unit cell of silk is composed by a two-phase nanostructure, reflecting the geometry of silk as shown in Figure 2-1a. A schematic of the model setup is depicted in Figure 2-1b, showing how a simple combination of beta-sheet nanocrystals as well as semi-amorphous regions is modeled by beads connected via nonlinear springs in serial arrangement.

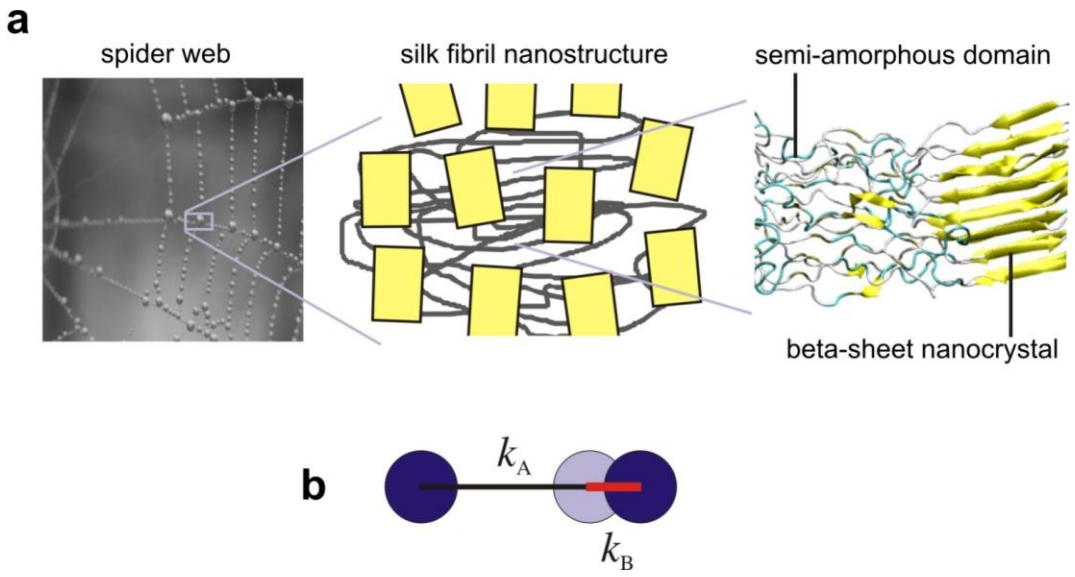

Figure 2-1: Hierarchical structure of spider silk and model formulation. **a,** Hierarchical structure of spider silk. The nanostructure of silk fibrils consists of two major constituents, a semi-amorphous region and beta-sheet nanocrystals. The focus of this study is the representation of the structure of spider silk through a mesoscale level model, where beta-sheet nanocrystals embedded in a soft matrix are described based on a coarse-grained approach. **b,** Representation of a spider silk mesoscale structure based on the coarse-grained model. The model is defined by a combination of a crystalline and a semi-amorphous region and mimics silk's nanostructure as shown in panel a. The mechanical characteristic of each constituting phase is informed from atomistic level molecular dynamics simulations.

A multiscale computational bottom-up investigation of spider silk, the approach employed in this work, is a powerful tool to understand its mechanical properties from a fundamental perspective. At length-scales on the order of tens of nanometers, spider silk appears as an entanglement of polypeptide chains, with two distinct domains that consist of (A) a semi-amorphous region [25, 48] and (B) a highly-ordered crystalline domain consisting of beta-sheet nanocrystals [45]. The silk constitutive unit is modeled as a combination of these two domains, namely a

crystalline beta-sheet region and a semi-amorphous domain, as shown in Figure 2-1b. The structure and mechanical behavior of these domains have been previously explored by atomistic simulations [10, 47] (see Figure 2-2) , making it possible now to feed a complete set of constitutive parameters directly from lower molecular scales.

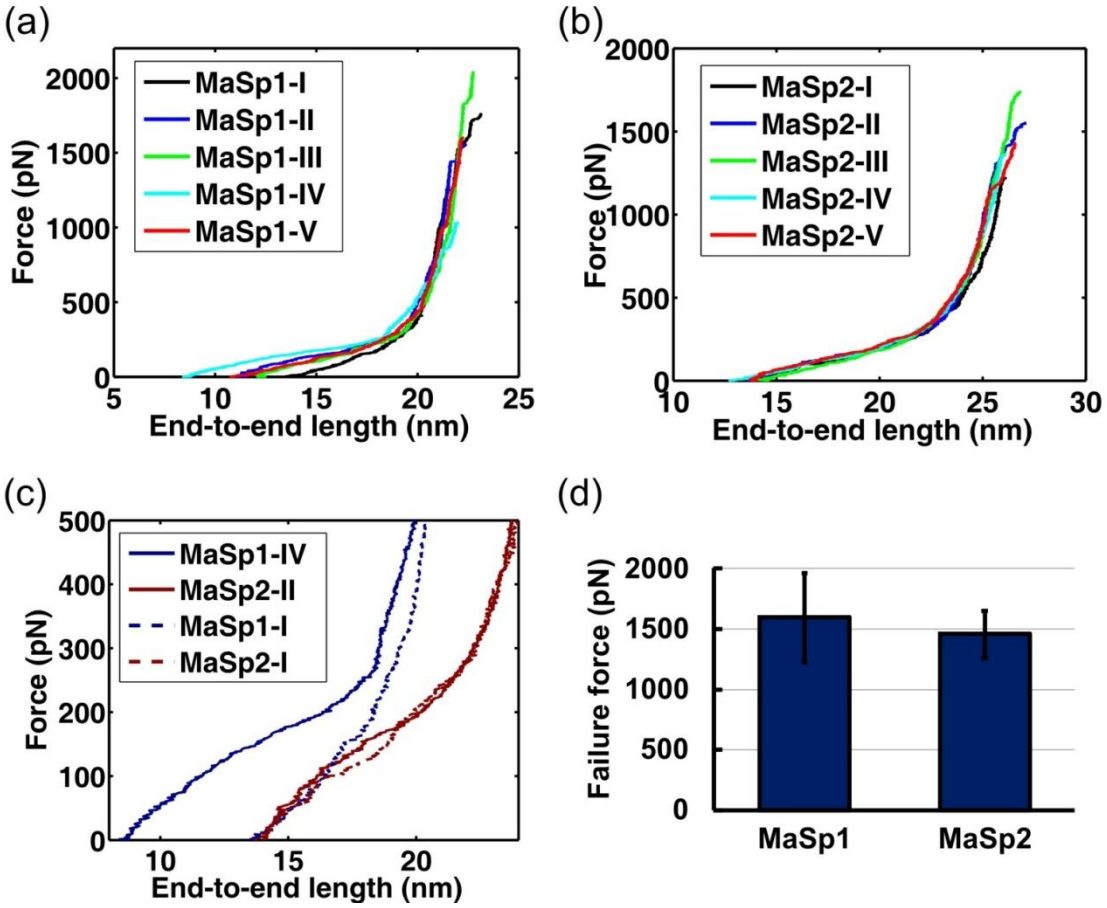

Figure 2-2: Force-displacement curves of the silk unit cell, for protein MaSp1 (**a**) and MaSp2 (**b**). The force represents the response of the structure to shear load, and its values are normalized per polypeptide strand. The behavior is characterized by an initial stiff regime (magnified in (**c**)), followed by a plateau and a final covalent regime that precedes structural failure. (**d**) shows the failure force values for MaSp1 and MaSp2, together with their variation around the average value. [Figure reprinted from Ref. [47]]

A model made up of a series of springs is a simple, yet powerful way to link nanostructural features and their associated mechanical signatures to the aggregate mechanical behavior at the silk-fibril scale. The serial spring assumption is reasonable at the nanoscale since in the sequence of spider silk the crystalline domains are followed by the glycine-rich repeats that form the semi-amorphous regions, resulting in a serial constitutive unit that is the fundamental building block of more complex hierarchies at larger scales [49].

2.1.1 Model formulation and parameter identification

Full-atomistic simulations of the mechanical properties of the semi-amorphous regions of spider silk have been performed in earlier studies [10, 47]. A representative volume element containing 15 polypeptide chains is used to derive the constitutive behavior (see Figure 2-3).

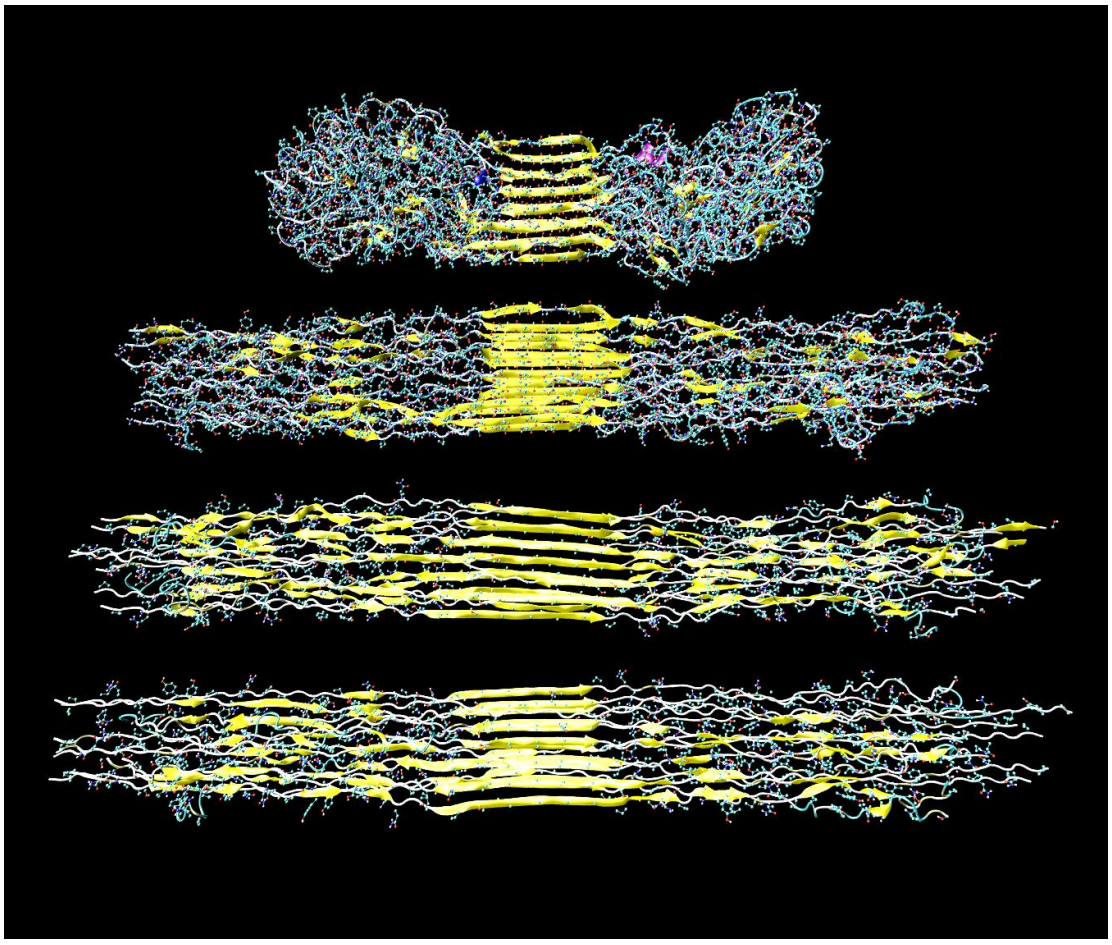

Figure 2-3: Representation of the molecular structure of the spider silk unit cell under increasing levels of deformation. Silk's unit cell is represented by a beta-sheet nanocrystal surrounded by semi-amorphous regions rich in beta-turns and 3_1-helices. Increasing levels of deformation are applied to the structure with the aim to determine its mechanical response until failure. [Figure reprinted from Ref. [47]].

This approach of considering more than one chain in the atomistic mechanical characterization allows to obtain a distribution of mechanical responses, and compute their averaged value. When compared to a single-chain mechanical characterization, this approach also accounts for the various interactions between chains within the

semi-amorphous domain. This is critical for example to accurately describe the constitutive properties of 3_1-helices that involve multiple polypeptide chains.

The effective force-extension behavior derived from the large molecular assembly is then normalized by the force, area and length per single polypeptide chain, to develop an appropriate constitutive law. The results from these analyses are used directly to determine the parameters of the present coarse-grained model representing a single amorphous domain and a single beta-sheet nanocrystal.

We approximate the force-displacement behavior of the two constituting phases of silk under tensile loading with a multi-linear model. Numerical values of all parameters developed here are given in Tables 1 and 2, and details on the mathematical formulation and parameter identification are given below.

Table 1: Model parameters for the semi-amorphous region in the mesoscale model.

Model parameter	**Value**
$k_{A,1}$ (pN/Å) – Initial regime	9.9
$k_{A,2}$ (pN/Å) – Intermediate regime	3.96
$k_{A,3}$ (pN/Å) – Final regime	103.84
$\Delta L_{A,1}$ (Å) – First transition point	12.0
$\Delta L_{A,2}$ (Å) – Second transition point	43.8
$L_{A,0}$,(Å) – Initial length	90.0

Table 2: Model parameters for the beta-sheet nanocrystal in the mesoscale model.

Model parameter	**Beta-sheet nanocrystal size**		
	3 nm crystal	**6.5 nm crystal**	**10 nm crystal**
$k_{B,1}$ (pN/Å) – Beta-sheet nanocrystal initial stiffness	576	205.5	67.53
$k_{B,2}$ (pN/Å) – Second-regime stiffness	5.76	N/A	N/A
$\Delta L_{B,1}$(Å) – Softening point	2.36	N/A	N/A
$\Delta L_{B,2}$ (Å) – Breaking point	5.8	4.5	6.63
$F_{\max}$ (pN) – Maximum tensile strength	1,380	925	447
$L_{B,0}$ (Å) – Initial length	0		

2.1.1.1 Semi-amorphous region

Atomistic simulations revealed a characteristic three-stage deformation pattern, where an initial stiff regime is followed by a yielding point and a long plateau, and eventual significant stiffening as the polypeptide's backbone is being stretched [10, 47]. This behavior is associated to the presence and the breaking of secondary structures such as 3_1-helices and beta-turns, which are rich in intra-chain and inter-chain hydrogen bonding [23, 45]. At larger strains, the structure enters a final high-stiffness regime, characterized by the stretching of covalent bonds along the protein backbone.

Values for the stiffness of the three different regimes of the semi-amorphous domain are extracted from atomistic simulation data [10, 47]. By fitting the atomistic simulation results with a tri-linear function, it's possible to obtain the tangent stiffnesses as a function of the displacement, where $\Delta L_A = L_A - L_{A,0}$ describes the

deformation of the semi-amorphous region (relative to the initial length). The stiffness as a function of deformation is then given by:

$$k_A(\Delta L_A) = \begin{cases} k_{A,1} & \Delta L_A < \Delta L_{A,1} \\ k_{A,2} & \Delta L_{A,1} \le \Delta L_A \le \Delta L_{A,2} \\ k_{A,3} & \Delta L_A > \Delta L_{A,2} \end{cases} \quad (1)$$

where the values for $k_{A,i}$ as well as the transition deformations $\Delta L_{A,1}$ and $\Delta L_{A,2}$ are summarized in Table 1. The force versus deformation of the amorphous domain is given by the following law:

$$F_A(\Delta L_A) = \begin{cases} k_{A,1}\Delta L_A & \Delta L_A < \Delta L_{A,1} \\ k_{A,1}\Delta L_{A,1} + k_{A,2}(\Delta L_A - \Delta L_{A,1}) & \Delta L_{A,1} \le \Delta L_A \le \Delta L_{A,2} \\ k_{A,1}\Delta L_{A,1} + k_{A,2}(\Delta L_{A,2} - \Delta L_{A,1}) + k_{A,3}(\Delta L_A - \Delta L_{A,2}) & \Delta L_A > \Delta L_{A,2} \end{cases} \quad (2)$$

The resulting force-deformation curve of the semi-amorphous region is shown in Figure 2-4.

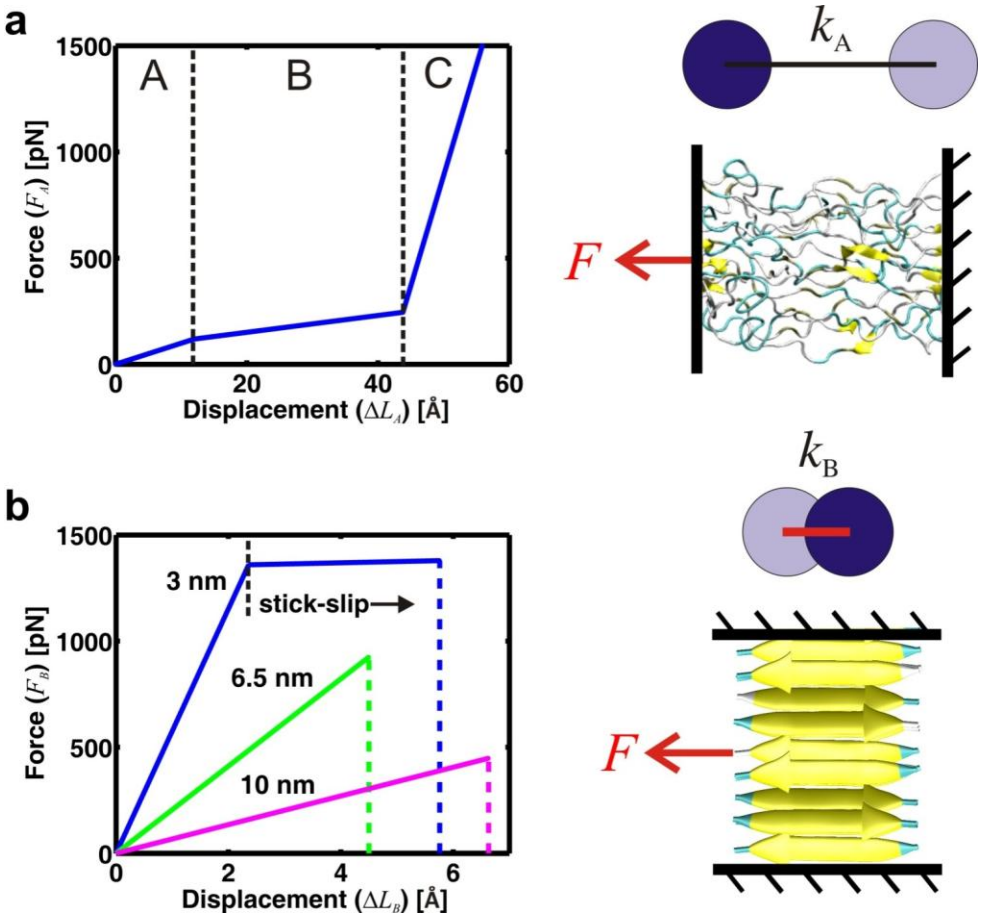

Figure 2-4: Constitutive behavior of the two elements represented in the coarse-grained model of silk (obtained from full atomistic molecular dynamics simulation results as reported in [4, 10, 47]). **a,** Mechanical behavior of the glycine rich semi-amorphous domain as reported in [47], consisting of three regimes (A: homogeneous stretching of the protein structure, B: onset of yielding and unraveling of the semi-amorphous domains via the breaking of H-bonds, C: stretching of protein backbone). **b,** Mechanical behavior of beta-sheet nanocrystals under lateral loading. The smallest beta-sheet nanocrystal size (3 nm) shows the characteristic stick-slip phenomenon due to repeated breaking and reformation of H-bonds (modeled here as an elastic-plastic yielding behavior), a phenomenon that is lost in larger beta-sheet nanocrystals. Larger beta-sheet nanocrystals (>3 nm) show a more brittle and at the same time weaker and softer mechanical behavior as shown in [4]), reflected in the constitutive behavior shown in panel **b**.

2.1.1.2 Beta-sheet nanocrystals

The beta-sheet nanocrystal is modeled as a nonlinear spring, where the force-displacement characteristic is informed from atomistic simulation results [4, 10, 47, 50, 51]. The beta-sheet nanocrystal is modeled as two beads superimposed on one another, and the bond between these beads characterizes the mechanical response of the crystal.

From atomistic simulations [4] it was found that the properties of the beta-sheet nanocrystals vary as a function of crystal size, where small crystals are stiffer, dissipate more energy through a stick-slip mechanism and fail at higher force values. The effect of the variation in size of beta-sheet nanocrystals on silk's mechanical behavior is considered by scaling the stiffness, strength and energy dissipation capacity of the beta-sheet nanocrystals according to size-effects observed in atomistic simulations. To account for these effects, beta-sheet nanocrystals of different size feature distinct mechanical properties [35, 52, 53] in this model.

The beta-sheet crystal stiffness is modeled as a function of the crystal deformation computed as $\Delta L_B = L_B - L_{B,0}$. The expression for the stiffness k_B as a function of deformation ΔL_B is then given by

$$k_B(\Delta L_B) = \begin{cases} k_{B,1} & \Delta L_B < \Delta L_{B,1} \\ k_{B,2} & \Delta L_B \geq \Delta L_{B,1} \end{cases} \tag{3}$$

where $\Delta L_{B,1}$ is the beta-sheet nanocrystal transition point as defined in Table 2 and shown in Figure 2-4b.

The force as a function of deformation is given by the following expression

$$F_B(\Delta L_B) = H(\Delta L_B)\begin{cases} k_{B,1}\Delta L_B & \text{if } \Delta L_B < \Delta L_{B,1} \\ k_{B,1}\Delta L_{B,1} + k_{B,2}(\Delta L_B - \Delta L_{B,1}) & \text{if } \Delta L_B \geq \Delta L_{B,1} \end{cases}, \tag{4}$$

where the Heaviside function H is defined as $H(\Delta L_B) = 1$ for $\Delta L_B < L_{B,2}$ and $H(\Delta L_B) = 0$ for $\Delta L_B \geq L_{B,2}$.

The failure point, $\Delta L_{B,2}$ depends on the crystal size as summarized in Table 2. The transition point $\Delta L_{B,1}$representing the onset of stick-slip motion only exists in the smallest 3 nm beta-sheet nanocrystal case. For the larger beta-sheet nanocrystals (6.5 nm and 10 nm cases), the force on the linear spring is simply given as

$$F_B(\Delta L_B) = H(\Delta L_B) \cdot k_{B,1} \Delta L_B . \quad (5)$$

The spring constants are calculated by dividing the maximum tensile strength by the softening deformation for the 3 nm case, and by the breaking point for the larger-crystal cases. The second, softer regime for the small-crystal case is assumed to feature a constant stiffness equal to 1% of the initial one, approximating the stick-slip behavior observed in atomistic simulations through an elastic-plastic model [4].

The calculation of the breaking point is done by maintaining the dissipated-energy proportion between beta-sheet nanocrystals of different size. Explicit atomistic simulations suggest that a 3 nm crystal is approximately three times tougher than a 6.5 nm-crystal, and in the context of the bilinear spring model [4] this results in a breaking point value of 5.8 Å. It has to be noted that atomistic calculations on strength and effective stiffness of beta-sheet nanocrystals are based on the pull-out force required to separate a single strand from the crystal, to be consistent with the normalization for a single polypeptide strand.

The maximum tensile strength of beta-sheet nanocrystals of different size [4] is derived directly from atomistic simulation for the 3 nm and 6.5 nm beta-sheet nanocrystals [4], while it is linearly extrapolated for the 10 nm case. To be consistent with the force values of the semi-amorphous domain, the maximum strength is directly calculated from simulations in implicit solvent for a 3 nm-crystal system; and

the large beta-sheet nanocrystal strengths are then determined using the strength ratio from explicit simulations.

The softening point for the 3 nm beta-sheet nanocrystal is extracted from explicit simulation results, as well as the breaking point for the 6.5 nm beta-sheet nanocrystal. In the 10 nm case, the breaking point is linearly extrapolated, keeping the same ratio of increase in breaking deformation as in the other two cases 6.5 nm and 10 nm). Both extrapolations for the 10 nm beta-sheet nanocrystal are performed in order to study a limiting case in the analysis of the effects of crystal size.

2.1.2 Parameter sensitivity

Since all constitutive elements feature a multi-linear elastic behavior, it is possible to predict a linear behavior in the response of the system to a parameter variation, either resulting from a different mechanical signature or from an error in the parameter estimate. Of particular interest is the dependence of the overall strength on the strength of the beta-sheet nanocrystal. Given the fact that the large-deformation behavior (including the fracture behavior) is controlled solely by the beta-sheet nanocrystal phase, a percentage variation in the maximum tensile strength of the beta-sheet nanocrystal correlates directly with the maximum tensile strength of the overall structure.

2.1.3 Model setup and computing techniques

The MATLAB script provided in the *Appendix A1* is used for calculating the stress-strain behavior of the one-dimensional serial spring model discussed in this chapter. The effective stiffness of the system under tensile stretch is given by a serial arrangement of two springs and corresponds to

$$k_{\mathrm{T}}(\Delta L_A, \Delta L_B) = \frac{k_A(\Delta L_A) k_B(\Delta L_B)}{k_A(\Delta L_A) + k_B(\Delta L_B)} \tag{6}$$

Force-displacement calculations are carried out by applying displacement increments to the system, and computing the relative deformations of the serial springs as a function of their instantaneous stiffness.

2.1.3.1 Calculation of stress and toughness

The displacement of each element can be computed based on eq. (6) such that total deformation equals $\Delta L_T = \Delta L_A + \Delta L_B$ at any point, and forces can be evaluated from equations (2) and (4), (5). Stress values are derived from force calculations by considering a A = 10 Å x 10 Å square cross-sectional area (this estimate for the effective area of a single polypeptide chain is based on a geometric analysis of the spider dragline silk nanostructures obtained in earlier atomistic simulation studies [10, 47]) along the whole system length such that $\sigma = F / A$, where σ is the computed stress, F is force per chain and A denotes the cross-sectional area associated with a single polypeptide chain.

Mechanical toughness is calculated measuring the area under the force-extension curve (until structural failure) by means of a trapezoidal numerical integration.

2.2 Results and Experimental Validation

In the spider silk mesoscale model illustrated in this chapter, each constituent has a mechanical signature informed from full atomistic simulation [4, 10, 47] as illustrated in Figure 2-4. This model, albeit extremely simple, is capable of describing the key features of the nanomechanics of spider silk, without the introduction of any experimental parameters.

The model is applied to simulate the mechanical deformation of silk according to a tensile loading condition shown in Figure 2-5a. The analysis begins by considering a system with a beta-sheet nanocrystal size of 3 nm that reflects the size found in

natural silks. The resulting stress-strain curve shown in Figure 2-5b displays the characteristic shape observed in silks, that is, it displays an early yield point, leading to a significant softening followed by a severe stiffening effect.

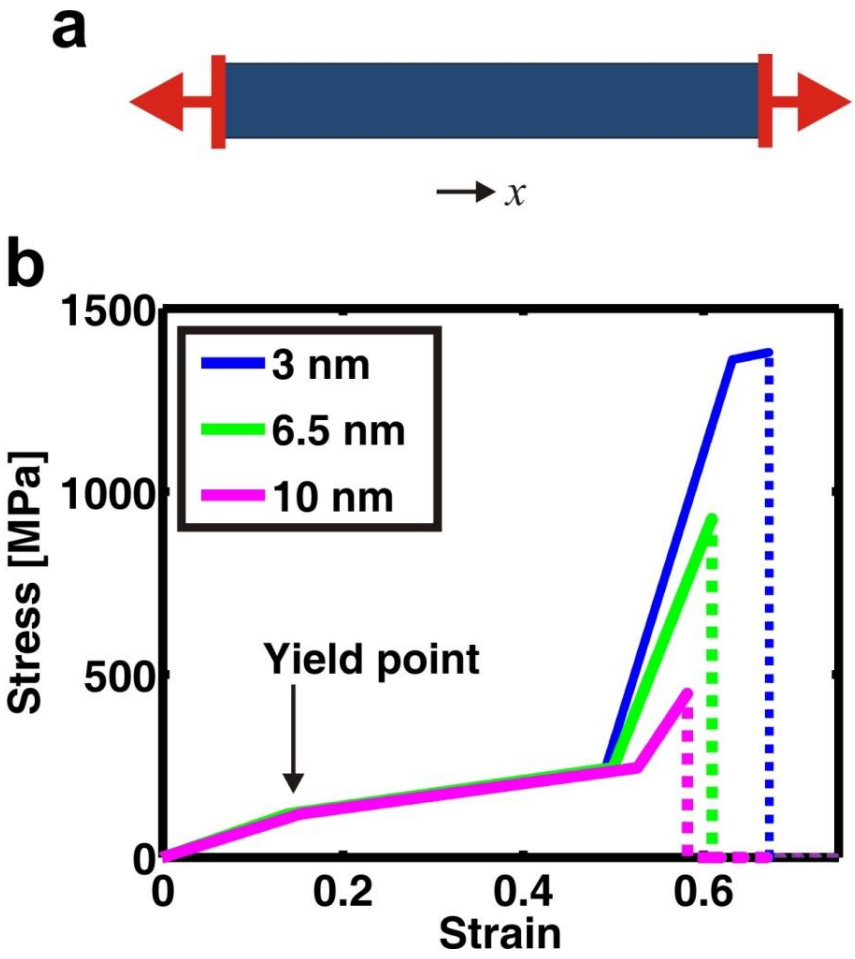

Figure 2-5: Stress-strain response of a silk fibril under tensile loading, for varying beta-sheet nanocrystal size. **a,** Schematic of model setup and loading geometry of tensile testing. **b,** Stress-strain response of spider silk based on different beta-sheet nanocrystal sizes, ranging from 3 to 10 nm. The behavior after rupture has occurred is displayed with dotted lines. The results reveal a remarkable dependence of the stress-strain response on the beta-sheet nanocrystal size. Overall, the stress-strain behavior observed here is in good agreement with experimental results.

A detailed analysis reveals that the initial regime is characterized by a relatively high tangent modulus (830 MPa) owing to the homogeneous stretching of semi-amorphous regions that are rich in hydrogen bonding in the form of 3_1-helices and beta-turns [8, 23, 45]. The onset of rupture of the hydrogen bonds in the semi-amorphous domains leads to yielding at strain values of around 13%, evident from a sudden drop in the tangent stiffness. The tangent modulus of this softer regime is much lower, around 310 MPa. During this plateau regime, protein chains in the semi-amorphous region gradually align along the pulling direction [6, 54], a mechanism that is mediated by the significant hidden length of polypeptide stored in this geometry.

At a strain value of around 50%, the stress-strain curve enters a high-stiffness regime (with a much higher tangent stiffness of around 8 GPa). At this point, the semi-amorphous region has been completely stretched out and the beta-sheet nanocrystals begin to sustain larger strains. An interesting event observed in the stress-strain plot is a small softening regime starting at around 63% strain, immediately prior to failure.

A detailed analysis of this phenomenon shows that this is due to the stick-slip failure mechanism of the beta-sheet nanocrystals, a mechanism first described in [4]. This final high-stress regime contributes significantly to the overall toughness as it accounts for approximately 20% of the total energy dissipated before failure. When the applied force reaches the maximum tensile strength at strain values of 67%, individual beta-strands are completely pulled out, and failure occurs at a stress of 1,379 MPa. This maximum stress level—on the order of GPa—is in quantitative agreement with results from experimental studies [6].

It’s now considered a systematic variation of the beta-sheet nanocrystal size of up to 10 nm, and its impact on the mechanical properties is studied to quantify the dependence of the crystal size on the overall mechanical behavior. The motivation for this analysis is to validate earlier hypotheses, showing that small changes in the crystal size translates to altogether different overall mechanical response in spider

silk [4, 6]. The results of the mechanical analysis are shown in Figure 2-5b, where we plot the stress-strain curves for varying beta-sheet nanocrystal sizes.

The most important finding is the observation that the size of beta-sheet nanocrystals—at otherwise completely identical conditions—severely affects the mechanical response. The analysis shown in Figure 2-5b clearly shows that larger-crystal systems (*i.e.* 6.5 nm and 10 nm beta-sheet nanocrystals) have a behavior that deviates significantly from the reference small-crystal case, especially at high levels of deformation. Silk fibrils with larger beta-sheet nanocrystals break at significantly lower stress values, and also show a shorter (61% and 58% strain, respectively) and much softer third regime, with a tangent modulus of 6 GPa and 3.6 GPa, respectively. The initial and intermediate regimes, however, are comparable to the case with the smallest beta-sheet nanocrystal, where the transition points and stiffness values do not vary substantially between the two systems.

These results demonstrate that even a slight increase in beta-sheet nanocrystal size leads to a significant loss of strength and toughness of the system (Figure 2-6). As shown in Figure 2-6a, with a value of 925 MPa, the 6.5 nm-crystal case shows a decrease of approximately 33% with respect to the reference system with the smallest beta-sheet nanocrystal. The drop is even larger for the 10 nm-crystal case, which fails at 447 MPa, at 67% less than the reference case with the smallest (3 nm) beta-sheet nanocrystal.

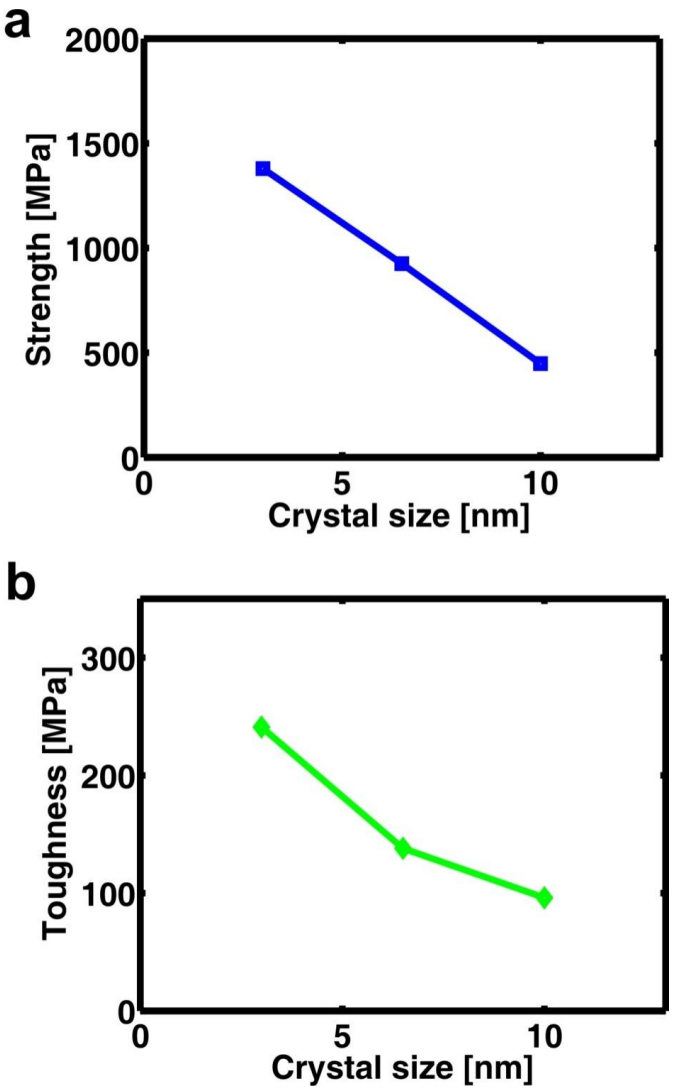

Figure 2-6: Variation of strength and toughness with beta-sheet nanocrystal size. **a**, Variation of strength with beta-sheet nanocrystal size. The plot illustrates that silk fibers employing larger beta-sheet nanocrystals have a diminished strength of 925 and 447 MPa for the 6.5 and 10 nm crystal cases, compared with the small-crystal (3 nm) system, which breaks at 1,379 MPa. **b**, Variation in the toughness (toughness modulus) of the silk constitutive unit as a function of beta-sheet nanocrystal size. Enhanced mechanical properties of small beta-sheet nanocrystals play a governing role in the overall behavior. An increase in the toughness (modulus) from 96 MPa to 138 MPa and 241 MPa is observed when beta-sheet nanocrystal size is reduced from 10 nm to 6.5 nm and 3 nm.

The drop of the maximum stress further lead to considerably lower toughness values than those found in the reference small-crystal case (Figure 2-6b). A decrease of 43% and 60% is measured for the 6.5 nm and the 10 nm case, in comparison to the toughness value for the reference small beta-sheet nanocrystal case (241 MPa).

Silk deformation mechanisms at different strain levels and for varying beta-sheet nanocrystal sizes are now studied. Figure 2-7 shows the relative contribution of the semi-amorphous domain and the beta-sheet nanocrystal to overall deformation for the three beta-sheet nanocrystal sizes considered here.

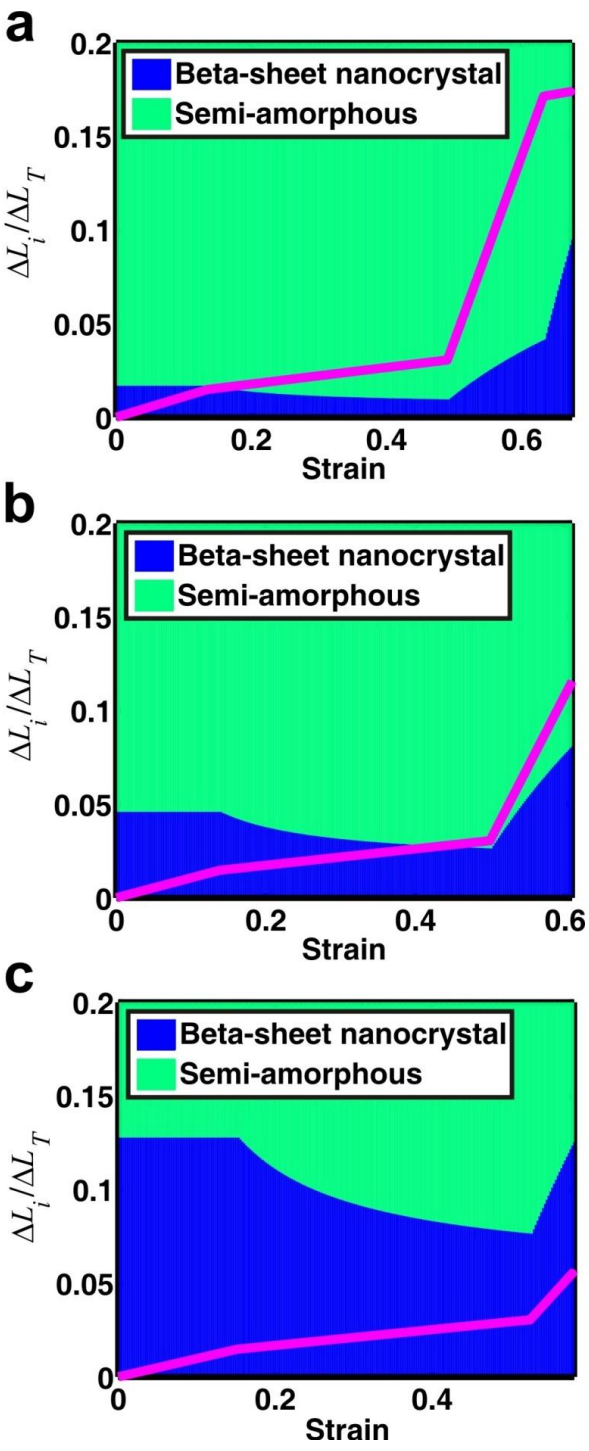

Figure 2-7: Deformation mechanisms of silk constitutive elements, as a function of beta-sheet nanocrystal size (3 nm in panel **a**, 6.5 nm case in panel **b**, and 10 nm in **c**). The plot shows the relative contribution of beta-sheet nanocrystal deformation and deformation of the semi-amorphous region as a function of strain. **a,** Since the beta-sheet nanocrystal is much stiffer than the semi-amorphous phase, its contribution to the total deformation is initially small. The softening of the semi-amorphous phase results in an even smaller contribution for the beta-sheet nanocrystal as deformation is increased. However, when the semi-amorphous region enters the stiff covalent regime, the beta-sheet nanocrystals deform more significantly. The final regime, with a drastic drop in beta-sheet nanocrystal properties due to stick-slip phenomena, determines a noticeable increase of beta-sheet nanocrystal deformation, finally leading to failure of the system. This panel illustrates that beta-sheet nanocrystals contribute to deformation primarily in the final stages of deformation. **b** and **c,** Since the larger beta-sheet nanocrystals are less stiff, their contribution to deformation is larger than in the small beta-sheet nanocrystal case (panel **a**). Note that the data shown is zoomed into 20% on the *y*-axis to focus on the range of contributions of the beta-sheet nanocrystals more clearly.

In the smallest crystal system (3 nm), deformation of the beta-sheet nanocrystals start to play a significant role once the semi-amorphous region begins to stiffen at around 50% strain, and clearly dominate deformation when the stick-slip mechanisms of beta-sheet nanocrystal deformation is triggered (Figure 2-7a). The dominance of beta-sheet nanocrystal deformation at large strains has been hypothesized in earlier experimental studies, but is here for the first time shown from a molecular perspective and with a direct link to underlying molecular mechanisms.

In the larger crystal cases of 6.5 nm and 10 nm, however, the beta-sheet nanocrystal contribution to deformation reaches much larger levels even for small deformation (Figure 2-7b-c). The reason for this is the much softer behavior of the beta-sheet nanocrystals (as illustrated in Figure 2-4b), which results in greater displacements in the nanocrystal region. This observation demonstrates the importance of the great stiffness of beta-sheet nanocrystals to enable the specific deformation mechanisms that are crucial to silk's mechanical properties.

Next comes a comparison of the maximum deformation of the semi-amorphous region at failure, for different beta-sheet nanocrystal sizes. As shown in Figure 2-8, semi-amorphous regions are less stretched in the systems with larger beta-sheet nanocrystals. The maximum strains reached in the semi-amorphous region is 61% in the 3 nm beta-sheet nanocrystal case, 56% in the 6.5 nm case, and around 51% in the 10 nm beta-sheet nanocrystal. This is an important observation, which suggests that the increase of the beta-sheet nanocrystal size prevents the material to take full advantage of the entire potential—the hidden length—of the semi-amorphous regions, which severely affects silk's extensibility and energy dissipation capacity [55, 56].

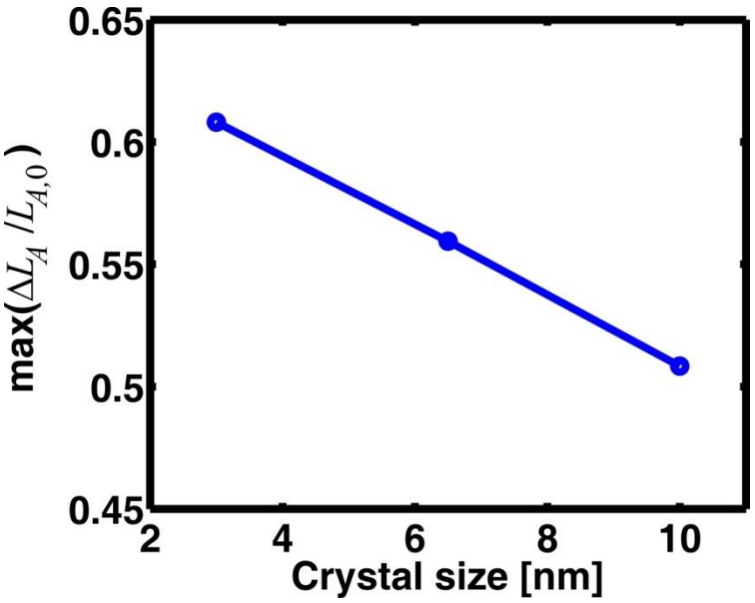

Figure 2-8: Deformation of semi-amorphous region in silk, as a function of beta-sheet nanocrystal size. The analysis reveals that larger beta-sheet nanocrystals prohibit the semi-amorphous region from fully extending, reducing the energy dissipation capacity of the material. In the 10 nm-case, the semi-amorphous region deforms only up to around 51% its initial length, while it can reach values of 56% and 61% in the 6.5 and 3 nm cases.

Overall, the results of our study are in excellent agreement with experimental data, where a similar variation of the beta-sheet nanocrystal size and its impact on larger-scale mechanical properties was reported recently [6], showing a drastic drop in toughness when beta-sheet nanocrystal size increases (in experiments [6], the change in the beta-sheet nanocrystal size was achieved via a change of the reeling speed. A drop of the strength from approximately 1,500 MPa to 300 MPa was observed as the beta-sheet nanocrystal size was increased, in reasonable agreement with the results shown in Figure 2-6a).

It has to be noticed that the strain values in the three systems investigated here are larger than those found in experimental studies (between 10% and 50% more). This phenomenon can be explained based on two points. First, in this one-dimensional

model we consider an ideal and rather simplified structure that completely lacks the statistical variability and structural defects. This fact generally leads to enhanced strength and extensibility in comparison to experimental results. Second, we underline that physiologically spun silks (*i.e.,* the small-crystal case) undergo a substantial pre-stretching at the orifice [6, 57]. However, the one-dimensional model described in this chapter does not include this effect and we consequently expect an overestimation of the stretching capacity of the material.

The more complex two-dimensional model described in Chapter 3 will directly include variability of silk structure, spacing and other parameter including the effect of pre-stretching, with the aim to allow for an even better comparison with experimental data.

2.3 Discussion

The most important finding of the study described in this chapter is that it has revealed the mechanistic interplay of the two constitutive phases in silks, semi-amorphous regions and highly organized beta-sheet nanocrystals, as well as the effect of structural changes on the overall mechanical behavior of silks.

It is found that semi-amorphous regions unravel first when silk is being stretched, leading to the large extensibility of silk. Conversely, the large-deformation mechanical properties and ultimate tensile strength of silk are controlled by the strength of beta-sheet nanocrystals, which is directly related to their size.

An important discovery is that small beta-sheet nanocrystals are crucial to reach outstanding levels of strength and toughness, as shown clearly in Figure 2-6. A key observation from the current study is that the unraveling of semi-amorphous regions is severely influenced by the size of the beta-sheet nanocrystals, and that only ultra-small crystals provide the basis for silks to take full advantage of extensibility and

energy dissipation capacity, and enable the material to reach very high levels of failure stresses (Figure 2-6 and Figure 2-8). Small-crystal systems guarantee the required cross-linking strength that is necessary for the semi-amorphous domains to fully extend and to enter a high-stiffness covalent regime when beta-sheet nanocrystals are being stretched and eventually fail.

The resulting capacity to sustain large tensile force as well as extension enhances the strength and energy dissipation ability of the material. Overall, the confinement of beta-sheet nanocrystals to the nanoscale is essential for the superior mechanical properties of silks, as this is crucial to reach high extensibility and high levels of stress.

These results further show that the severe change of the mechanical properties of spider silk under relatively small variations of the size of beta-sheet nanocrystals can be explained solely based on structural effects (Figure 2-4 and Figure 2-5). These findings also relate the characteristic yielding point in the stress-strain curve (see Figure 2-5b), observed universally for many types of silks, to the onset of failure of semi-amorphous regions when H-bonded 3_1-helices and beta-turns begin to rupture.

Chapter 3

Parametric study of a two-dimensional mesoscale model

The one-dimensional model described in Chapter 2 is a powerful tool to model silk's characteristic behavior and to describe key characteristic phenomena related to the silk unit cell. However, there are intrinsic limitations of a one-dimension model to describe geometric features found in silks at larger scales, such as a specific distribution of the nanostructure, density variations, and others.

The goal of this chapter is to shed light on the mechanical behavior of the silk threads at dimensions of hundred of nanometers, by directly including the distribution of beta-sheet nanocrystals and semi-amorphous domains in a two-dimensional network model. The importance of a computational study of silk's behavior at the mesoscale comes from the fact that despite significant advances in experimental techniques, approaches such as SEM or x-ray diffraction could thus far only provide limited insight into the atomic resolution structure of spider silk, given its great complexity and its semi-amorphous nature.

Another aim of this Chapter is to further gain insight in silk's nanostructure by means of computational simulations, thus obtaining an understanding of sub-micron scales not yet possible by experimental techniques. It is explored how basic unit cells further assemble at a higher dimensional hierarchy to form the overall silk thread. A bottom up approach is consistently employed, taking advantage of atomistic results and preliminary mesoscale evidence (as described in Chapter 2) in order to climb the dimensional hierarchy of silk.

3.1 Strengths and limitations of a two-dimensional model

A complete understanding of the mechanical signature of silk, at different dimensional scales, requires the development of models that are able to take into account key physical phenomena defining silk's mechanical behavior. Models have to explain relevant features at a defined scale, avoiding at the same time the introduction of unnecessary complexities that make the model heavy and non-efficient.

A two-dimensional model of spider silk structure has the possibility, compared to a 1D model, to describe key physical phenomena taking place at a scale of hundreds of nanometers such as crystal concentration and structural homogeneity. The 1D model described in the previous chapter has intrinsic limitations in describing geometric features found in silks at larger scales, such as the specific distribution of the nanostructure, density variations, presence of defects and others.

A possible future implementation of a three-dimensional model could further improve our capacity to model spider silk mechanical properties. Whereas the advantages of a three-dimensional model are still to be evaluated, the challenges of a more complex modeling of the silk structure are evident, for example the necessary assumptions on three-dimensional branching of crystalline structures, necessary to realistically represent the complex and entangled three-dimensional arrangement of the polypeptide chains.

A coarse-grain representation of a physical system intrinsically carries some assumptions and limitations with it, and consequently an increase in complexity of the model is always a trade-off between a possible gain in understanding and an excessive approximation of the physics of the system. Advantages and drawbacks of a more complex three-dimensional model will have to be carefully weighed,

considering that the present 2D model is by itself able to represent key physical phenomena occurring in the three-dimensional space, such as the effect of crystal size. The agreement of outcomes between 1D and 2D model also suggests that the current models are able by themselves to correctly represent the right physics of spider silk nanostructure and to predict the effect and the outcome of parameter variations.

Although the current two-dimensional model cannot justify all phenomena that characterize silk behavior, it can correctly model, reproduce and predict key phenomena and interesting features of spider silk up to the scale of hundreds of nanometers.

3.2 Materials and Methods

3.2.1 Geometry setup and silk network generation

An appropriate modeling of spider silk structure at the mesoscale of hundreds of nanometers requires knowledge of the geometry of the system under investigation. Previous work has shown that the coarse-grained basic unit cell of spider silk consists of a serial arrangement of one semi-amorphous and one crystalline domain, and that this structure is by itself able to represent some of the characteristic mechanical behavior of silk, as shown in Chapter 2.

For the present two-dimensional analysis, a random network is generated (see Figure 3-1) in a square space and has the goal to model the geometry by which silk unit cells assemble at a larger scale. Nodes represent the beta-sheet nanocrystals, while bonds model the semi-amorphous inter-crystalline regions.

The introduction of structural randomness in the model allows statistical variability of the initial length of the constitutive unit cells, thereby facilitating random crack-propagation processes leading to material failure (see Figure 3-2).

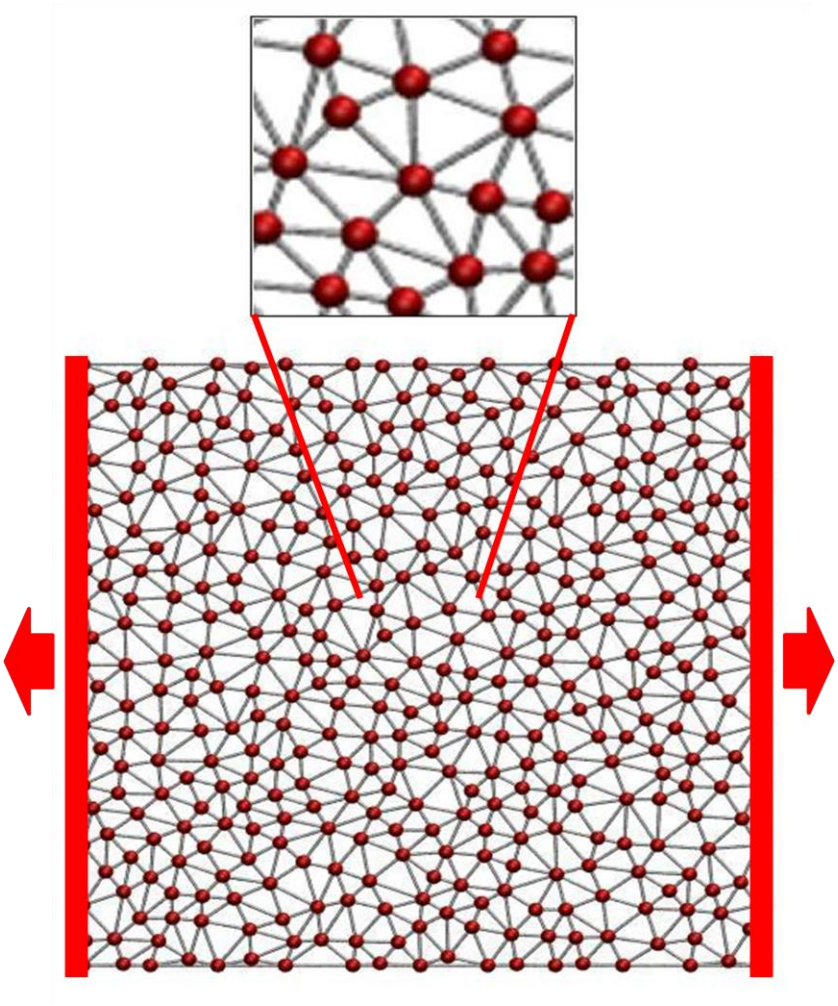

Figure 3-1: Schematic of the mesoscale two-dimensional model. Schematic illustration of the model and the loading conditions. The system consists of a random yet homogeneous network of polypeptide chains where the beads represent beta-sheet nanocrystals and the lines represent amorphous domains. Tensile strain is applied by moving the edges at a constant deformation rate, and stress is computed using the virial stress formulation.

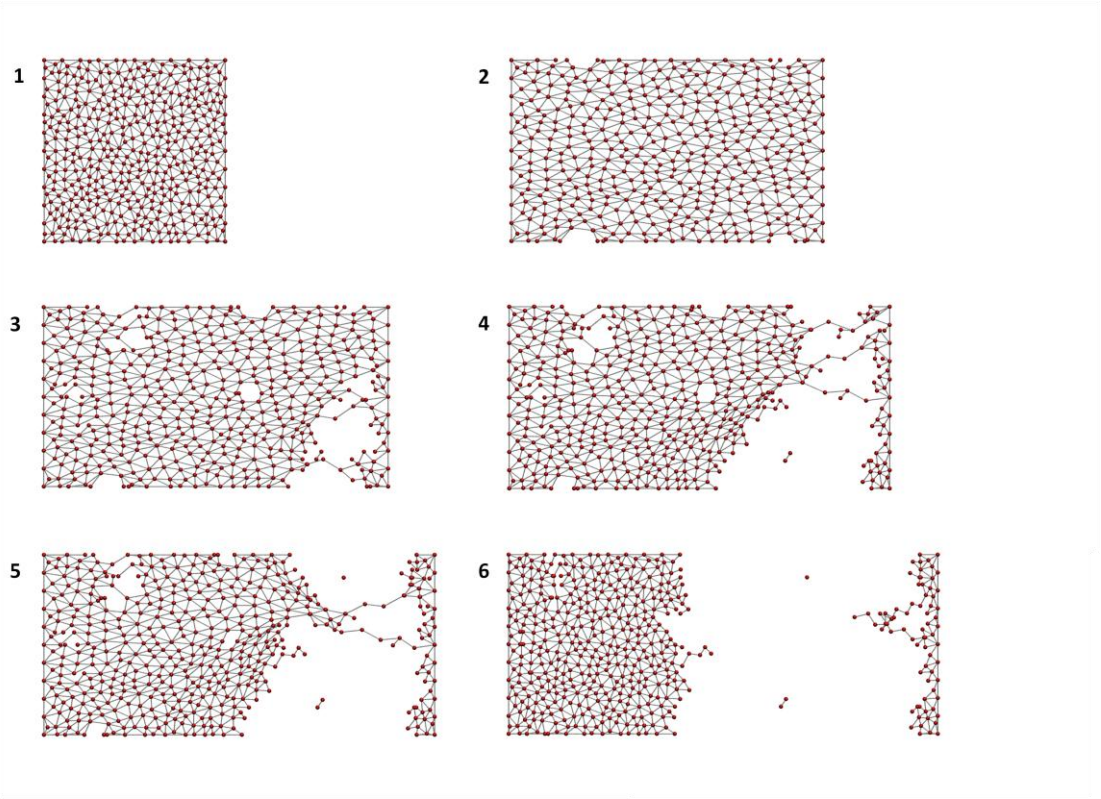

Figure 3-2: Spider silk network under increasing levels of loading. Deformation is applied at constant rate to the system. Cracks generate and propagate through the network, leading to failure of the overall structure.

A MATLAB script (in *Appendix A2*) is used to generate the initial geometry, where nodes are positioned along the boundaries of a square representative area following a regular distribution. This is done in order to ensure an even spacing between the crystals that are located along the boundaries and has the aim to minimize non-homogeneity that could lead to the nucleation of early cracks at the boundaries. Coordinates of the interior nodes of the matrix are generated using a uniform random distribution, while a recursive cycle checks that all points satisfy a lower threshold limit (cutoff) on the inter-nodal distance, ensuring that all distances between neighboring beta-sheet nanocrystals fall above this value.

This check ensures a homogeneous distribution of nodal points within the boundaries. Bonds between nodes are then generated through a Delaunay-triangulation algorithm, which ensures that no node falls into the triangle's circumcircle, which is the unique circle that passes through each of the triangles three vertices [58]. A schematic of the matrix generation process is shown in Figure 3-3.

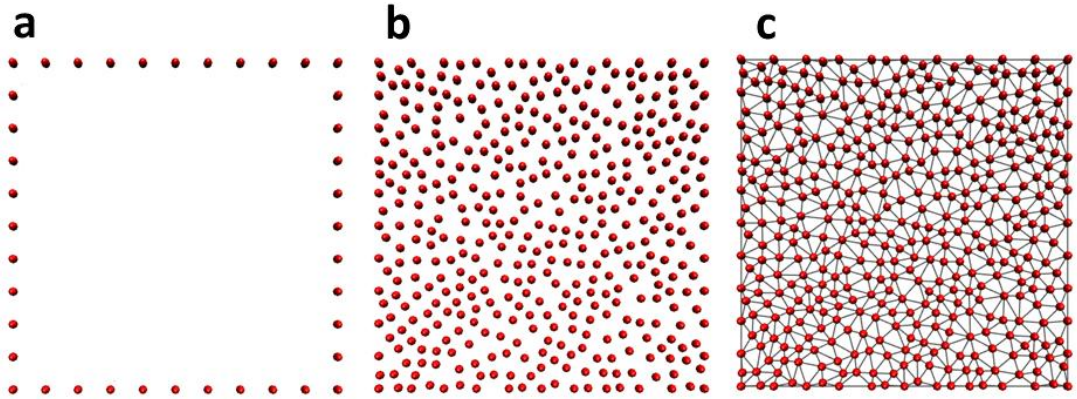

Figure 3-3: Matrix generation process. Schematic showing how the silk random matrix is generated. **a.** Equally-spaced points are distributed along the edges of a square shape. **b.** Random points are positioned within the borders of the square shape. **c.** Inter-crystalline bonds, connecting the nodes of the network, are created through a Delaunay-triangulation algorithm.

The total size of the reference system is L_x = 600 nm by L_y =600 nm with periodic boundary conditions, and the average inter-crystalline distance is imposed to be 90 Å in the reference system, consistently with the parameters used in the one-dimensional unit-cell system described in [19] and in the previous Chapter. A study of the effect of the system size has been performed by varying the system dimensions in a range from 500 Å to 9000 Å, with results not showing any significant difference in the silk stress-strain behavior.

Given an average size of the whole silk fibril of a few microns [6, 59], our simulations are performed in a dimensional scale about one order of magnitude smaller than experiments in literature [60-62].

3.2.2 Model formulation and parameter identification

Full-atomistic simulations of the mechanical properties of the semi-amorphous regions of spider silk have been performed in earlier studies [10, 47]. The results from these analyses are used directly to determine the parameters of the reference coarse-grained unit cell, formed by an amorphous domain in series with a beta-sheet nanocrystal [19] as described in Chapter 2.

The two-dimensional model described in this Chapter consistently use the same parameters employed for the one-dimensional model, described in Figure 2-4 and summarized in Table 1-2. Two distinct types of bonds are introduced: semi-amorphous bonds between distinct crystals in the network and crystal bonds between the crystalline domain itself. These last bonds model the properties of silk polypeptides and their assembly into beta-sheet secondary structures. Analogously to what has been done for the one-dimensional model, we approximate the force-displacement behavior of the two constituting phases of silk under tensile loading with a multi-linear model (see Figure 2-4).

Given the random-matrix generation process previously described, statistical variability exists for the length of the semi-amorphous regions L_A, that is, the length of the bonds between two crystals of the network. Each amorphous-region length L_A is defined as $L_A = r_{ij} = | r_i - r_j |$, where r_i and r_j are the Cartesian coordinates of the two beads involved in the semi-amorphous bond at a given deformation state. In the reference unit-cell, the initial semi-amorphous length $L_{A,0}$ = 90 Å, while the crystal-bond length $L_{B,0} = 0$ for every crystal bond, where $L_B = r_{ij} = | r_i - r_j |$ and r_i , r_j are the coordinates of the beads involved in the crystal bond.

Numerical values of all model parameters are consistent with values used for the silk unit cell and given in Tables 1 and 2, while details on the mathematical formulation and parameter identification are described below.

3.2.2.1 Semi-amorphous region

Values for the stiffness of the three different regimes of the semi-amorphous domain are extracted from atomistic simulation data [10, 47]. The behavior shows an initial stiff regime, followed by a yielding point, a long plateau and a final high-stiffness regime as described in detail in Chapter 2. By fitting the atomistic simulation results with a tri-linear function, the tangent stiffness is obtained as a function of the displacement, where $\Delta L_A = L_A - L_{A,0}$ describes the deformation of the semi-amorphous region (relative to the initial state) and L_A represents the semi-amorphous length as previously defined.

In order to be consistent with the assumptions of the one-dimensional mesoscale model [19], an equal chain-density has to be ensured across the cross-section area. The number of chains across the cross-section area is calculated along the length of the whole network and an average value is then computed and used to calculate the density of the 2D system. Given a density of 0.01 chains/Å^2 for the 1D model, it is possible to ensure equal chain density in the 2D model by means of a parameter α_1 that scales the forces of the whole system so that the mechanical analogous is obtained of systems with equal chain density.

The parameter α_1 is defined as the ratio between one-dimensional and two-dimensional chain density, as follows:

$$\alpha_1 = \frac{d_{1D}}{d_{2D}}, \tag{7}$$

where d_{1D} and d_{2D} are defined as the chain density in the 1D system and 2D system, and chain density is defined as the number of chains per total cross-section area.

A second parameter α_2 accounts for changes in the semi-amorphous initial length, with respect to the reference 90 Å case on which parameters are derived from atomistic simulations. Variations in length can be either systematic or random. A systematic variation of the average inter-crystal spacing is performed in this work with the aim to study the effect of different spacing on the overall mechanical response. Random variations are instead due to the distribution around an average value of initial lengths, whose spread around the mean value depends on the homogeneity of the structure.

Each semi-amorphous polypeptide chain is characterized by an equal elastic modulus E and chain cross-section area A_0, and its stiffness is then related to the amorphous-region initial length $L_{A,0}$ by

$$K_A = \frac{EA_0}{L_{A,0}}, \tag{8}$$

showing inverse proportionality between semi-amorphous stiffness and initial length. The scaling parameter α_2 is defined as $\alpha_2 = \overline{L_0} / L_{A,0}$, where $\overline{L_0} = 90$ Å is the average equilibrium distance (and the initial length of the semi-amorphous region in the reference system). The formulation expressed in equation (2) is able to effectively capture the fact that longer chains behave in a softer fashion.

The semi-amorphous stiffness as a function of deformation is given, for every bond, by the equation:

$$k_A(\Delta L_A) = \alpha_2 \begin{cases} k_{A,1} & \Delta L_A < \Delta L_{A,1} \\ k_{A,2} & \Delta L_{A,1} \le \Delta L_A \le \Delta L_{A,2} \\ k_{A,3} & \Delta L_A > \Delta L_{A,2} \end{cases} \quad (9)$$

where the values for $k_{A,i}$ as well as the transition deformations $\Delta L_{A,1}$ and $\Delta L_{A,2}$ are summarized in Table 1. The force versus deformation for each amorphous domain is given by the following law:

$$F_A(\Delta L_A) = \alpha_1\alpha_2 \begin{cases} k_{A,1}\Delta L_A & \Delta L_A < \Delta L_{A,1} \\ k_{A,1}\Delta L_{A,1} + k_{A,2}(\Delta L_A - \Delta L_{A,1}) & \Delta L_{A,1} \le \Delta L_A \le \Delta L_{A,2} \\ k_{A,1}\Delta L_{A,1} + k_{A,2}(\Delta L_{A,2} - \Delta L_{A,1}) + k_{A,3}(\Delta L_A - \Delta L_{A,2}) & \Delta L_A > \Delta L_{A,2} \end{cases} \quad (10)$$

where α_1, α_2 are scaling parameters accounting for crystal density and variations in inter-crystal spacing as previously described. Analogously to what stated in Chapter 2, shows the resulting force-deformation curve of the semi-amorphous region for the reference case, where $\alpha_1 = \alpha_2 = 1$.

3.2.2.2 Beta-sheet nanocrystals

Each beta-sheet nanocrystal in the two-dimensional system is modeled as a stack of four bonded beads with zero initial equilibrium distance. Each bond models the cross-linking effect of cooperative H bonds within the beta-sheet nanocrystal [4, 50, 51] and characterizes its mechanical response. Bonds are modeled as multi-linear springs and the force-displacement characteristic is informed from pull-out atomistic simulations [4, 10, 47, 50, 51], where both explicit and implicit-solvent simulations have shown agreement in the description of the beta-sheet nanocrystal constitutive behavior. We consider the effect of the variation in size of beta-sheet nanocrystals on the mechanical behavior by scaling the stiffness, strength and energy dissipation capacity of the beta-sheet nanocrystals according to size-effects observed in atomistic simulations and analogously to what has been done for the one-dimensional basic

unit-cell [19]. To account for these size effects, beta-sheet nanocrystals of different size feature distinct mechanical properties [35, 52, 53].

Beta-sheet nanocrystal stiffness is modeled as a function of beta-sheet nanocrystal deformation, expressed as $\Delta L_B = L_B - L_{B,0}$, where L_B represents the crystal-bond length as previously described and where $L_{B,0} = 0$ for every crystal bond. The formulation for the stiffness k_B as a function of deformation ΔL_B is then given by

$$k_B(\Delta L_B) = \begin{cases} k_{B,1} & \Delta L_B < \Delta L_{B,1} \\ k_{B,2} & \Delta L_B \geq \Delta L_{B,1} \end{cases} \tag{11}$$

where $\Delta L_{B,1}$ is the beta-sheet nanocrystal transition point as defined in Table 2 and shown in Figure 2-4b. The effect of crystal size is modeled by changing the values of parameter $k_{B,1}$ and $k_{B,2}$, as well as $\Delta L_{B,1}$ and $\Delta L_{B,2}$ as summarized in Table 2.

The force as a function of deformation for the 3 nm-crystal is given by the following expression

$$F_B(\Delta L_B) = \alpha_1 H(\Delta L_B) \begin{cases} k_{B,1}\Delta L_B & \text{if } \Delta L_B < \Delta L_{B,1} \\ k_{B,1}\Delta L_{B,1} + k_{B,2}(\Delta L_B - \Delta L_{B,1}) & \text{if } \Delta L_B \geq \Delta L_{B,1} \end{cases}, \tag{12}$$

where the Heaviside function H is defined as $H(\Delta L_B) = 1$ for $\Delta L_B < L_{B,2}$ and $H(\Delta L_B) = 0$ for $\Delta L_B \geq L_{B,2}$ and the parameter α_1 accounts for the system-density scaling as previously described.

The failure point, $\Delta L_{B,2}$ depends on the crystal size as summarized in Table 2. For the larger beta-sheet nanocrystals (6.5 nm and 10 nm cases), the force on the linear spring is given as

$$F_B(\Delta L_B) = \alpha_1 H(\Delta L_B) \cdot k_{B,1}\Delta L_B . \tag{13}$$

The added value of the model described in this Chapter is the possibility to vary a wider number of system parameters and study how this affects the overall mechanical behavior.

3.2.3 Parametric study formulation

Parameters relative to the geometry of the system and the mechanical behavior of the constitutive elements will be varied in this study. The goal is to check the robustness of the model, its capacity to represent different mechanical conditions and validate the results with experimental evidence.

In detail, the effect on silk mechanical response of the following parameters is studied:

- different inter-crystalline spacing;
- different crystal homogeneity;
- prestretch;
- combined effect of crystal size, inter-crystalline spacing and prestretch;
- water content.

3.2.3.1 Effect of different beta-sheet nanocrystal spacing on the silk mechanical properties

Silk polypeptide chains are present in a semi-liquid phase in the spider's silk glands. The silk solidification process taking place at the spider's orifice during the spinning drastically affects the mechanical properties of the silk thread [6].

Formation of the crystals is a complex process, requiring the chains to have, at the same time, a suitable relative position and enough time to nucleate. When the silk is extruded, it passes through a long duct, where the shearing of the fluid drives the protein to align in the direction of the flow and to come close to each other: faster

spinning increases this phenomenon and thus the probability of having the geometrical suitable conditions for crystal formation [6].

More crystals in the same amount of silk correspond to a higher crystal concentration and a smaller intercrystalline distance. The nucleation time plays a role in defining the size of the crystals, where large crystals are only possible at low spinning rate (long nucleation time).

An increase in crystal density is accompanied by a decrease in inter-crystalline spacing and in the length of the silk unit cell, with value ranging from 6 nm to 24 nm.

3.2.3.2 Effect of crystal homogeneity

Silk structures can show different levels of crystal homogeneity. Different levels of homogeneity can be obtained by changing the degree of order in the Delaunay-triangulation network.

A larger cutoff value ensures great homogeneity of crystal distribution and thus a change in its value determines different homogeneity levels. The range for the threshold limit varies between 0.2 and 1.0 times the optimal value for the cutoff distance. The optimal value is intended as the maximum value for the cutoff that allows the random-matrix generation algorithm to be solved.

Homogeneity of the system is changed by varying the lower-threshold value for the inter-nodal distance during the random-network formation.

The cutoff coefficient for a random matrix generated as above is expressed by the following equation:

$$\text{cutoff} = \frac{1}{25\sqrt{\left(\frac{N_{\text{int}}}{400}\right)}} * \text{cutoffCoef} \quad , \tag{14}$$

where N_{int} is the number of internal points to the network and cutoffCoef is a coefficient that varies between 0.2 and 1.0 as described above.

A diminished value for the threshold results in a clustering of crystals in certain regions, where the result is a local crystal distribution which is less homogeneous and a system with altered mechanical properties. A quantitative estimate of the level of homogeneity could be obtained analyzing the distribution of bond lengths around the average value: if amorphous-region bond lengths tend to be closer to the average value the level of homogeneity of the structure is higher.

3.2.3.3 Effect of prestretch

As mentioned above, semi-liquid spider silk passes through a long and tiny duct when silk is being spun; the resulting shear forces have the double effect to partially align the polypeptide chains along the longitudinal direction and to pre-stretch the molecules of a quantity that is proportional to the spinning speed [6]. Faster-spun silk is characterized by better oriented and more pre-stretched polypeptide chains. This means that the equilibrium structure (no load applied) of the silk unit cell is not completely folded and consequently it has less hidden length that can be unraveled when pulling the silk thread [6].

A higher spinning speed determines increased levels of pre-stretch in the semi-amorphous regions of silk [6]. In the pre-stretched case, the equilibrium structure of silk is partially unfolded even when no load is applied, determining yielding and stiffening to occur at lower displacement values than the reference case.

Modeling of pre-stretch can be done according to different hypotheses as shown in Figure 3-4. Constant feature is the fact that pre-stretch is modeled by a variation of the displacement at the transition points (from 0% to 80% variation). This drop in strain can be imposed keeping the initial stiffness constant or alternatively keeping the forces at the transition points to be constant.

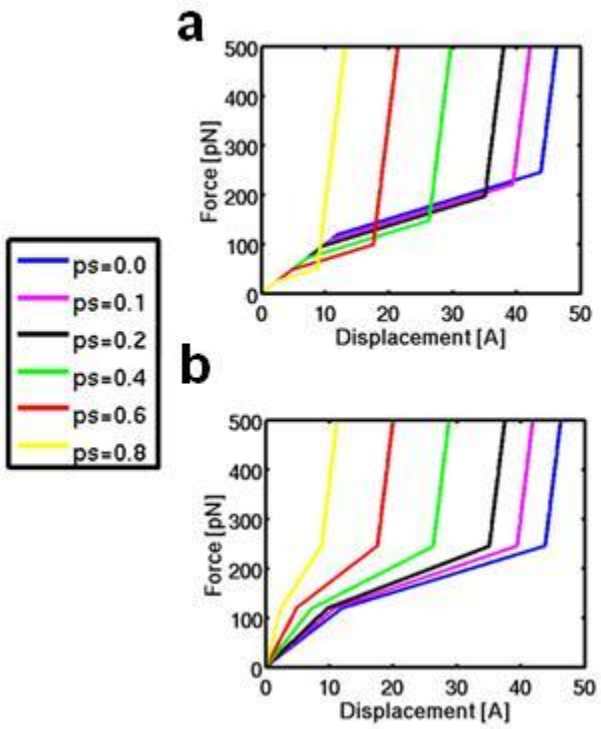

Figure 3-4: Different hypotheses for the modeling of pre-stretch. **a.** Pre-stretch is modeled by a variation of the displacement at the transition points (from 0% to 80% variation), keeping the initial stiffness constant. The initial and the plateau regimes are shorter at increasing levels of pre-stretch, with yielding and stiffening occurring at lower force levels. **b.** Different hypothesis for the modeling of pre-stretch: force at yielding and stiffening points is kept constant, while the displacement is changed and decreased up to 80%. As a consequence, initial and plateau stiffness increases as the level of pre-stretch grows.

The initial and the plateau regimes are shorter at increasing levels of pre-stretch: yielding and stiffening occur at lower force levels if constant stiffness is imposed, while initial and plateau stiffness increases as the level of pre-stretch grows under the hypothesis of constant forces.

In the present work both hypotheses for the modeling of pre-stretch in silk are investigated. $\Delta L_{A,1}$ and $\Delta L_{A,2}$ are the amorphous transition points for the reference

case and the pre-stretched transition points $\Delta L'_{A,1}$ and $\Delta L'_{A,2}$ are defined as $\Delta L'_{A,i} = (1 - ps)\Delta L_{A,i}$, where *ps* is defined as a prestretch factor varying between 0 (no prestretch) and 0.8 (max level of prestretch investigated in this study).

Stiffness of the semi-amorphous region $k_A(\Delta L_A)$ is divided by a factor $(1 - ps)$ in the hypothesis of constant force, while it is not modified with respect to the reference case under the hypothesis of constant stiffness.

3.2.3.4 Combined effect of crystal size, inter-crystalline spacing and pre-stretch

The speed by which silk is spun at the spider's orifice affects simultaneously the size of the beta-sheet nanocrystals, their average spacing and the level of pre-stretch of the semi-amorphous regions. All these factors lead to different stress-strain constitutive behaviors and are introduced into the model as described above. The overall effect of silk spinning speed is studied by a simultaneous combined variation of these three parameters and all their possible combinations. For each crystal dimension the whole range of possible pre-stretches is studied, and for each level of pre-stretch different inter-crystalline distances are taken into exam.

3.2.3.5 Effect of water

An increase in hydration promotes the entry of water molecules into the spider silk network, leading to a softer, more extensible structure [59, 63]. A schematic representation of this effect is shown in Figure 3-5 (note that this figure is not the result of an actual simulation, but rather based on a rendering of the effect of water on the hydrogen bonding of two generic protein molecules). Water molecules interfere with the formation of H bonds within silk polypeptide chains: higher levels of hydration determine a decrease in inter- and intra-chain hydrogen bonding and lead to a softer and more extensible behavior for the semi-amorphous region.

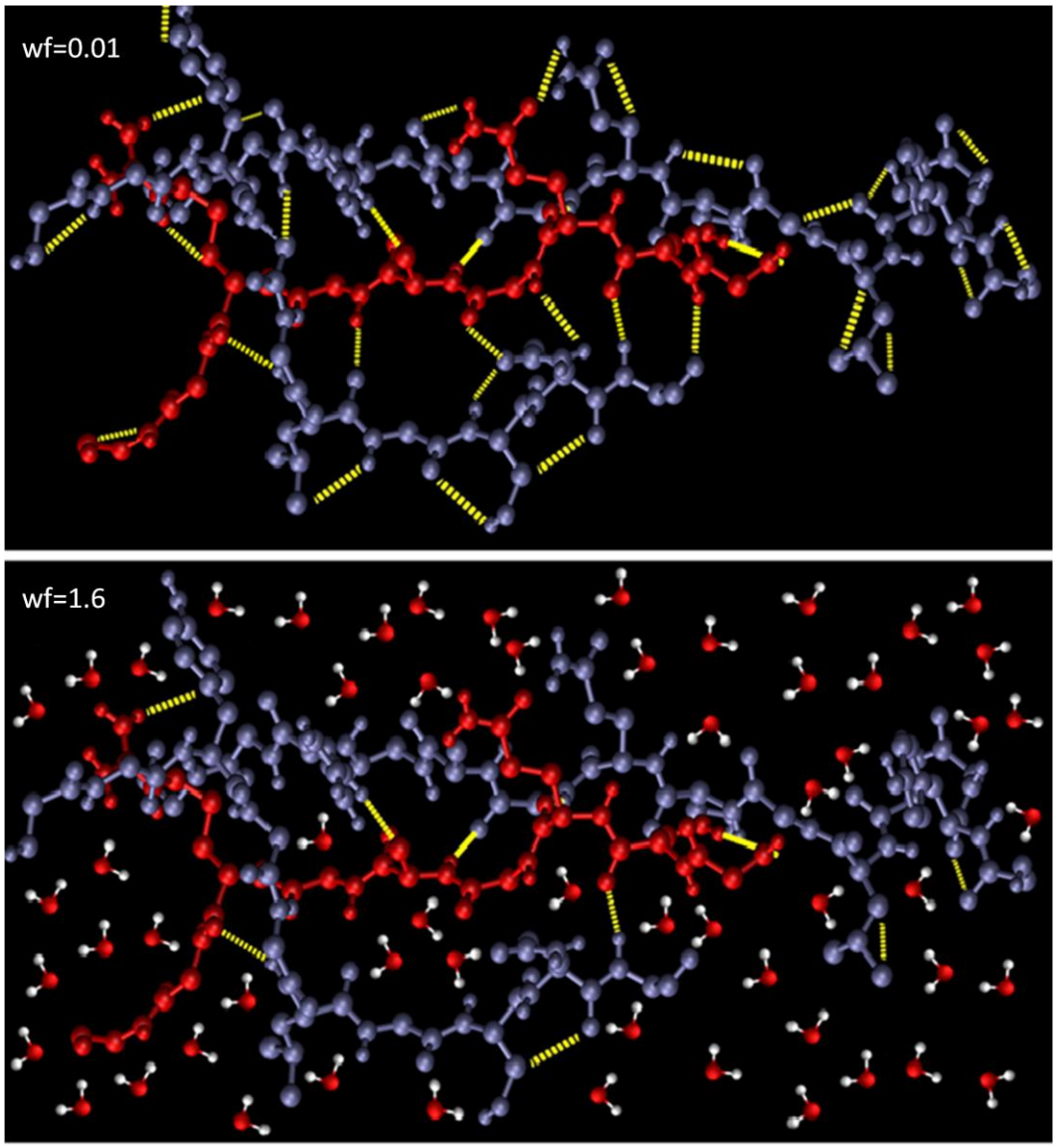

Figure 3-5: Effect of system hydration. Schematic representation of the effect of water on the spider silk structure. Water molecules enter the silk network and interfere with the formation of H bonds within polypeptide chains: higher levels of hydration determine a decrease in inter- and intra-chain hydrogen bonding and lead to a softer and more extensible behavior for the semi-amorphous region.

The effect of water is modeled by modifying the initial stiffness and extensibility of the semi-amorphous region, with the assumption to keep equal values of yielding and stiffening force. The level of hydration is accounted by means of a water factor, where higher values represent a more hydrated structure and a softer initial behavior.

The model aims to study the effect of water on the initial regime and on the entity of the drop in stiffness at the yielding point. Water contribution is modeled by a progressive softening of the initial regime: the transition point occurs at same force levels, but higher deformations lead to smaller initial-stiffness values. The transition deformation ΔL_A is rescaled to be $\Delta L_A^{'} = wf * \Delta L_A$, where wf is a water-factor varying between 0.01 and 1.6. The reference value $wf = 1$ refers to a partially hydrated structure, whose behavior has been derived from atomistic simulations. Analogously, the initial amorphous stiffness k_A is scaled to be $k_A^{'} = k_A / wf$, to ensure equal transition forces in all systems.

3.2.4 Computing technique

LAMMPS Molecular Dynamics code is used for the simulations [64]. The force field is modified introducing multi-linear harmonic bond potentials as previously described, with the aim to model the bonding interactions within the crystalline and the semi-amorphous domains (for the code, see *Appendix A3*). We notice that since the basis of the model is atomistic simulation, the (multi-linear) spring constants directly take into account the effects of solvent and molecular friction, while additional parameters for viscosity and other effects are not considered in this work.

Pulling simulations are performed at constant volume and constant energy (NVE ensemble) at room temperature (300 K - with Berendsen control of Temperature every 60 fs). The time step is 1 fs and the total simulation time 1.5 ns. Pulling velocity is $6*10^{-16}$ m/s and the strain rate is 10^{-9} s^{-1}. The initial structure is initially at

equilibrium and homogeneous deformation is applied to the entire system every 500 time steps (for details, see input file in *Appendix A4*).

In order to deform the network, fixed boundary conditions constrain the system vertical edges while tensile strain is applied to the simulation box, which is deformed cyclically and transfers the deformation to the silk structure. Using this technique, deformation is applied instantaneously and homogeneously to every point of the network. Simulations using Steered Molecular Dynamics (SMD) have been previously performed, but did not allow a homogeneous distribution of deformation and led to high stress values in localized points of the network, with the arise of cracks leading to early material failure.

The network structure is further constrained in its transversal direction via periodic boundary conditions, in order to exclude the effect of Poisson ratio (shrinking) and its effect on cross-section area. Additional simulations have been preformed relaxing this constraint: no significant difference in the mechanical behavior has been noticed, confirming the validity of this simplifying assumption.

The output of the pulling simulations, which is the component of the virial stress tensor along the x (pulling) direction, is calculated and averaged over the entire system. The stress is defined according to the virial approach [15, 65], where the volume is calculated assuming a thickness of T=10 Å, consistently with the one-dimensional analysis performed in Ref. [19] and in Chapter 2 of this thesis work.

The output is further time-averaged every 500 time steps and data post-processing is performed using python and MATLAB scripts, with Visual Molecular Dynamics (VMD) as a graphical interface [66]. Mechanical toughness is calculated measuring the area under the force-extension curve (until structure breaking) by means of a trapezoidal numerical integration.

3.3 Results and discussion

3.3.1 Variation of crystal size

The findings presented in Chapter 2 for a one-dimensional silk unit cell show how a variation in size of the beta-sheet nanocrystals affects the overall system mechanical behavior, with small crystals leading to enhanced values of maximum strength and toughness. Aim of this section is to show whether such a variation in crystal size affects the behavior of silk also at a larger scale, with silk polypeptide entanglements represented by the two-dimensional coarse-grained random network previously described. Molecular dynamics simulations are used to characterize the mechanical behavior of the system under stretching and for varying system conditions as described in the *Materials and Methods* section of this Chapter.

Figure 3-6a represents a cluster of poly(Ala) residues, creating a highly-order stacked structure and the basic unit of beta-sheet nanocrystals. Figure 3-6b is a graphical representation of beta-sheet nanocrystals of different size, with values from 3 nm up to 10 nm.

The resulting stress-strain curves shown in Figure 3-6c provide evidence that the size of beta-sheet nanocrystals drastically affects silk's overall mechanical response also in a silk two-dimensional model, with smaller-crystal systems showing enhanced properties in terms of maximum tensile strength and dissipated energy.

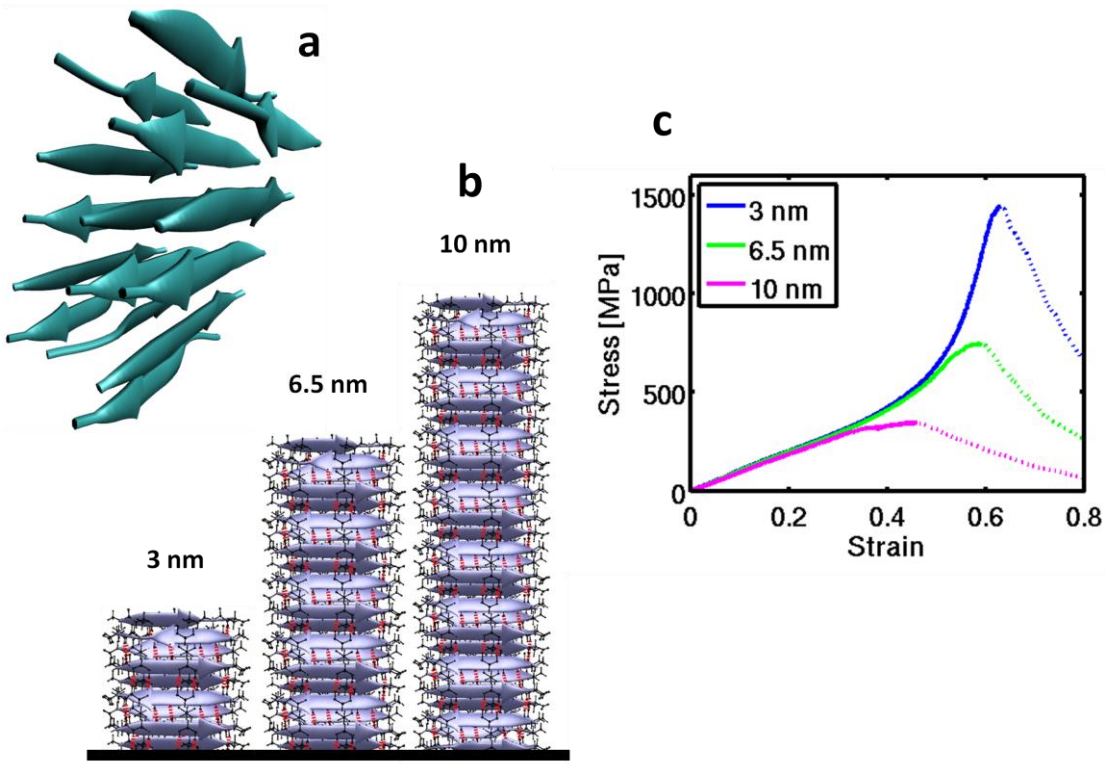

Figure 3-6: Influence of the beta-sheet nanocrystal size on the tensile stress-strain behavior. **a,** three dimensional representation of a cluster of poly(Ala) residues that represent the basic unit of silk nanocrystals. Anti-parallel beta-sheets are formed by protein strands linked by hydrogen bonding. **b**, Different dimensions of beta-sheet nanocrystals (3 nm, 6.5 nm, 10 nm). The number of strands clustered to form beta-sheet structures affects the load distribution within the crystal and its overall mechanical response, as described in [4]. c, Predicted stress-strain curves of spider dragline silk illustrating the influence of beta-sheet nanocrystal size. The behavior after rupture is displayed with dotted lines. The results show that failure stress and strain depends strongly on the beta-sheet nanocrystal size: for the systems studied (ranging from 3nm to 10nm), a slight yielding behavior is observed at around 15% strain, and failure occurs between 45% and 65% strain. Failure stresses lie in a range from around 400 MPa to 1500 MPa, where smaller crystals lead to higher strength as well as higher tensile strain.

The analogy of results in a one-dimensional and two-dimensional arrangement confirms that the mechanical properties and deformation mechanisms of silk—in particular the sensitivity of the properties with respect to the size of beta-sheet nanocrystals—are well preserved when increasing the complexity of the system. Most importantly, the similarity of results from the one- and two-dimensional models confirm that the approach employed to coarse grain the spider-silk unit cell into a one-dimensional model is suitable to capture the key physics of material deformation also at larger scales.

Results show that an increase in beta-sheet nanocrystal size leads to a significant loss of strength and toughness of the overall system. The maximum value of tensile strength for the small crystal case is 1447 MPa in the 2D system. As shown in Figure 3-6c, with a value of around 745 MPa, the 6.5 nm-crystal case shows a decrease of approximately 50% with respect to the reference system with the smallest beta-sheet nanocrystal. The drop is even larger for the 10 nm-crystal case, which fails at 345 MPa, at 76% less stress than the reference case with the smallest (3 nm) beta-sheet nanocrystal.

The drop in maximum stress also leads to toughness values that are considerably lower than the reference small-crystal case (see Figure 3-6c). A decrease of 26% and 64% is measured for the 6.5 nm and the 10 nm case respectively, in comparison to the toughness value of 260 MPa for the 3 nm reference case.

3.3.2 Variation of intercrystalline distance

The probability of beta-sheet nanocrystal formation is increased at higher reeling speed, thanks to better orientation of the poly(Ala) regions [6]. Crystal size and crystal concentration are two highly-correlated phenomena, showing nevertheless different effects on silk's mechanical behavior. In the present analysis the effect of crystal spacing is first studied separately, while it will be later combined with the concurrent effect of crystal size and pre-stretch level.

Results from mesoscale simulations on the random matrix described above show that a shorter average intercrystalline distance in the denser case increases the failure stress and the toughness of the system and is accompanied by a significant decrease of the strain levels (see Figure 3-7).

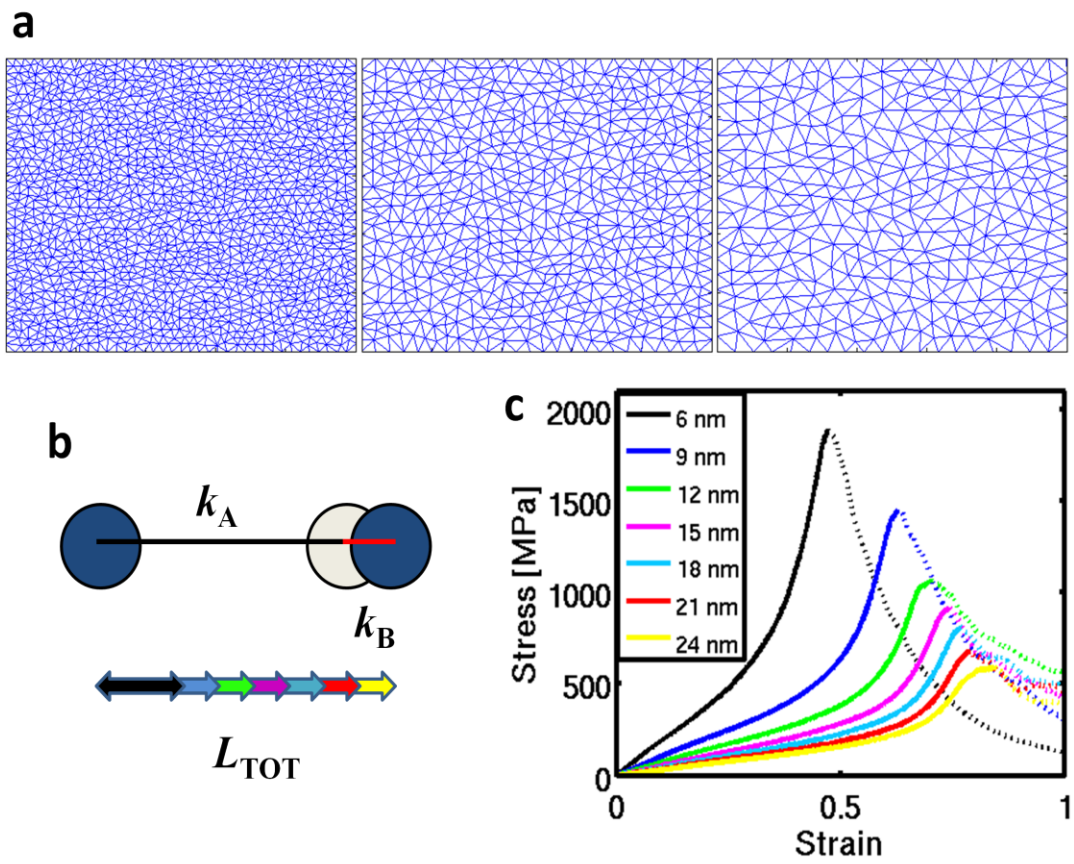

Figure 3-7: Influence of beta-sheet nanocrystal spacing on the silk mechanical properties. **a,** Silk networks with different beta-sheet nanocrystal spacing. In experiments, reeling speed and the associated crystal nucleation time affect the properties of beta-sheet nanocrystals in the network: higher reeling speeds better orient the poly(Ala) regions and increase the probability of beta-sheet nanocrystal formation, thus increasing their density and decreasing the inter-crystalline space. **b,** Schematic representation of the silk unit cell, formed by a series of an amorphous domain and a beta-sheet nanocrystal. A change in crystal density corresponds to a change in length of the silk unit cell, with values ranging from 6 nm to 24 nm. Stiffness values for the amorphous domain depend on the length of the unit cell as discussed in *Materials and methods* section. **c,** Stress-strain curves, showing the mechanical behavior of silk networks characterized by different inter-crystalline spacing. A decrease in spacing determines increased values of maximum tensile strength, together with an upward shift of the characteristic curve at all levels of strain.

Crystal spacing drastically affects the maximum tensile strength, with values ranging between 600 MPa and 1900 MPa. Concurrent with increasing maximum stress is a decrease in failure strain from around 80% to 50%. This characteristic behavior is confirmed by experimental evidence, where the mechanics of silks spun at different velocities has been studied [2]. These results demonstrate that in a 2D model an increase in maximum tensile strength does not depend only on beta-sheet nanocrystal strength but also on crystal concentration and stiffness of the amorphous domains.

A stiffer amorphous region resulting from decreased inter-crystalline spacing (for details see *Materials and Methods* section) affects the mechanical behavior at all levels of deformations, leading to an upward shift of the overall curve. A higher crystal concentration plays a role particularly at high deformation levels, drastically increasing the maximum tensile stress.

Considering a variation of inter-crystalline length between the reference case (inter-crystalline spacing of 9 nm) and the value of 24 nm, it is possible to see a drop of maximum tensile strength from 1447 MPa to 592 MPa (-60%) and a decrease in toughness from 260 to 151 MPa (-42%). Strain at failure concurrently increase from 63% to 85% (+35%).

The study of the effect of crystalline superconcentration, modeled by an average inter-crystalline distance of 6 nm, also yields interesting results. The curve (Figure 3-7c) shows an increase of maximum tensile stress of 30% with respect to the reference (9 nm) case and tops a value of 1883 MPa. Toughness is also increased from 260 to 279 MPa.

Intermediate values of inter-crystalline distance result in a mechanical behavior whose curve lies in-between the two extreme cases of 6 nm and 24 nm.

Figure 3-8 shows a series of snapshots of spider silk networks with different intercrystalline distance at different deformation levels.

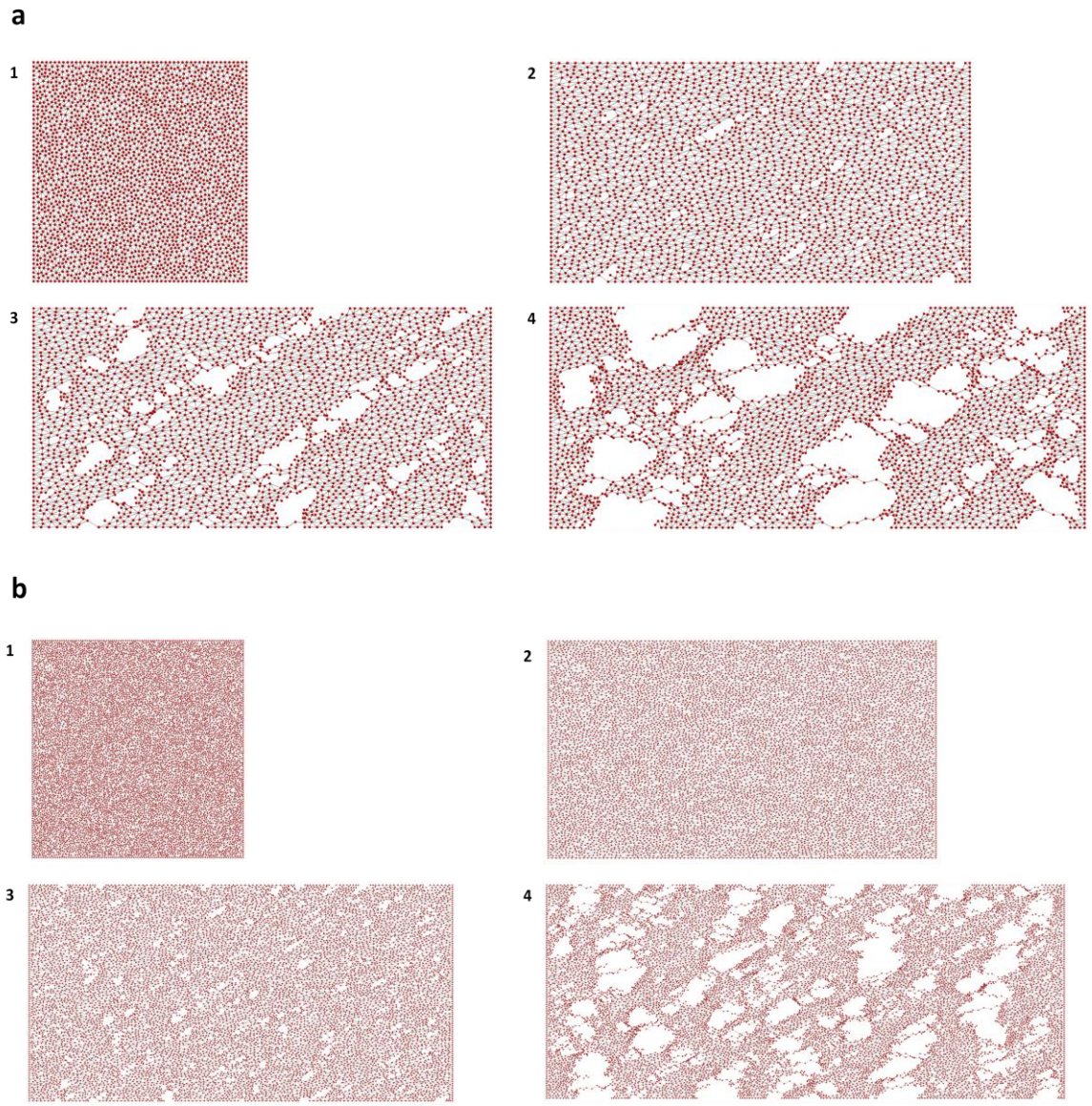

Figure 3-8: Spider silk networks of different density (different inter-crystal spacing – **a,b**) under increasing levels of loading. Deformation is applied at constant rate to the systems.

Besides showing the effect of inter-crystalline spacing on the maximum stress, strain and toughness, another outcome of this study is the discovery that in a two-dimensional model, the maximum stress value does not depend uniquely on the value of crystal strength (as in the one-dimensional model) but it rather depends on a combination of multiple factors such as amorphous stiffness and crystal concentration.

3.3.3 Variation of crystal homogeneity

Crucial in the analysis of the mechanical properties of a material is the study of defects and their repercussion on the overall mechanical response. A study of structural homogeneity variation shows how a divergence from an ideal structure leads to different mechanical properties.

The curves represented in Figure 3-9 show an increase of up to 20% in maximum tensile strength for homogeneous structures when compared to, while they do not show a significant variation in maximum strain values. Highly homogeneous structures are characterized by a more pronounced sigmoidal behavior, with a marked yielding and final stiff regime.

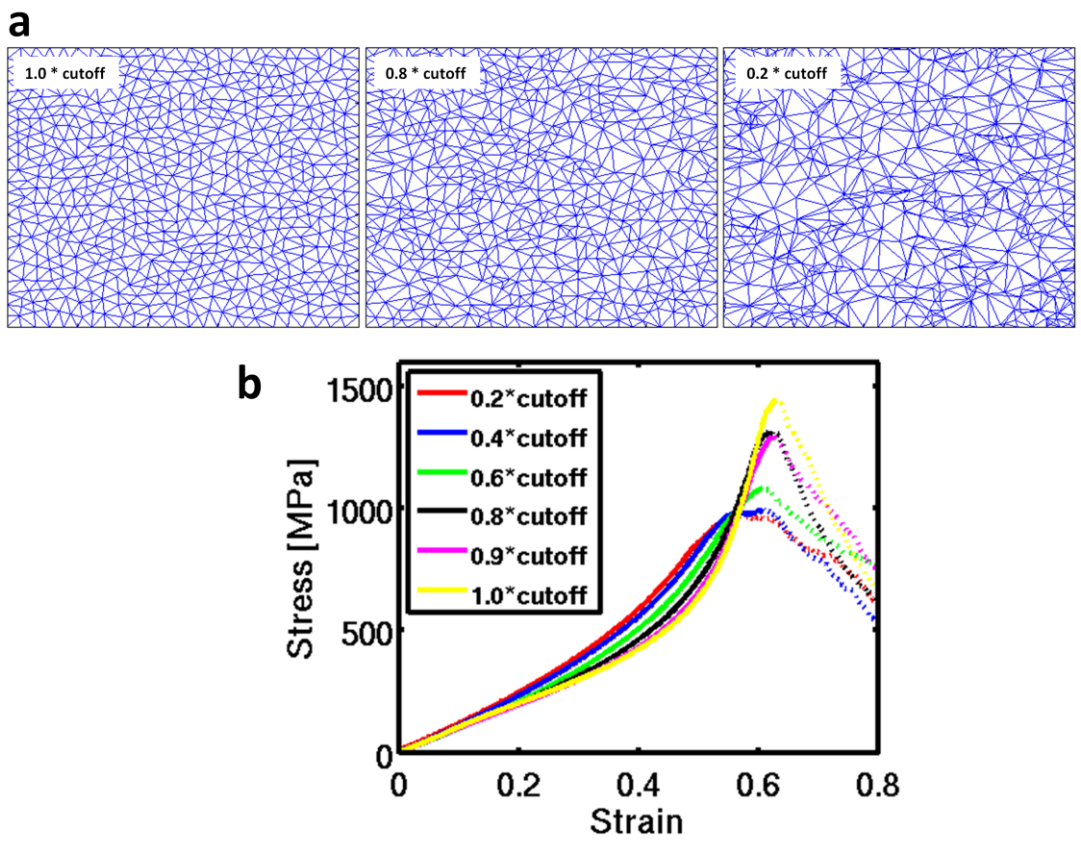

Figure 3-9: Effect of structural homogeneity. **a.** Silk structures with different crystal homogeneity, obtained by changing the degree of order in the Delaunay triangulation scheme. The coordinates of the nodes in the matrix are generated using a uniform random distribution, while a recursive cycle checks that all points satisfy a lower threshold limit on the inter-nodal distance. The order parameter is defined by a lower threshold limit (cutoff), ensuring that all distances between neighboring beta-sheet nanocrystals fall above this value. A larger cutoff value ensures great homogeneity of crystal distribution. The range for the threshold limit varies between 0.2 and 1.0 times the optimal value for the cutoff distance. **b.** Study of the effect of crystal homogeneity on the mechanical behavior of the silk network. Homogeneous structures show an increase of up to 20% in maximum tensile strength while they do not show a significant variation in maximum strain values. Highly homogeneous structures are characterized by a more pronounced sigmoidal behavior, with a marked yielding and final stiff regime.

The main finding of this section is that a lack of crystal homogeneity in the silk structure modifies the overall mechanical response, with particular reference to the failure mechanisms: with increased crystal homogeneity, the stress-strain curve shows an increase in maximum tensile strength, without any significant variation in the maximum strain level.

3.3.4 Effect of pre-stretch

The resulting stress-strain curves in Figure 3-10 show the effect of silk pre-stretch on the mechanical behavior of the overall structure. Different results are obtained when assuming different hypotheses as described in *Materials and Methods* section.

Faster spinning determines increased levels of pre-stretch in the semi-amorphous regions of silk. In the pre-stretched case, the equilibrium structure of silk is partially unfolded even when no load is applied.

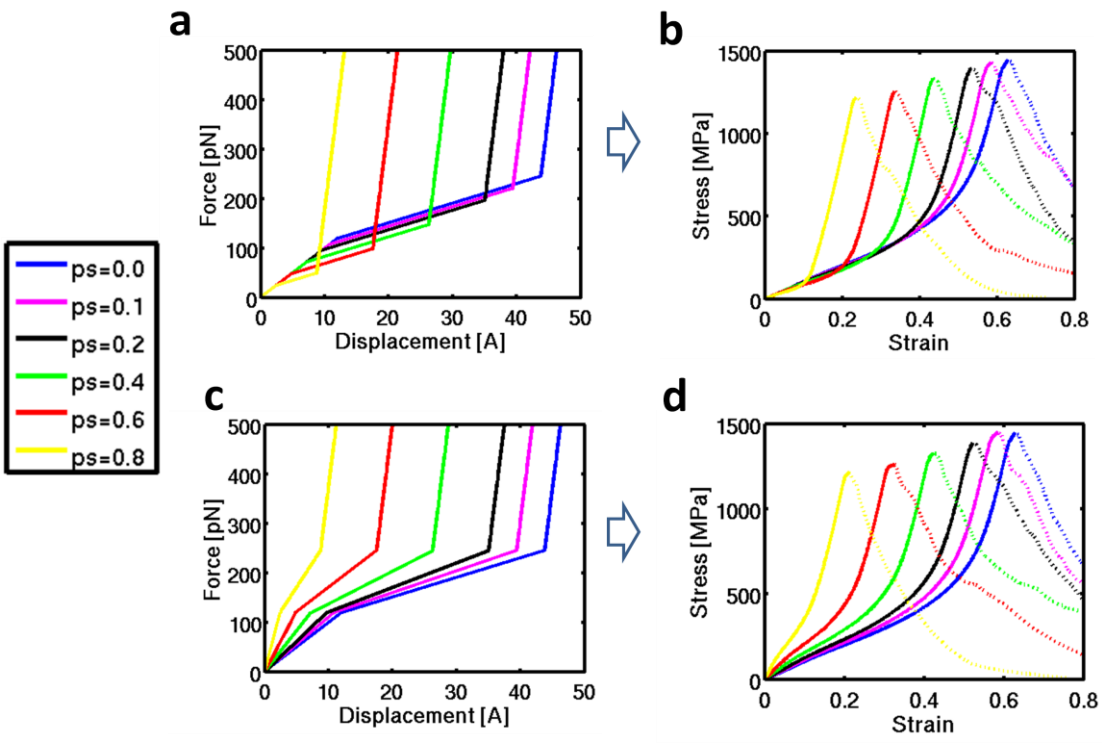

Figure 3-10: Effect of semi-amorphous region pre-stretch. Faster spinning determines increased levels of pre-stretch in the semi-amorphous regions of silk. In the pre-stretched case, the equilibrium structure of silk is partially unfolded even when no load is applied, determining yielding and stiffening to occur at lower displacement values than the reference case. Modeling of pre-stretch can be done according to different hypotheses. **a.** Pre-stretch is modeled by a variation of the displacement at the transition points (from 0% to 80% variation), keeping the initial stiffness constant. **b.** Predicted spider silk stress-strain curves at different levels of pre-stretch. Highly pre-stretched structures show a significant drop in maximum strain (from 65% to 25%) and a concurrent decrease in toughness and failure stress. **c.** Different hypothesis for the modeling of pre-stretch: force at yielding and stiffening points is kept constant, while the displacement is changed and decreased up to 80%. **d.** predicted stress-strain curves at different pre-stretch values, hypothesis of constant force at transition points. Increased values of pre-stretch lead to lower values of maximum stress, strain and toughness, together with an upward shift of the whole curve at all levels of strain.

Figure 3-10b,d show that, either assuming the hypothesis of constant stiffness or constant force, the initial and the plateau regimes of the resulting stress-strain curves are shorter at increasing levels of pre-stretch, with yielding and stiffening occurring at lower force levels. Highly pre-stretched structures show a significant drop in maximum strain (failure strain shifts from 65% strain to 25% strain) and a concurrent decrease in toughness and in failure stress.

With the hypothesis of constant stiffness (for details, see *Materials and Methods* section of this chapter), maximum stress decreases from 1447 to 1217 MPa and toughness from 260 to 85 MPa (see Figure 3-10b) when going from a structure characterized by 0 pre-stretch (reference case) to a structure characterized by a pre-stretch factor of 0.8. Assuming the hypothesis of constant force, maximum stress decreases to 1252 MPa and toughness to 102 MPa in the case of prestretch factor equal to 0.8.

As shown above, different hypotheses on the modeling of pre-stretch give approximately the same drop in maximum stress for a pre-stretched system, while the hypothesis of constant stiffness leads to a sharper drop in toughness than the hypothesis of constant force. The two different hypotheses change the shape of the silk stress-strain curve especially at low levels of deformation, with a gradual upward shift evident in the hypothesis of constant force and for increasing levels of pre-stretch, but lacking in the hypothesis of constant stiffness.

It’s important to underline that this pre-stretch effect will have to be properly combined with a crystal-size effect, since both phenomena happen simultaneously when silk is being spun.

Simulation results on a two-dimensional model of spider silk that include the effect of pre-stretch give results where strain levels that are much closer to experimental evidences [6]. This fact confirms that a study of pre-stretch can help to explain the

reason for the gap, in terms of maximum strain, between simulations and experiments as it has been noticed at the end of Chapter 2.

3.3.5 Combined effect of crystal size, inter-crystalline spacing and pre-stretch variation

Figure 3-11 and Figure 3-12 show how different spinning conditions affect the overall spider silk mechanical behavior. This is done by simultaneously varying the parameters defining crystal size, inter-crystalline spacing and level of pre-stretch, all factors concurrently affected by the silk spinning conditions and speed.

Figure 3-11 shows the curves obtained by all possible combinations of these three parameters when they vary in the ranges described above. The result is an area of the stress-strain plot that can be explored by different spider silk systems. As clearly shown in Figure 3-12, the stress value at failure can go from about 100 MPa to almost 2000 MPa, while system toughness can range from 10 to almost 300 MPa.

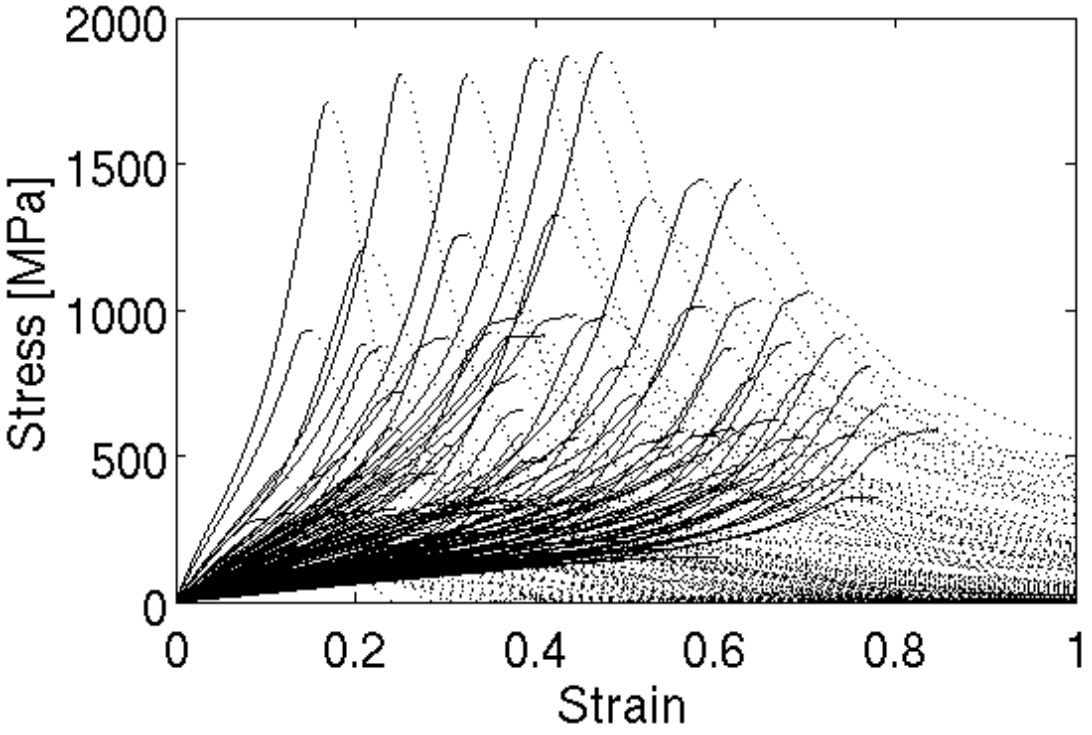

Figure 3-11: Combined effect of crystal size, spacing and pre-stretch. Combined effect of crystal size, crystal density and level of pre-stretch on the mechanical behavior of silk. The speed by which silk is spun affects simultaneously the size of the crystallites, their average spacing and the level of pre-stretch of the semi-amorphous regions. All these factors lead to different stress-strain constitutive behaviors. All the curves define an area of the stress-strain plane that can be explored by the present two-dimensional mesoscale model by varying characteristic parameters of silk.

When plotting toughness versus maximum stress, as it has been done in Figure 3-12, it is possible to see how the level of pre-stretch and the inter-crystal spacing play a role in changing these two fundamental parameters for the description of silk mechanical properties. Both an increase in inter-crystalline spacing and in pre-stretch level determine a significant drop in toughness. At the same time, a change in inter-crystalline spacing leads to a sharper decrease in maximum stress than what a decrease of pre-stretch leads to.

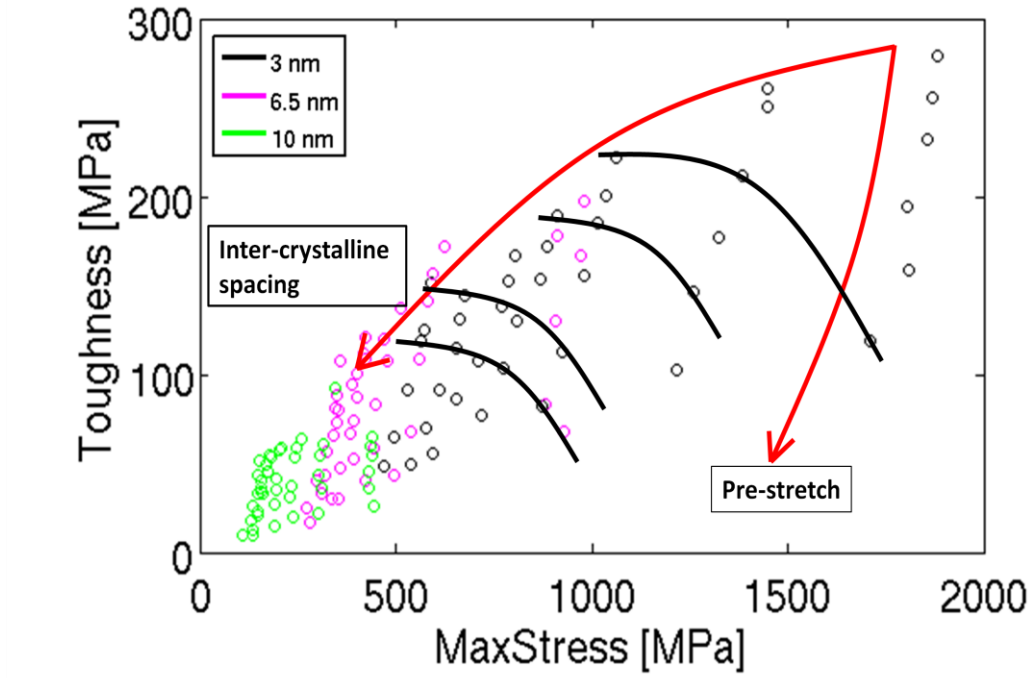

Figure 3-12: Silk toughness plotted as a function of maximum stress. Toughness is plotted over maximum stress for varying levels of pre-stretch, inter-crystalline spacing and crystal size. Points referred to crystals of different size are plotted in different colors, showing increased values of maximum stress and toughness for smaller (3 nm) crystals. An increase in inter-crystalline spacing leads to a drastic drop in both maximum stress and toughness, while an increase in pre-stretch mainly affects the toughness levels. By appropriately varying the controlling parameters, it is possible to obtain a curve with downward concavity, and thus a mechanical behavior able to couple high values of both material properties.

The presence of arches in Figure 3-12 is aimed to underline that by appropriately varying the controlling parameters it's possible to obtain a concave downwards curve, and thus a mechanical behavior able to couple high values of both toughness and maximum stress.

3.3.6 Effect of hydration

The level of hydration highly influences the mechanical properties of a silk system, since water molecules can penetrate within the polypeptide network, interfere with the level of hydrogen bonding and change the stiffness and extensibility features of the semi-amorphous domains. Here we analyze the effect of different hydration levels and how the presence of water affects the characteristic mechanical features of spider silk. The reference case has a water factor equal to 1 and represents a semi-amorphous structure which is partially hydrated, as it has been studied in atomistic implicit-solvent simulations [47]. A variation in the level of hydration is studied by varying the value of the water factor and leads to the different stress-strain characteristic curves shown in Figure 3-13b, c.

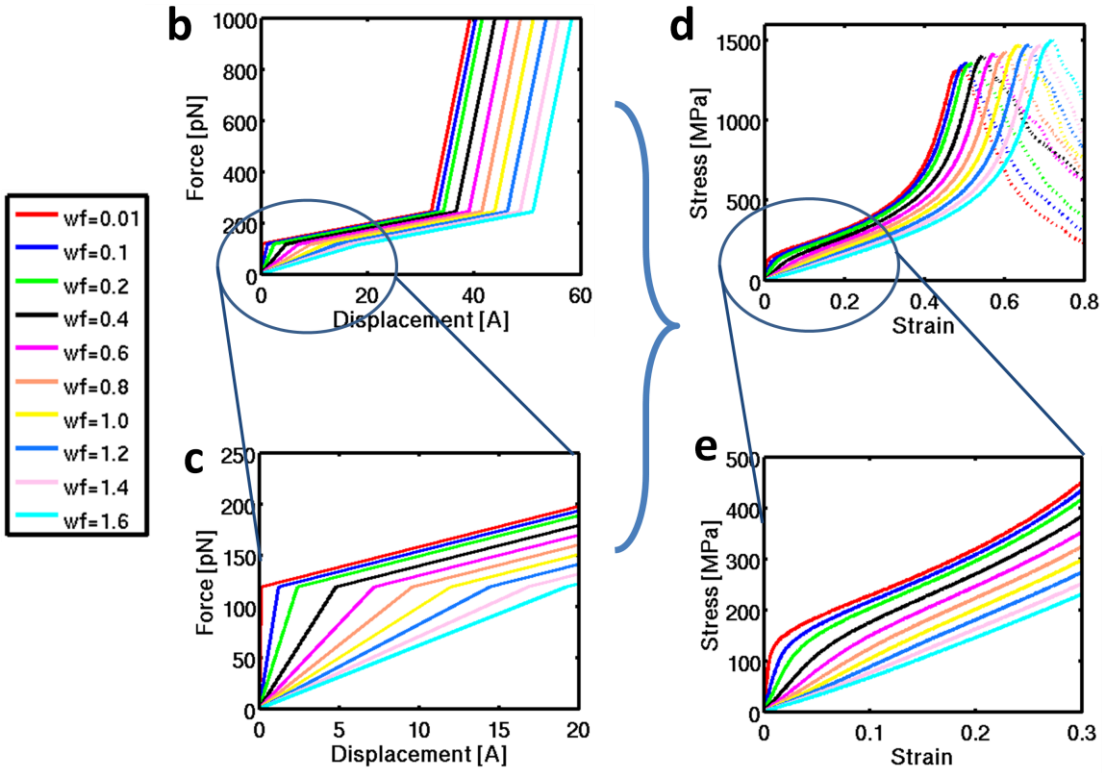

Figure 3-13: Effect of system hydration. **b-c.** The effect of water is modeled by modifying the initial stiffness and extensibility of the semi-amorphous region, with the hypothesis to keep equal values of yielding and stiffening force. The level of hydration is accounted by means of a water factor, varying between 0.4 and 1.6: higher values represent a more hydrated structure and a softer initial behavior. **c.** shows a magnified image of the region around the yielding point: the current model aims indeed to study the effect of water on the initial regime and on the entity of the yielding. **d** and **e** (magnified). stress-strain behavior of spider silk at different hydration values. Higher values of hydration lead to a yielding which is less pronounced and which occur at higher strain values. The reference case (with a water factor equal to 1) refers to a partially-hydrated original structure, whose characteristic parameters are obtained from atomistic simulations in implicit solvent [10, 47]. These predicted results are in agreement with recent experimental evidences about supercontraction and the effect of water on silk threads.

Figure 3-5 shows a schematic representation of the effect of water on the spider silk structure: higher levels of hydration determine a decrease in inter- and intra-chain hydrogen bonding and lead to a softer and more extensible behavior for the semi-amorphous region (see Figure 3-13b,c). The effect of water is modeled by modifying the initial stiffness and extensibility of the semi-amorphous region, with the hypothesis to keep equal values of yielding and stiffening force. The level of hydration is accounted by means of a water factor, varying between 0.4 and 1.6: higher values represent a more hydrated structure and a softer initial behavior of the semi-amorphous regions.

The current model aims to study the effect of water to the limited extent of the initial regime and the yielding point. Figure 3-13d,e shows how an increase in hydration leads to a softer and more extensible initial regime and how a higher values of hydration leads to a yielding which is less pronounced and which occur at higher strain values.

These results are overall in agreement with experimental data [59], where an increase in hydration has shown to lead to a significant softening of the whole structure, to the gradual disappearance of the yielding point and to the supercontraction phenomenon characteristic of silk [57, 67].

Chapter 4

Conclusions and outlook to future research

This Chapter is aimed to summarize the key findings of this thesis work, distinguishing the results and scientific accomplishments gained by the development of the one-dimensional model described in Chapter 2 and the two-dimensional model described in Chapter 3.

The work has helped to fill the gap in the understanding of the linkage between the atomistic and macroscopic description of spider silk and has provided critical insight into the molecular and supra-molecular arrangement making up the structure of silk.

At the same time, the work developed for this thesis has opened new opportunities for future research and provided new scientific questions on the modeling and understanding of spider silk mechanical behavior.

4.1 Summary of key findings and significance

The key contribution of this thesis work is in the development and application of a framework of structural and mechanical understanding of the behavior of silk protein materials, with the use of a purely computational bottom up approach and validated by a direct comparison with experimental evidence. Figure 4-1 is referred to recent experimental results [6] on the mechanical properties of spider dragline silk. The plots show two systems characterized by different beta-sheet nanocrystal size, showing how nanoconfinement to smaller crystals leads to higher values of toughness and maximum tensile stress. These values are quantitatively comparable, in terms of maximum tensile strength, with simulation results obtained in the study described in this thesis work. Overall, goal of this work is to create a link between the understanding of silk's mechanical behavior at the nanoscale and its mechanical behavior at the macroscale.

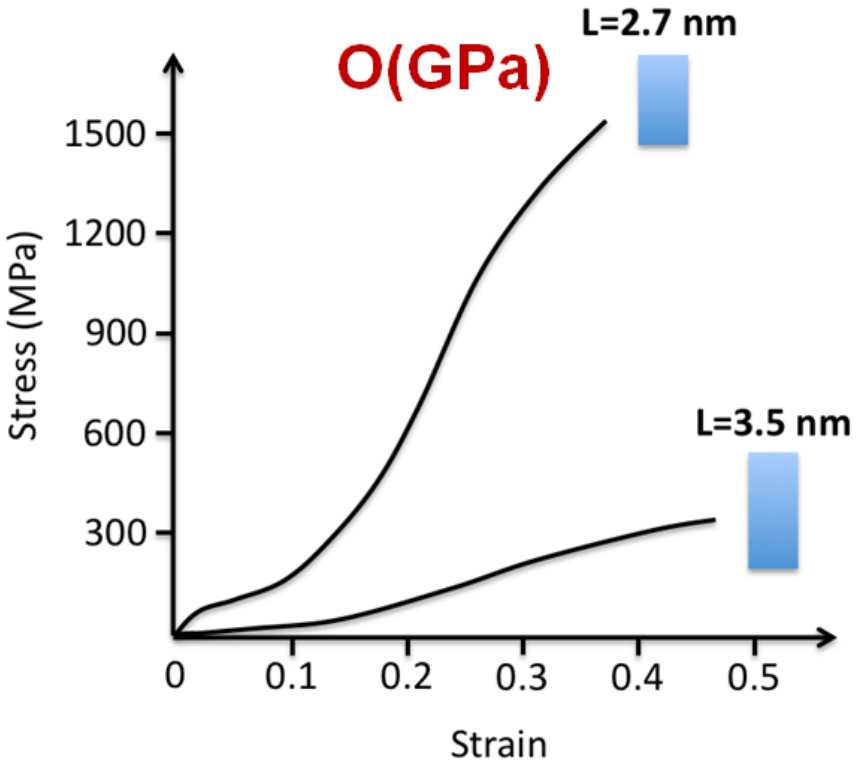

Figure 4-1: Schematic representation of the experimental stress-strain behavior of silks, characterized by different size of beta-sheet nanocrystals. It's evident a sigmoidal behavior in the small-crystal case, characterized by a yielding point and a final covalent stiff regime. Larger crystals show instead a slightly enhanced capacity to strain but much smaller values of maximum stress and toughness [6]. [courtesy of Sinan Keten]

These finding shed light on the structure and interplay of different constitutive elements that make up the behavior and peculiar features of spider silk. A model has been developed to allow an understanding of the role of the two fundamental constituents of silks at the intermediate, mesoscale level.

The aim has been to understand the fundamentals of silk's unique material properties, by deriving evidence directly from an atomistic level, without the need to introduce any experimental parameter. The atomistic-informed computational model described in this work has demonstrated to be able to correctly represent key features of spider silk mechanical behavior, and has provided insight into the underlying mechanicistc reason of experimental evidences.

4.1.1 Contribution of the one-dimensional model of silk unit cell

The most important finding of the study described in Chapter 2 and relative to the one-dimensional silk unit cell has been revealing the mechanistic interplay of the two constitutive phases of silk at the scale of tens and potentially hundred of nanometers. Structural changes on silk's semi-amorphous regions and on its highly-organized beta-sheet nanocrystals have shown to drastically affect silk's overall mechanical behavior (see Figure 2-5 and Figure 3-6).

When silk is being stretched, semi-amorphous regions have shown to unravel first leading to the large extensibility of silk, which is concurrently made possible by the high ultimate tensile strength of beta-sheet nanocrystals (See Figure 2-7). The large-deformation mechanical properties of silk have shown to be controlled by the strength of beta-sheet nanocrystals, which are directly related to their size. An important discovery is that beta-sheet nanocrystals of small dimension are crucial to reach high levels of strength and toughness, since they guarantee the required cross-linking strength that is necessary for the semi-amorphous domain to fully extend and enter a high-stiffness covalent regime, when beta-sheet nanocrystals are being stretched and eventually fail.

Only ultra-small crystals enable the material to reach very high levels of failure stress and provide the possibility to take full advantage of all silk's extensibility and energy dissipation capacity.

Unraveling of semi-amorphous regions is severely influenced by the size of beta-sheet nanocrystals and part of the secret of silk's outstanding mechanical properties relies in a correct balance of these interplaying factors: capacity to sustain large tensile force as well as capacity to unravel and extend.

Overall, the confinement of beta-sheet nanocrystals has shown to be essential for the superior mechanical properties of silk, as it is crucial to reach high extensibility and high levels of stress and toughness. The study has also demonstrated that silk's peculiar behavior can be modeled using evidences derived solely by computational atomistic simulations, without any introduction of experimental parameter. In particular these findings have related the characteristic yielding point in the stress-strain curve, universally observed for many types of silk, with the rupture of H bonds in 3_1 helices and beta turns of semi-amorphous regions.

4.1.2 Contribution of the two-dimensional model

The development of a two-dimensional mesoscale model of spider silk has been crucial to identify and explain key features of spider silk behavior that cannot be justified by a simple one-dimensional model, such as crystal concentration and structural homogeneity. Molecular dynamics techniques have been used to simulate the variation of a variety of system conditions and perform a parametric study of their effect on the overall silk's mechanical behavior.

A complete understanding of the mechanical signature of silk requires indeed the development of a model that can take into account key physical phenomena such as the effect of water and system hydration, the effect of crystal density and homogeneity as well as the level of pre-stretch of the protein chains. The robustness and flexibility of the current model has been checked by validating computational evidences with experimental results, showing great agreement but opening at the same time interesting directions for future research, in the pursuit of an always better understanding of the phenomena underlying experimental evidences.

The importance of this computational study of silk's behavior at the nanoscale comes from the fact that experimental techniques can only provide limited insight into the nanostructure of silk, making computing techniques the only suitable tool for such investigation. A bottom-up approach is consistently employed to climb the dimensional hierarchy of silk and to study the effect of different system conditions: for every parameter variation, the physical underlying reason has been taken in consideration, has been modeled and its consequence on the overall system has been analyzed.

Key findings of the two-dimensional model can be summarized as follows:

- a variation in size of beta-sheet nanocrystals affect the mechanical behavior of spider silk also at larger scales, with smaller crystal systems showing enhanced properties in terms of maximum tensile strength and dissipated energy (see Figure 3-6). The analogy of results in a one-dimensional and two-dimensional system confirms that the deformation mechanisms of silk are well preserved when increasing the complexity of the system;
- a shorter average inter-crystalline distance, corresponding to denser silk structures, increases the failure stress and toughness of the system and is accompanied by a significant decrease of the strain levels (see Figure 3-7). A main outcome of this study is the discovery that in a two-dimensional model the maximum stress value does not depend solely on the value of crystal strength (as in a one-dimensional model) but it rather depends on a combination of multiple factors such as amorphous stiffness and crystal concentration;
- a variation in crystal homogeneity leads to a significant variation of silk's mechanical properties (see Figure 3-9), with highly homogeneous structures showing an increase of up to 20% in maximum stress and a more pronounced sigmoidal behavior, with a marked yielding and final stiff regime. No significant variations of the strain levels have been shown as a consequence of a change in homogeneity;

- different hypotheses on the modeling of pre-stretch (constant stiffness and constant force) give approximately the same variation in maximum stress, with highly-prestretched structures leading to a drop in maximum strength and toughness (see Figure 3-10). The hypothesis of constant force for the transition points of the semi-amorphous domain changes the shape of the silk stress-strain curve especially at low levels of deformation, with a gradual upward shift concurrent with higher levels of pre-stretch;
- a study of the combined effect of crystal size, inter-crystalline spacing and pre-stretch (Figure 3-11 and Figure 3-12) determines an area in the stress-strain plot where the silk characteristic curves lie given the present model. Plotting toughness versus maximum stress it is possible to see how an increase in inter-crystalline spacing or an increase in the pre-stretch level determines a decrease in toughness and maximum stress values;
- a change in the level of hydration (see Figure 3-13) influences the mechanical properties of a silk system, determining a decrease in inter and intra-molecular bonding, to a more extensible initial regime and to a yielding point which is less pronounced and occurring at higher strain values. These results are overall in agreement with experimental data, where an increase in hydration has shown to lead to a significant softening of the whole structure, accompanied by the gradual disappearance of a clear yielding point.

4.2 Open questions and future developments

While answering some of the questions on spider silk's structural conformation and mechanical properties, the current study has at the same time opened new lines of research, that use the models described in this thesis work to further improve the understanding of silk's mechanical secrets.

Exciting future research perspectives that have been opened and on which research is currently undergoing can be summarized as follows:

- the effect of imperfections has just been explored in the present work, in terms of variations in homogeneity. A more systematic study of defects, crack formation and propagation patterns as well as system flaws and void in the network will shed further light in the mechanics of silk, especially at failure;

- a single type of geometry and matrix generation process has been studied in this project. Work is undergoing to understand how different conformation and generation processes can affect the system mechanical behavior, increasing the number of parameters that could be used to tune silk's mechanical properties with the aim to even better describe experimental evidences;

- the current model is able to describe the silk's behavior until rupture. An interesting perspective opened by the current study is the possibility to improve and adapt the model so that it can describe the silk behavior after breaking, analyzing how local stress distribution change when cracks generate and propagate, leading the structure to complete failure.

- the current model is based on multi-linear elements, that do not include the effect of visco-elastic phenomena and energy-dissipation events. Exploratory research is undergoing to identify the viability of a model which can include also these effects and consequently allow a study of the effect of cyclical loading on silk structure. Booster to curiosity in this field is the fact that experimental evidences show that silk has a strongly visco-elastic dissipative behavior that cannot be modeled by any model currently existing. When capturing preys, spider silk threads are cyclically loaded, making the exploration of this mechanical effect particularly exciting;

- new force-fields, new simulation techniques and new simulation parameters for the current model could be investigated, with the goal to bring the

potentialities of this model to its full extent and to validate its robustness with regards to different computational tools;

- the current modeled has been based on a restrict number of pioneering atomistic simulations, limited especially by the complexity of the system, the high simulation times and the difficulty of directly validate results with experimental evidences. The perspectives opened by the work described in this thesis and the possibility to now compare and validate computational results with experiments have leaded to a renovated interest for atomistic simulations on spider silk, with specific regards to the understanding of how different system parameters affect the silk structure and behavior at the nanoscale level. Of particular interest is the study of the effect of water on the silk unit cell and the analysis of its consequences on the stress-strain curve at all levels of deformation. The results from these new atomistic simulations will be used in the future to back up what now are just hypotheses on the effect of parameters on silk's constitutive-elements behavior. Scope of the parametric study described in this work has been to anticipate how a specific parameter variation affects the overall silk behavior and arise the curiosity to fully understand the phenomena from a fundamental atomistic perspective;

- thrilling research is undergoing to develop the first molecularly informed macroscale study of a whole spider web [61, 68-71]. The results obtained in this work have made possible to link the atomistic scale with the macroscale of spider silk, passing through the mesoscale of tens and hundreds of nanometers. It is consequently now possible to use the acquired knowledge to bring the bottom-up multiscale analysis of spider silk to its final stage, developing a macroscale model of the silk web completely backed up by computational studies at lower scales. It is possible to envision the early development of a three-dimensional macroscale model that could simulate the behavior of the whole spider web in different loading conditions: when preys

of different kind hit the spider web, a different mechanical load is applied. It will soon be possible to simulate and predict the behavior of the spider web when undergoing a whole range of mechanical loadings.

The work described in this thesis has helped to open a window in the understanding of silk's astonishing mechanical properties, has arisen enhanced curiosity in the field and provided the research community with a mesoscale two-dimensional model. The current study will eventually work as a tool and starting point for future developments in silk's mechanical understanding and has overall contributed in the process of unraveling the secrets of one of the most enigmatic and exciting biological materials.

Appendix

A1. MATLAB code for the simulation of the 1D system

```
%all lengths are in A
function [y]=onedimensional(type, color);
%type can be s (small), l (large) or xl (extralarge)
npoints=5000;   %how many points I have in the plot
strain=0.7;     %how much i strain the whole structure
crlength=0;    %initial length of the crystal
amlength=90;    %initial length of the amorphous region
length=crlength+amlength    %total system length;
if type=='s';
k11=576; %the crystal has purely elastic behavior
%all stiffnesses in pN/A
k12=0.01*k11;
r11=2.36; %value in A
r12=5.8;
elseif type =='l';
k11=205.5;
k12=205.5;
r11=4.5;
r12=4.5;
elseif type =='xl';
k11=67.53;
k12=67.53;
r11=6.63;
```

```
r12=6.63;

end

k21=9.9;

k22=3.96;

k23=103.84;

r21=0.13;    %fraction of initial length of amorphous

r22=0.49;    %fraction of initial length of amorphous

k2=k21;  %need to specify this for the first step of the cycle

k1=k11;

for i=1:npoints+1;

    dl(i,1)=(i-1)/npoints*strain*length;    % total deformation as a
function of step

 if i==1;    %only for first step

    dl1(i,1)=k2/(k1+k2)*dl(i,1);    % deformation of each spring as
a function of total length

    dl2(i,1)=k1/(k1+k2)*dl(i,1);

 else

    dl1(i,1)=dl1(i-1,1)+k2/(k1+k2)*(dl(i,1)-dl(i-1,1));

    dl2(i,1)=dl2(i-1,1)+k1/(k1+k2)*(dl(i,1)-dl(i-1,1));

 end

    if dl2(i,1)>=r21*amlength;   %semi-amorphous spring reaches 1st
transition point

        if dl2(i,1)>=r22*amlength;   %semi-amorphous spring reaches
2nd transition point

        k2=k23; %assigment of the new k

        else

        k2=k22;

        end

    end

    if dl1(i,1)>=r11;   %crystal spring reaches transition point

       k1=k12;
```

```
    end

    k(i,1)=k1*k2/(k1+k2); %overall system stiffness in a series of
springs

      if dl1(i,1)<=r12;     %i make sure the crystal is not broken

        if i==1;    %particular only for first step

        f(i,1) = k(i,1)*dl(i,1);

        else

        f(i,1) = f(i-1,1)+k(i,1)*(dl(i,1)-dl(i-1,1));

        end

    else f(i,1)=0;  %if crystal is broken the total force goes to
zero

   end

end

 %conversion to stress; number in MPa:

sigma = f*1;  %this value depends on the area used to calculate the
stress

top=max(sigma)

maxstress=top;

location=find(sigma(:)==top);

initial=sigma(1:location);

dl5=dl(1:location);

sigma5=sigma(1:location);

plot(dl/length, sigma, [':',color], 'HandleVisibility', 'off');

hold on;

plot(dl5/length, initial, color);

set(gca, 'XTick', [ 0.3 0.6 .9])

xlim ([0 1.1])

xlabel('Strain');

ylabel('Stress [MPa]');

toughness=trapz(dl5/length, sigma5
```

A2. MATLAB code for the generation of the random 2D matrix

```
function randommatrix(averagelength, totlength, cutoffcoeff);

close all

averagelength
totlength


Ninternal=double(int32(1.1*totlength^2/(sqrt(3)/2*averagelength^2)))

Nbord=double(int32(sqrt(Ninternal)));

cutoff=1/(25*(sqrt(Ninternal/400)))*cutoffcoeff;

xpart=(1/Nbord)*[0:1:Nbord]';
xin=[xpart zeros(Nbord+1,1); xpart ones(Nbord+1,1); zeros(Nbord-1,1)
xpart(2:end-1); ones(Nbord-1,1) xpart(2:end-1)];
for i=1:4*Nbord
    xf(i)=xin(i,1);
    yf(i)=xin(i,2);
end
i=4*Nbord+1;

cutoffsq=cutoff^2;
%cutoff2sq=cutoff2^2;
while i<Ninternal+Nbord+1
    X= rand(1,2);
    x=X(1);
    y=X(2);
    use=1;
    for j=1:i-1
        if ((x-xf(j))^2+(y-yf(j))^2<cutoffsq), use=0; end
    end
    if (use==1)
       xf(i)=x;
       yf(i)=y;
       i=i+1;
    end
end
TRI=delaunay(xf,yf);
triplot(TRI,totlength*xf,totlength*yf);
set(gca, 'Xtick', [0:totlength/5:totlength]);
set(gca, 'ytick', [0:totlength/5:totlength]);

TRI3=[TRI(:,1) TRI(:,2);TRI(:,2) TRI(:,3);TRI(:,3) TRI(:,1)];
TRI4 = sort(TRI3')';
saaa=unique(TRI4,'rows');
```

```
numbering = [1:1:length(xf)];
%first layer of beads
numbering2 = [1:1:size(saaa,1)];
%amorphous bonds
numbering3 = [length(xf)+1:1:2*length(xf)];
%second layer of beads
numbering4 = [size(saaa,1)+1:1:length(xf)+size(saaa,1)];
%crystal bonds numbering -- 1
numbering5 = [2*length(xf)+1:1:3*length(xf)];
%third layer of beads
numbering6 =
[length(xf)+size(saaa,1)+1:1:2*length(xf)+size(saaa,1)];
%crystal bonds numbering -- 2
numbering7 = [3*length(xf)+1:1:4*length(xf)];
%fourth layer of beads
numbering8 =
[2*length(xf)+size(saaa,1)+1:1:3*length(xf)+size(saaa,1)];
%crystal bonds numbering -- 3

% Positioning of the four layers of beads:

Xfin1 = [numbering' ones(length(xf),1) ones(length(xf),1)
totlength*xf' totlength*yf' zeros(length(xf),1)];
Xfin2 = [numbering3' ones(length(xf),1) ones(length(xf),1)
totlength*xf' totlength*yf' zeros(length(xf),1)];
Xfin3 = [numbering5' ones(length(xf),1) ones(length(xf),1)
totlength*xf' totlength*yf' zeros(length(xf),1)];
Xfin4 = [numbering7' ones(length(xf),1) ones(length(xf),1)
totlength*xf' totlength*yf' zeros(length(xf),1)];
Xfin = [Xfin1; Xfin2; Xfin3; Xfin4];

% Creation of the amorphous bonds:

for i = 1:size(saaa,1); %loop to attach crystals such that if X1>X2
attach to second crystal bead
   if  Xfin(saaa(i,1),4)<Xfin(saaa(i,2),4);
       if Xfin(saaa(i,1),5)<Xfin(saaa(i,2),5);
            saaa(i,1)=saaa(i,1)+length(xf);
            saaa(i,2)=saaa(i,2)+2*length(xf);
       else
            saaa(i,1)=saaa(i,1)+3*length(xf);
       end
   else
       if Xfin(saaa(i,1),5)<Xfin(saaa(i,2),5);
            saaa(i,2)=saaa(i,2)+3*length(xf);
       else
            saaa(i,1)=saaa(i,1)+2*length(xf);
            saaa(i,2)=saaa(i,2)+length(xf);
       end
   end
end

bondfin1 = [numbering2' 2*ones(size(saaa,1),1) saaa];
%amorphous bonds
```

```
bondfin2 = [numbering4' 1*ones(length(xf),1) numbering'
numbering3'];     %how crystals are bound --1
bondfin3 = [numbering6' 1*ones(length(xf),1) numbering3'
numbering5'];     %how crystals are bound --2
bondfin4 = [numbering8' 1*ones(length(xf),1) numbering5'
numbering7'];     %how crystals are bound --3

bondfin = [bondfin1; bondfin2; bondfin3; bondfin4];
dlmwrite('nodes.txt',Xfin,'delimiter','\t','precision',6);
dlmwrite('bonds.txt',bondfin,'delimiter','\t','precision',6);

clear all;
```

A3. Modified bond-harmonic file

```
/* ----------------------------------------------------------------------
   LAMMPS - Large-scale Atomic/Molecular Massively Parallel
Simulator

------------------------------------------------------------------------- */

#include "math.h"
#include "stdlib.h"
#include "bond_harmdifflengths.h"
#include "atom.h"
#include "neighbor.h"
#include "domain.h"
#include "comm.h"
#include "update.h"
#include "neighbor.h"
#include "force.h"
#include "memory.h"
#include "error.h"

using namespace LAMMPS_NS;

/* ---------------------------------------------------------------------- */

BondHarmdifflengths::BondHarmdifflengths(LAMMPS *lmp) : Bond(lmp) {}

/* ---------------------------------------------------------------------- */

BondHarmdifflengths::~BondHarmdifflengths()
{
  if (allocated) {
    memory->sfree(setflag);
    memory->sfree(k);
    memory->sfree(r0);
  }
}

/* ----------------------------------------------------------------------*/

void BondHarmdifflengths::compute(int eflag, int vflag)
{
  int i1,i2,n,type,factor;
  double
delx,dely,delz,ebond,fbond,xFac,rfactor,softp,rcut,r00,length,chainf
actor,lengthfactor,prestretch;
  double rsq,r,dr,rk;
  int c1,c2,c3,c4,c5,c6,c7,c8;
  double rsoft1, rbreak1,k11, k12, r21, r22, k_pick, k21, k22, k23 ;

  ebond =0.0;
  if (eflag || vflag) ev_setup(eflag,vflag);
  else evflag = 0;
```

```
double **x = atom->x;
double **f = atom->f;
int **bondlist = neighbor->bondlist;
int nbondlist = neighbor->nbondlist;
int nlocal = atom->nlocal;
int newton_bond = force->newton_bond;
int currentstep = update->ntimestep;

r00=3.615;

if (currentstep==0) {
   for (n = 0; n < nbondlist; n++) {
     i1 = bondlist[n][0];
     i2 = bondlist[n][1];

     delx = x[i1][0] - x[i2][0];
     dely = x[i1][1] - x[i2][1];
     delz = x[i1][2] - x[i2][2];
     domain->minimum_image(delx,dely,delz);

     rsq = delx*delx + dely*dely + delz*delz;
     r = sqrt(rsq);
     rlist[n]=r;
     }
  }

for (n = 0; n < nbondlist; n++) {
  i1 = bondlist[n][0];
  i2 = bondlist[n][1];
  type = bondlist[n][2];

if (newton_bond) factor = 2;
  else {
    factor = 0;
    if (i1 < nlocal) factor++;
    if (i2 < nlocal) factor++;
  }
  rfactor = 0.5 * factor;

  delx = x[i1][0] - x[i2][0];
  dely = x[i1][1] - x[i2][1];
  delz = x[i1][2] - x[i2][2];
  domain->minimum_image(delx,dely,delz);

  rsq = delx*delx + dely*dely + delz*delz;
  r = sqrt(rsq);

  r00=rlist[n];

  //type1:

  chainfactor=3.75;
  if (type==1){
```

```
      rsoft1 = r00+2.36;
      rbreak1 = r00+5.8;
      k11=8.2842*chainfactor;

      if (r <= rbreak1){

      if (r <= rsoft1){
        k_pick = k11;

    dr = r - r00;
    rk = k_pick * dr;

      if (r > 0.0)
    fbond = -2.0*rk/r;
    else fbond = 0.0;

       }
      if (r > rsoft1){

      k12 = 0.01*k11;   //second slope is 1% of the initial
    k_pick = k12;

    dr = r - rsoft1;
    rk = k_pick * dr;

      if (r > 0.0)
    fbond = -2.0*(((rsoft1-r00)*k11)+rk)/r;
    else fbond = 0.0;
      }
      }
      else fbond = 0.0;

      }

 // Type 2 amorphous region

      length=r0[2];

      prestretch=k[1];

      if (type==2){

      lengthfactor=60/(length-30);

      r21 = r00+0.2*(1-prestretch)*(r00-30);
      r22 = r00+0.73*(1-prestretch)*(r00-30);

      k21=0.1424*chainfactor*lengthfactor/(1-prestretch);
      k22=0.0570*chainfactor*lengthfactor/(1-prestretch);
      k23=1.4935*chainfactor*lengthfactor;

if (r <= r22){


      if (r <= r21){
```

```
        k_pick = k21;

    dr = r - r00;
    rk = k_pick * dr;

      if (r > 0.0)
    fbond = -2.0*rk/r;
    else fbond = 0.0;

       }
      if (r > r21){
        k_pick = k22;

    dr = r - r21;
    rk = k_pick * dr;

      if (r > 0.0)
    fbond = -2.0*(((r21-r00)*k21)+rk)/r;
    else fbond = 0.0;

        }
   }

 if (r > r22) {

   k_pick = k23;

   dr = r - r22;
   rk = k_pick * dr;

   if (r > 0.0)
     fbond = -2.0*(((r21-r00)*k21)+ ((r22-r21)*k22) + rk)/r;
   else fbond = 0.0;
   }

    }

    if (newton_bond || i1 < nlocal) {
      f[i1][0] += delx*fbond;
      f[i1][1] += dely*fbond;
      f[i1][2] += delz*fbond;
    }

    if (newton_bond || i2 < nlocal) {
      f[i2][0] -= delx*fbond;
      f[i2][1] -= dely*fbond;
      f[i2][2] -= delz*fbond;
    }

    if (evflag)
ev_tally(i1,i2,nlocal,newton_bond,ebond,fbond,delx,dely,delz);

     }
}
```

```
/* ----------------------------------------------------------------------*/

void BondHarmdifflengths::allocate()
{
  allocated = 1;
  int n = atom->nbondtypes;
  int maxbond = atom->nbonds;

  k = (double *) memory->smalloc((n+1)*sizeof(double),"bond:k");
  r0 = (double *) memory->smalloc((n+1)*sizeof(double),"bond:r0");
//  rlist = (double *) memory-
>smalloc((maxbond+1)*sizeof(double),"bond:rlist");
  rlist = memory->create_1d_double_array(0,maxbond,"bond:rlist");

  setflag = (int *) memory-
>smalloc((n+1)*sizeof(int),"bond:setflag");
  for (int i = 1; i <= n; i++) setflag[i] = 0;
}

/* ----------------------------------------------------------------------
   set coeffs for one or more types
------------------------------------------------------------------------- */

void BondHarmdifflengths::coeff(int narg, char **arg)
{
  if (narg != 3) error->all("Incorrect args for bond coefficients");
  if (!allocated) allocate();

  int ilo,ihi;
  force->bounds(arg[0],atom->nbondtypes,ilo,ihi);

  double k_one = atof(arg[1]);
  double r0_one = atof(arg[2]);

  int count = 0;
  for (int i = ilo; i <= ihi; i++) {
    k[i] = k_one;
    r0[i] = r0_one;
    setflag[i] = 1;
    count++;
  }

  if (count == 0) error->all("Incorrect args for bond
coefficients");
}

/* ----------------------------------------------------------------------
   return an equilbrium bond length
------------------------------------------------------------------------*/

double BondHarmdifflengths::equilibrium_distance(int i)
{
  return r0[i];
}
```

```
/* ----------------------------------------------------------------------
   proc 0 writes out coeffs to restart file
------------------------------------------------------------------------*/

void BondHarmdifflengths::write_restart(FILE *fp)
{
  fwrite(&k[1],sizeof(double),atom->nbondtypes,fp);
  fwrite(&r0[1],sizeof(double),atom->nbondtypes,fp);
}

/* ----------------------------------------------------------------------
   proc 0 reads coeffs from restart file, bcasts them
------------------------------------------------------------------------*/

void BondHarmdifflengths::read_restart(FILE *fp)
{
  allocate();

  if (comm->me == 0) {
    fread(&k[1],sizeof(double),atom->nbondtypes,fp);
    fread(&r0[1],sizeof(double),atom->nbondtypes,fp);
  }
  MPI_Bcast(&k[1],atom->nbondtypes,MPI_DOUBLE,0,world);
  MPI_Bcast(&r0[1],atom->nbondtypes,MPI_DOUBLE,0,world);

  for (int i = 1; i <= atom->nbondtypes; i++) setflag[i] = 1;
}

/* ----------------------------------------------------------------------*/

double BondHarmdifflengths::single(int type, double rsq, int i, int
j)
{
  double r = sqrt(rsq);
  double dr = r - r0[type];
  double rk = k[type] * dr;
  return rk*dr;
}
```

A4. LAMMPS input file

```
# Initialization

units       real
atom_style  angle
timestep    1.0     #fs for units=real

# Atom Definition - Indicate input geometry file

read_data   random.data

# Neighbor Settings

neighbor    20 bin
neigh_modify      every 50 delay 50

# Force Fields and Interactions

bond_style      harmdifflengths
bond_coeff  1 0.0 0.0     # k1; r01

bond_coeff  2 0.0 30.0    # k2; r02

# Basic Output

dump        first01 all xyz 10000 random.xyz

dump        first02 all atom 10000 random.atom

# Set Ensemble

fix         1 all nve

# -------------------------------------------------------

region      1 block -5.0 5.0 INF INF INF INF units box
region      2 block 5990.0 6010.0 INF INF INF INF units box

group       fix_left region 1
group       fix_right region 2
group       fixx union fix_left fix_right

thermo          500

# Initial Conditions

fix             2 fixx setforce 0.0 0.0 0.0

velocity        all create 5.00 574654   #T value; random_seed
velocity        fixx set 0.00 0.00 0.00  units box    #i give value
in velocity                                                 units,
not in T
```

```
fix             3 all setforce NULL 0.0 0.0
velocity        all set NULL 0.0 0.00  units box

# ---------------------------------------------------------
#     END OF BASIC SET-UP
# ---------------------------------------------------------


run         10000

fix         hold_temp all temp/berendsen 5.0 5.0 60.0 #only when
stretching

compute           max_x all reduce max x
compute           min_x all reduce min x

compute         stress all stress/atom
compute         s all reduce sum c_stress[1] c_stress[2] c_stress[3]

fix             stressout all ave/time 10 10 500 c_s[1] c_s[2]
c_s[3] c_max_x c_min_x file stress.data

fix         stretch all deform 500 x scale 2.5 units box

run         1500000

# ---------------------------------------------------------
#     END OF SIMULATION
# ---------------------------------------------------------
```

References

1. Becker, N., et al., *Molecular nanosprings in spider capture-silk threads.* Nature Materials, 2003. **2**(4): p. 278-283.
2. Shao, Z.Z. and F. Vollrath, *Materials: Surprising strength of silkworm silk.* Nature, 2002. **418**(6899): p. 741-741.
3. Vollrath, F. and D.P. Knight, *Liquid crystalline spinning of spider silk.* Nature, 2001. **410**(6828): p. 541-548.
4. Keten, S., et al., *Nanoconfinement controls stiffness, strength and mechanical toughness of [beta]-sheet crystals in silk.* Nat Mater, 2010. **9**(4): p. 359-367.
5. Vollrath, F. and D. Porter, *Spider silk as a model biomaterial.* Applied Physics A-Materials Science & Processing, 2006. **82**(2): p. 205-212.
6. Du, N., et al., *Design of superior spider silk: From nanostructure to mechanical properties.* Biophysical journal, 2006. **91**(12): p. 4528-4535.
7. Vollrath, F. and D. Porter, *Spider silk as archetypal protein elastomer.* Soft Matter, 2006. **2**(5): p. 377-385.
8. Porter, D., F. Vollrath, and Z. Shao, *Predicting the mechanical properties of spider silk as a model nanostructured polymer.* The European Physical Journal E: Soft Matter and Biological Physics, 2005. **16**(2): p. 199-206.
9. Rammensee, S., et al., *Assembly mechanism of recombinant spider silk proteins.* Proceedings of the National Academy of Sciences of the United States of America, 2008. **105**(18): p. 6590-6595.
10. Keten, S. and M.J. Buehler, *Atomistic model of the spider silk nanostructure.* Applied physics letters, 2010. **96**(153701).
11. Vollrath, F., *Spider webs and silks: Tracing evolution from molecules to genes to phenotypes.* Nature, 2003. **426**(6963): p. 121-122.
12. Buehler, M.J. and Y.C. Yung, *Deformation and failure of protein materials in physiologically extreme conditions and disease.* Nature Materials, 2009. **8**(3): p. 175-188.

13. Elliott, W.H. and D.C. Elliott, *Biochemistry and Molecular Biology*. Oxford University Press, 2001.
14. Kajava, A., J. Squire, and D. Parry, *beta-structures in fibrous proteins.* fibrous proteins: amyloids, prions and beta proteins, 2006. **73**: p. 1-+.
15. Buehler, M.J., *Atomistic modeling of materials failure.* Springer, 2008.
16. Keten, S. and M.J. Buehler, *Strength limit of entropic elasticity in beta-sheet protein domains.* Physical Review E (Statistical, Nonlinear, and Soft Matter Physics), 2008. **78**(6): p. 061913.
17. Fraser, P. and W. Bickmore, *Nuclear organization of the genome and the potential for gene regulation.* Nature, 2007. **447**(7143): p. 413-417.
18. Keten, S., *Size-Dependent Mechanical Properties of Beta-Structures in Protein Materials.* Doctoral Thesis Work, 2010.
19. Nova, A., et al., *Molecular and nanostructural mechanisms of deformation, strength and toughness of spider silk fibrils.* NanoLetters, 2010.
20. Nova, A., et al., *Mechanics of spider silk fibrils.* in submission, 2010.
21. LeDuc, P.R. and D.N. Robinson, *Using Lessons from Cellular and Molecular Structures for Future Materials.* Advanced Materials, 2007. **19**: p. 3761-3770.
22. Hayashi, C.Y., N.H. Shipley, and R.V. Lewis, *Hypotheses that correlate the sequence, structure, and mechanical properties of spider silk proteins.* International Journal of Biological Macromolecules, 1999. **24**(2-3): p. 271-275.
23. van Beek, J.D., et al., *The molecular structure of spider dragline silk: Folding and orientation of the protein backbone.* Proceedings of the National Academy of Sciences of the United States of America, 2002. **99**(16): p. 10266-10271.
24. Lefevre, T., M.E. Rousseau, and M. Pezolet, *Protein secondary structure and orientation in silk as revealed by Raman spectromicroscopy.* Biophysical Journal, 2007. **92**(8): p. 2885-2895.

25. Kummerlen, J., et al., *Local structure in spider dragline silk investigated by two-dimensional spin-diffusion nuclear magnetic resonance.* Macromolecules, 1996. **29**(8): p. 2920-2928.
26. Gatesy, J., et al., *Extreme diversity, conservation, and convergence of spider silk fibroin sequences.* Science, 2001. **291**(5513): p. 2603-2605.
27. Holland, G.P., et al., *Determining secondary structure in spider dragline silk by carbon-carbon correlation solid-state NMR spectroscopy.* Journal of the American Chemical Society, 2008. **130**(30): p. 9871-9877.
28. Hayashi, C.Y. and R.V. Lewis, *Evidence from flagelliform silk cDNA for the structural basis of elasticity and modular nature of spider silks.* Journal of Molecular Biology, 1998. **275**(5): p. 773-784.
29. Brooks, A.E., et al., *An investigation of the divergence of major ampullate silk fibers from Nephila clavipes and Argiope aurantia.* Biomacromolecules, 2005. **6**(6): p. 3095-3099.
30. Gao, H.J., et al., *Materials become insensitive to flaws at nanoscale: Lessons from nature.* Proceedings of the National Academy of Sciences of the United States of America, 2003. **100**(10): p. 5597-5600.
31. Fossey, S.A., et al., *Conformational Energy Studies of Beta-Sheets of Model Silk Fibroin Peptides .1. Sheets of Poly(Ala-Gly) Chains.* Biopolymers, 1991. **31**(13): p. 1529-1541.
32. Xiao, S.B., et al., *Mechanical Response of Silk Crystalline Units from Force-Distribution Analysis.* Biophysical Journal, 2009. **96**(10): p. 3997-4005.
33. Thiel, B.L., K.B. Guess, and C. Viney, *Non-periodic lattice crystals in the hierarchical microstructure of spider (major ampullate) silk.* Biopolymers, 1997. **41**(7): p. 703-719.
34. Grubb, D.T. and L.W. Jelinski, *Fiber morphology of spider silk: The effects of tensile deformation.* Macromolecules, 1997. **30**(10): p. 2860-2867.
35. Philip, M.C., et al., *Mechanical and thermal properties of dragline silk from the spider Nephila clavipes.* Polymers for Advanced Technologies, 1994. **5**(8): p. 401-410.

36. Ball, P., *Made to measure : new materials for the 21st century*, ed. Anonymous. 1997, Princeton, N.J.: Princeton University Press. 458.
37. Vepari, C. and D.L. Kaplan, *Silk as a biomaterial.* Progress in Polymer Science, 2007. **32**(8-9): p. 991-1007.
38. Lewis, R.V., *Spider silk: Ancient ideas for new biomaterials.* Chemical Reviews, 2006. **106**(9): p. 3762-3774.
39. Rief, M., et al., *Reversible unfolding of individual titin immunoglobulin domains by AFM.* Science, 1997. **276**(5315): p. 1109-1112.
40. Marszalek, P.E., et al., *Mechanical unfolding intermediates in titin modules.* Nature, 1999. **402**(6757): p. 100-103.
41. Brockwell, D.J., et al., *Pulling geometry defines the mechanical resistance of a beta-sheet protein.* Nature structural biology, 2003. **10**(9): p. 731-737.
42. Eom, K., et al., *Relationship between the mechanical properties and topology of cross-linked polymer molecules: Parallel strands maximize the strength of model polymers and protein domains.* Journal of Physical Chemistry B, 2003. **107**(34): p. 8730-8733.
43. Lee, E.H., et al., *Mechanical strength of the titin Z1Z2-telethonin complex.* Structure (London, England : 1993), 2006. **14**(3): p. 497-509.
44. Sulkowska, J.I. and M. Cieplak, *Mechanical stretching of proteins - a theoretical survey of the Protein Data Bank.* Journal of Physics-Condensed Matter, 2007. **19**(28): p. -.
45. Termonia, Y., *Molecular Modeling of Spider Silk Elasticity.* Macromolecules, 1994. **27**(25): p. 7378-7381.
46. Lee, S.M., et al., *Greatly Increased Toughness of Infiltrated Spider Silk.* Science, 2009. **324**(5926): p. 488-492.
47. Keten, S. and M.J. Buehler, *Nanostructure and molecular mechanics of dragline spider silk protein assemblies.* Journal of the Royal Society Interface, 2010. **in press**.

48. Michal, C.A. and L.W. Jelinski, *Rotational-echo double-resonance in complex biopolymers: a study of Nephila clavipes dragline silk.* Journal of Biomolecular Nmr, 1998. **12**(2): p. 231-241.

49. Simmons, A.H., C.A. Michal, and L.W. Jelinski, *Molecular orientation and two-component nature of the crystalline fraction of spider dragline silk.* Science, 1996. **271**(5245): p. 84-87.

50. Keten, S. and M.J. Buehler, *Geometric Confinement Governs the Rupture Strength of H-bond Assemblies at a Critical Length Scale.* Nano Lett., 2008. **8**(2): p. 743-748.

51. Keten, S. and M.J. Buehler, *Asymptotic strength limit of hydrogen bond assemblies in proteins at vanishing pulling rates.* Physical Review Letters, 2008.

52. Oroudjev, E., et al., *Segmented nanofibers of spider dragline silk: Atomic force microscopy and single-molecule force spectroscopy.* Proceedings of the National Academy of Sciences, 2002. **99**(90002): p. 6460-6465.

53. Krasnov, I., et al., *Mechanical properties of silk: Interplay of deformation on macroscopic and molecular length scales.* Physical Review Letters, 2008. **100**(4)

54. Rousseau, M.E., et al., *Study of protein conformation and orientation in silkworm and spider silk fibers using Raman microspectroscopy.* Biomacromolecules, 2004. **5**(6): p. 2247-2257.

55. Fantner, G.E., et al., *Sacrificial bonds and hidden length dissipate energy as mineralized fibrils separate during bone fracture.* Nature Materials, 2005. **4**(8): p. 612-616.

56. Hartmann, M.A. and P. Fratzl, *Sacrificial Ionic Bonds Need To Be Randomly Distributed To Provide Shear Deformability.* Nano Letters, 2009. **9**(10): p. 3603-3607.

57. Papadopoulos, P., J. Sölter, and F. Kremer, *Hierarchies in the structural organization of spider silk—a quantitative model.* Colloid & Polymer Science, 2009. **287**(2): p. 231-236.

58. Shewchuk, J.R., *Delaunay refinement algorithms for triangular mesh generation.* Computational Geometry, 2002. **22**(1-3): p. 21-74.
59. Vehoff, T., et al., *Mechanical Properties of Spider Dragline Silk: Humidity, Hysteresis, and Relaxation.* Biophysical journal, 2007. **93**(12): p. 4425-4432.
60. Romer, L. and T. Scheibel, *The elaborate structure of spider silk Structure and function of a natural high performance fiber.* Prion, 2008. **2**(4): p. 154-161.
61. Alam, M.S., M.A. Wahab, and C.H. Jenkins, *Mechanics in naturally compliant structures.* Mechanics of Materials, 2007. **39**(2): p. 145-160.
62. Denny, M., *The physical properties of spider's silk and their role in the design of orb-webs.* Journal of Experimental Biology, 1976. **65**: p. 483-506.
63. Porter, D. and F. Vollrath, *The role of kinetics of water and amide bonding in protein stability.* Soft Matter, 2008. **4**(2): p. 328-336.
64. Plimpton, S., *Fast Parallel Algorithms for Short-Range Molecular-Dynamics.* Journal of Computational Physics, 1995. **117**(1): p. 1-19.
65. Zimmerman, J.A., et al., *Calculation of stress in atomistic simulation.* Modelling and Simulation in Materials Science and Engineering, 2004. **12**(4): p. S319-S332.
66. Humphrey, W., A. Dalke, and K. Schulten, *VMD: Visual molecular dynamics.* Journal of Molecular Graphics, 1996. **14**(1): p. 33-&.
67. Liu, Y., Z.Z. Shao, and F. Vollrath, *Relationships between supercontraction and mechanical properties of spider silk.* Nature Materials, 2005. **4**(12): p. 901-905.
68. Lin, L.H., D.T. Edmonds, and F. Vollrath, *Structural-Engineering of an Orb-Spiders Web.* Nature, 1995. **373**(6510): p. 146-148.
69. Wirth, E. and F.G. Barth, *Forces in the Spider Orb Web.* Journal of Comparative Physiology a-Sensory Neural and Behavioral Physiology, 1992. **171**(3): p. 359-371.
70. Aoyanagi, Y. and K. Okumura, *Simple Model for the Mechanics of Spider Webs.* Physical Review Letters, 2010. **104**(3)

71. Ko, F.K. and J. Jovicic, *Modeling of mechanical properties and structural design of spider web*. Biomacromolecules, 2004. **5**(3): p. 780-785.